2016

Modeling rogue waves in deep water

Maria Strawn
University of Central Florida

MODELING ROGUE WAVES IN DEEP WATER

by

MARIA STRAWN
B.S. University of Central Florida, 2010
M.S. University of Central Florida, 2012

A dissertation submitted in partial fulfillment of the requirements
for the degree of Doctor of Philosophy
in the Department of Mathematics
in the College of Sciences
at the University of Central Florida
Orlando, Florida

Summer Term
2016

Major Professor:
Constance Schober

ABSTRACT

The evolution of surface waves in deep water is governed by the nonlinear Schrödinger (NLS) equation. Spatially periodic breathers (SPBs) and rational solutions of the NLS equation are used as typical models for rogue waves since they exhibit many features of rogue waves.

A major component of the dissertation is the stability of solutions of the NLS equation. We address the stability of the rational solutions of the NLS equation used to model rogue waves using squared eigenfunctions of the associated Lax Pair. This allows us to contrast to the existing results for SPBs. The stability of the constant amplitude solution of the higher order NLS (HONLS) equation with additional novel perturbations, relevant to our subsequent study on downshifting, is considered next. In addition to the higher order perturbations, we include linear effects and nonlinear damping of the mean flow to the HONLS equation.

In addition to stability, we discuss rogue waves and downshifting. Permanent downshifting occurs when energy if permanently transferred from the initially dominant mode to lower modes and is observed in physical experiments and field studies of deep water waves. Although these experimental observations are well documented, neither NLS nor HONLS equations describe this behavior. Nonlinear damping of the mean flow, included in our stud-

ies, is shown to model permanent downshifting. We examine the interaction of rogue waves and downshifting in a sea state with both nonlinear and linear effects. We show that there are no rogue waves after permanent downshifting. Analytical and numerical analysis are provided to support the findings.

TABLE OF CONTENTS

LIST OF FIGURES

INTRODUCTION

Rogue waves have been described as large waves appearing out of no where which then disappear. They are frequently seen as walls of water that are preceded by deep troughs. Although we now know that they are more than legends, rogue waves were not observed by scientific measuring devices until 1995, when a wave exceeding 25 meters in height was recorded at a time when the average height of the largest third of the waves was only 12 meters. The Draupner wave (or New Year's wave) and the sea state were numerically simulated by Trulsen, et al. to investigate the conditions that led to this unique observation [1]. The rarity of rogue waves was quantified based on three weeks' satellite data collected by the European Space Agency in 2000 when at least 10 waves with height 25 meters or larger were recorded [2]. The frequency of the waves is strong evidence that rogue waves are not formed by linear wave interactions, so the governing equation must allow for nonlinear wave interactions.

Another interesting phenomena we peruse is that of frequency downshifting. In lab tank experiments, Lake et al. observed that initially periodic waveforms have different long-time behavior depending on the steepness of the initial waves [3]. When the waves had small steepness the initial condition would reappear periodically throughout the experiment.

When the initial waves had large steepness, however, the energy would move from the initially dominant wave numbers into lower frequency wave numbers. The lab tank results were later reproduced in numerical experiments [4]. Let us define the dominant wave number at a given time as the wave number, k, with the most energy. Downshifting occurs when the dominant mode decreases to a lower wavenumber in the course of the evolution of the solution.

Benjamin and Feir first observed solutions that have large growths despite being small perturbations of a constant background state [5]. The phenomena is called modulational instability (MI) and is a mechanism whereby small perturbations can lead to exponential growth in the low frequency components. Both rogue waves and frequency downshifting are associated with MI.

One model for describing ocean waves in deep water is the nonlinear Schrödinger equation (NLS). Solutions of NLS exhibit the modulational instability and anomalously large, steep waves. In particular, spatially periodic breathers (SPB) and rational solutions have the features of rogue waves. These two model solutions have been chosen as representative solutions that exhibit rogue waves. When investigating a model, features such as persistence and stability are very important. In [6] the periodic model was shown to have these features. In this work we show that although the rational solutions have the qualities of rogue waves, they do not have the desirable features of stability to perturbation and persistence.

The initial conditions used by Lake were small perturbations of a constant background, and this type of initial condition is viewed effectively as a rogue wave regime. We further examine the relationship between rogue waves and downshifting. This dissertation

explores the selection of appropriate perturbations to nonlinear Schrödinger equation to get downshifting. Earlier studies found that higher order perturbations of NLS are not sufficient to cause downshifting; some form of damping is needed. Although different methods of damping were examined to create downshifting of solutions, linear damping does not cause downshifting. In this dissertation we include nonlinear damping of the mean flow and linear effects from wind. Small amounts of nonlinear damping of the mean flow is shown to cause downshifting, and the interaction of the linear and nonlinear perturbations to HONLS are examined. After discussing the effects of various types of damping to the equation, the work in [7] is expanded further by also including additional families of initial conditions.

The document is arranged in the following chapters:

In Chapter 1 we outline the background information on the models in consideration, including history and definitions of the models. We also quantify rogue waves and demonstrate that both spatially periodic breathers and rational solutions can have waves that satisfy the criteria we define as having a rogue wave. We demonstrate that the rational solution is related to the spatially periodic breather by letting the period become infinitely large.

In Chapter 2 we discuss the the integrable nature of the governing equation and the associated framework. We begin with solving the Zakharov-Shabot eigenvalue problem for the eigenvalues and eigenvectors associated with a constant amplitude background state (the plane wave). The Bäklund-Gauge transformation is presented as a way to transform not only solutions, but also the associated eigenfunctions for the Zakharov-Shabot system.

In Chapter 3 we offer comparison of the stability of the two model solutions and an explanation of why we choose the spatially periodic breather for numerical implementation. Additionally, the analytical claims are supported by comparing the numerical resolution of the solutions.

In Chapter 4 we present the HONLS along with two different types of damping: linear and nonlinear. Special emphasis is paid to the particular form of HONLS and its retention of features of the zeroth order model. The topic of downshifting is introduced, and the linear instability of the plane wave for the full equation is presented.

In Chapter 5 we show that numerical experiments exhibit the expected behavior of each type of damping from the analytical expressions. The impact of the individual types of damping and the combination of the two types is examined in numerical experiments that focus on rogue waves and downshifting of solutions. The interaction between rogue waves and downshifting is examined, but we show that rogue waves are not required for downshifting to occur.

CHAPTER 1

ANALYTICAL BACKGROUND

1.1 Governing Equation

The nonlinear Schrödinger equation is frequently used to model the dynamics of deep water waves. In this section we briefly review the derivation of NLS from the water wave equations. There are are many variations of presentation for this derivation. The core of the discussion follows [8].

Let h be the depth of a fluid with density ρ, velocity $\vec{v}$, and kinematic viscosity ν being acted upon by body forces $\vec{f}$ and under pressure p. We establish a coordinate system with vertical component z and set $z = 0$ as the unperturbed free surface of the air-water interface. The displacement from the unperturbed surface is defined to be $\eta(x, t)$. It is assumed that the water cannot penetrate the lower boundary, so there is no exchange of particles in the z direction. This coordinate system is shown in Figure 1.1.

One of the fundamental principles of fluid mechanics is the conservation of mass. Since the fluid has density ρ and is moving with velocity $\vec{v}$, the flux of the fluid is $\rho\vec{v}$, so the

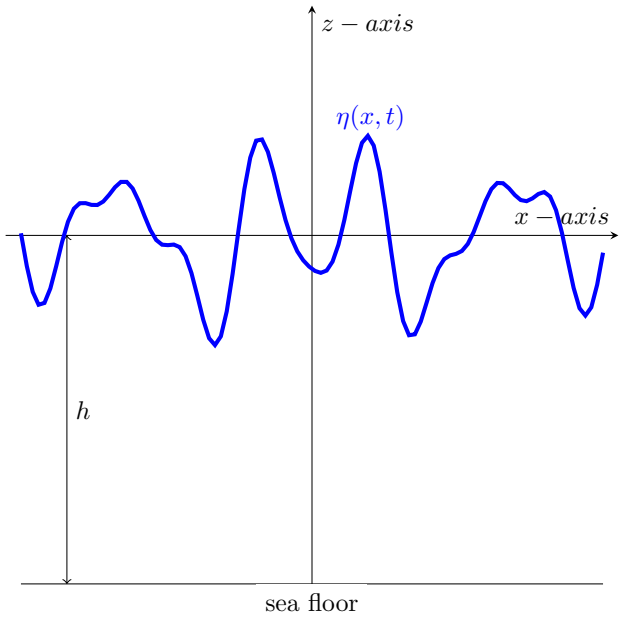

Figure 1.1: $\eta(x,t)$ is the surface elevation as measured from the x-axis which describes the profile of the sea surface, and h is the mean water depth.

conservation of mass equation is

$$\frac{\partial \rho}{\partial t} + \nabla \cdot (\rho \vec{v}) = 0 \tag{1.1.1}$$

and the conservation of momentum equation is

$$\frac{\partial \vec{v}}{\partial t} + (\vec{v} \cdot \nabla)\vec{v} = -\frac{1}{\rho}\nabla p + \vec{f} + \nu \nabla^2 \vec{v}. \tag{1.1.2}$$

From here we impose several conditions to adapt these equations to the physical situation of ocean waves. We assume that the density of the fluid, ρ, is constant in both space and time, and that the fluid is only undergoing irrotational motion. Because the motion is irrotational, $\nabla \times \vec{v} = \vec{0}$, there is a scalar-valued potential function ϕ that satisfies

$\vec{v} = \nabla\phi$. Thus (1.1.1) becomes

$$\nabla \cdot (\rho\nabla\phi) = \rho\nabla^2\phi = 0 \implies \nabla^2\phi = 0, \tag{1.1.3}$$

which is the Laplace equation.

We also neglect viscosity for this problem ($\nu = 0$) because we are considering surface gravity waves. Furthermore, because these are gravity waves we see that the only external force is due to gravity, g, and gravity only acts in the negative z direction for this problem. Thus, we can write $\vec{f} = \nabla(-gz)$. Combining this information with $\vec{v} = \nabla\phi$ equation (1.1.2) becomes

$$\nabla\frac{\partial\phi}{\partial t} + \nabla(\phi\nabla\phi) = -\frac{1}{\rho}\nabla p + \nabla(-gz),$$
$$\nabla\left[\frac{\partial\phi}{\partial t} + \phi\nabla\phi\right] = \nabla\left[-\frac{p}{\rho} - gz\right].$$

Integrating both sides with respect to the spatial variables and noting that $\nabla(\phi^2) = (\nabla\phi)\phi + \phi(\nabla\phi) = 2\phi\nabla\phi$ we have

$$\frac{\partial\phi}{\partial t} + \frac{1}{2}\nabla(\phi^2) = -\frac{p}{\rho} - gz + C(t),$$

where C is independent of the spatial variables but not independent of time. Shifting ϕ to $\hat{\phi}$, where

$$\hat{\phi} = \phi + \int_0^t \left[-\frac{p}{\rho} + C(\hat{t})\right] d\hat{t},$$

we see that $\hat{\phi}_t = -\frac{p}{\rho} + C(t)$, but the other terms in the equation stay the same. So by choosing a particular potential function we have at the top boundary

$$\frac{\partial\phi}{\partial t} + \frac{1}{2}\nabla(\phi^2) + g\eta = 0. \tag{1.1.4}$$

For the bottom interface, note that the normal vector is $-\vec{e}_z = - < 0, 0, 1 >$. The boundary at $z = -h$ is impermeable, so the velocity in the direction normal to that surface must be zero. In other words,

$$-(\vec{v} \cdot \vec{e}_z) = 0 \implies \nabla\phi \cdot \vec{e}_z = 0 \implies \phi_z = 0. \tag{1.1.5}$$

At the free surface S we have $S = \eta - z = 0$. In order to have the normal velocity of the surface match the normal velocity of the fluid we must have $S_t = 0$, or

$$\begin{aligned} \frac{1}{|\nabla S|}\frac{\partial S}{\partial t} + \frac{\nabla S}{|\nabla S|} \cdot \vec{v} &= 0, \\ \frac{\partial S}{\partial t} + \nabla S \cdot \vec{v} &= 0, \\ \frac{\partial S}{\partial t} + \nabla S \cdot \nabla\phi &= 0, \\ \eta_t + \phi_x\eta_x - \phi_z &= 0. \end{aligned}$$

Which brings us to the following differential equations and boundary conditions:

$$\begin{cases} \nabla^2\phi = 0 & -h < z < \eta, \\ \phi_z = 0 & \text{when } z = -h, \\ \eta_t + \eta_x\phi_x = \phi_z & \text{at } z = \eta, \\ \phi_t + \frac{1}{2}(\nabla\phi)^2 + g\eta = 0 & \text{at } z = \eta, \end{cases} \tag{1.1.6}$$

where ϕ is the potential function for the velocity, η is the surface elevation, and g is gravity.

The particular surface gravity waves we study have small amplitude relative to the depth of the waver and are slowly modulated. Let a be the size of the initial surface displacement and K the wavenumber of the carrier (or background) wave. The steepness of

the carrier wave with wavenumber K is aK. We require that the steepness is small, so we set $\epsilon = aK$, where $\epsilon \ll 1$. We also require that the modulation or change to the surface has a narrow bandwidth compared to the carrier wave. Finally, we concern ourselves only with deep water, so we assume $(Kh)^{-1} = \mathcal{O}(\epsilon)$.

Let θ be the phase of the carrier wave with complex amplitude A, where $\theta = kx - \omega t$. We expand the velocity potential, ϕ, and surface displacement, η as

$$\phi = \epsilon(A(\epsilon x, \epsilon t)e^{i\theta+kz} + A^*(\epsilon x, \epsilon t)e^{-i\theta+kz}) + \dots$$

$$\eta = \epsilon(B(\epsilon x, \epsilon t)e^{i\theta+kz} + B^*(\epsilon x, \epsilon t)e^{-i\theta+kz}) + \dots$$

Substituting these assumptions into (1.1.6) one finds the equations are not satisfied at each order unless the following conditions are met [9]:

$$\mathcal{O}(\epsilon\ ):\ \omega^2 = gk,$$
$$\mathcal{O}\left(\epsilon^2\right):\ \frac{\partial A}{\partial(\epsilon t)} + c_g\frac{\partial A}{\partial(\epsilon x)} = 0,$$

where c_g is the "group velocity" or the speed at which the wave envelope moves. The next order requires

$$\mathcal{O}\left(\epsilon^3\right):\ i\partial_t A + \partial_x^2 A + 2|A|^2 A = 0,$$

which is the equation that describes the complex amplitude of the surface. Renaming A to u we have the nonlinear Schrödinger equation equation (NLS),

$$iq_t + q_{xx} + 2|q|^2 q = 0, \tag{1.1.7}$$

where q is the complex wave envelope. is the leading order approximation to the wave dynamics which exhibit nonlinear focusing and modulational instability. The next several chapters will be devoted to examining the general background for the equation, including several types of solutions.

1.2 Lax pair, eigenvalue problem

The nonlinear Schrödinger equation is an integrable PDE [10] [11]. The Lax pair for (1.1.7) is

$$U(q,\lambda) \equiv \begin{bmatrix} -i\lambda & iq \\ iq^* & i\lambda \end{bmatrix} \qquad V(q,\lambda) \equiv \begin{bmatrix} i|q|^2 - 2i\lambda^2 & -q_x + 2i\lambda q \\ q_x^* + 2i\lambda q^* & -i|q|^2 + 2i\lambda^2 \end{bmatrix}, \tag{1.2.1}$$

where f^* indicates the complex conjugate of f.

The eigenfunction $\phi = [\phi_1, \phi_2]^T$ is a solution to the Lax pair if

$$\phi_x = U\phi \qquad \text{and} \qquad \phi_t = V\phi.$$

Lemma 1.2.1. *ϕ is continuously differentiable if, and only if, q is a solution of NLS* (1.1.7)*.*

Proof. We can write ϕ_{xt} and ϕ_{tx} as

$$\phi_{xt} = \frac{\partial}{\partial t}\left[\phi_x\right] = \frac{\partial}{\partial t}\left[U\phi\right] = U_t\phi + U\phi_t = (U_t + UV)\phi,$$
$$\phi_{tx} = \frac{\partial}{\partial x}\left[\phi_t\right] = \frac{\partial}{\partial x}\left[V\phi\right] = V_x\phi + V\phi_x = (V_x + VU)\phi,$$

so $\phi_{xt} = \phi_{tx}$ if, and only if $U_t - V_x = VU - UV$. In this case,

$$U_t - V_x = \begin{bmatrix} -i\left(qq_x^* + q^*q_x\right) & iq_t - 2i\lambda q_x + q_{xx} \\ iq_t^* - 2i\lambda q_x^* - q_{xx}^* & i\left(qq_x^* + u^*q_x\right) \end{bmatrix}$$

$$VU - UV = \begin{bmatrix} -i\left(qq_x^* + q^*q_x\right) & -2|q|^2q - 2i\lambda q_x \\ 2|q|^2q^* - 2i\lambda q_x^* & i\left(qq_x^* + q^*q_x\right) \end{bmatrix}$$

Noting that the elements on the diagonals are equal in the two matrices we see the equality of the off diagonal components reduces to $iq_t + q_{xx} + 2|q|^2q = 0$, and its conjugate. That is to say, $U_t - V_x = VU - UV$ if, and only if, q is a solution to (1.1.7). □

When u is a sufficiently simple solution, we can solve the system for ϕ directly. We begin by solving the temporal part of the Lax pair, specifically the eigenfunctions ϕ corresponding to the simplest solution to (1.1.7): the spatially independent plane-wave (Stokes wave) $q_a(x,t) = ae^{2ia^2t}$. In this case, $\phi_t = V\phi$ is

$$\begin{bmatrix} \phi_1 \\ \phi_2 \end{bmatrix}_t = \begin{bmatrix} ia^2 - 2i\lambda^2 & -2ia\lambda e^{2ia^2t} \\ -2ia\lambda e^{-2ia^2t} & -ia^2 + 2i\lambda^2 \end{bmatrix} \begin{bmatrix} \phi_1 \\ \phi_2 \end{bmatrix}. \tag{1.2.2}$$

Although this matrix is not time independent, it can be transformed into one that is. Let $\phi_1 = \hat{\phi}_1 e^{ia^2t}$ and $\phi_2 = \hat{\phi}_2 e^{-ia^2t}$. Then

$$(\phi_1)_t = (\hat{\phi}_1)_t e^{ia^2t} + ia^2\hat{\phi}_1 e^{ia^2t} \quad \text{and} \quad (\phi_2)_t = (\hat{\phi}_2)_t e^{-ia^2t} - ia^2\hat{\phi}_1 e^{-ia^2t}.$$

Substituting this into (1.2.2), the problem becomes

$$\begin{bmatrix} \hat{\phi}_1 \\ \hat{\phi}_2 \end{bmatrix}_t = \begin{bmatrix} -2i\lambda^2 & -2ia\lambda \\ -2ia\lambda & 2i\lambda^2 \end{bmatrix} \begin{bmatrix} \hat{\phi}_1 \\ \hat{\phi}_2 \end{bmatrix}. \tag{1.2.3}$$

This is a constant coefficient linear homogeneous system. The solution is of the form $\hat{\phi}_j = \chi_j e^{\mu t}$, where χ_j are constant in t (but not necessarily in x) and μ are the eigenvalues of the coefficient matrix.

$$\begin{vmatrix} -2i\lambda^2 - \mu & -2ia\lambda \\ -2ia\lambda & 2i\lambda^2 - \mu \end{vmatrix} = -(2i\lambda^2 + \mu)(2i\lambda^2 - \mu) - (-2ia\lambda)^2$$

$$= 4\lambda^4 + \mu^2 + 4\lambda^2 a^2.$$

Requiring the determinant to be zero and solving for μ, the eigenvalues are found to be

$$\mu_\pm = \pm\sqrt{-4\lambda^2(\lambda^2 + a^2)} = \pm 2i\lambda\sqrt{\lambda^2 + a^2} = \pm 2i\lambda k, \tag{1.2.4}$$

where

$$k \equiv \sqrt{\lambda^2 + a^2}. \tag{1.2.5}$$

So the solutions to (1.2.3) are

$$\hat{\phi}^\pm = \begin{bmatrix} \chi_1 e^{\mp 2i\lambda k t} \\ \chi_2 e^{\mp 2i\lambda k t} \end{bmatrix},$$

which implies that the solutions to (1.2.2) are

$$\phi^\pm = \begin{bmatrix} \chi_1 e^{ia^2 t} e^{\mp 2i\lambda k t} \\ \chi_2 e^{-ia^2 t} e^{\mp 2i\lambda k t} \end{bmatrix}. \tag{1.2.6}$$

where χ_i are independent of t but may depend on x.

Now we incorporate the spatial dependence of the eigenfunctions. Because U and V satisfy the Lax pair, solutions to the eigenvalue problem which involves the spatial part of

the Lax pair are time independent (or isospectral). Thus, if the eigenfunctions satisfy the spatial part of the Lax pair at $t = 0$, then they satisfy the spatial part of the Lax pair for all t.

Since $\phi(x,0) = [\chi_1, \chi_2]^T$, $u(x,0) = a$, and $u^*(x,0) = a$, the problem becomes

$$\begin{bmatrix} \chi_1 \\ \chi_2 \end{bmatrix}_x = \begin{bmatrix} -i\lambda & ia \\ ia & i\lambda \end{bmatrix} \begin{bmatrix} \chi_1 \\ \chi_2 \end{bmatrix}. \tag{1.2.7}$$

This is another constant coefficient linear homogeneous system. Assume the solution has the form $\chi_j = c_j e^{\mu x}$, where c_j is constant in both x and t. Substituting this into (1.2.7) yields

$$\begin{bmatrix} \chi_1 \\ \chi_2 \end{bmatrix}_x = \mu \begin{bmatrix} \chi_1 \\ \chi_2 \end{bmatrix} = \begin{bmatrix} -i\lambda & ia \\ ia & i\lambda \end{bmatrix} \begin{bmatrix} \chi_1 \\ \chi_2 \end{bmatrix} \quad \text{or,}$$

$$\begin{bmatrix} -i\lambda - \mu & ia \\ ia & i\lambda - \mu \end{bmatrix} \begin{bmatrix} \chi_1 \\ \chi_2 \end{bmatrix} = \begin{bmatrix} 0 \\ 0 \end{bmatrix}. \tag{1.2.8}$$

Calculating these new eigenvalues, note that

$$\begin{vmatrix} i\lambda - \mu & ia \\ ia & -i\lambda - \mu \end{vmatrix} = (i\lambda - \mu)(-i\lambda - \mu) - (ia)^2 = \lambda^2 + \mu^2 + a^2 = 0$$

Thus $\mu^2 = -(\lambda^2 + a^2)$ or $\mu_\pm = \pm i\sqrt{\lambda^2 + a^2} = \pm ik$, where k is defined as in (1.2.4). Thus $\chi_\pm$ are two linearly independent solutions of (1.2.8), where $\chi^+ = \vec{c}e^{ikx}$ and $\chi^- = \vec{c}e^{-ikx}$. In order for χ^+ to satisfy (1.2.7), c_1 and c_2 must satisfy

$$\begin{bmatrix} -i\lambda \mp ik & ia \\ ia & i\lambda \mp ik \end{bmatrix} \begin{bmatrix} c_1 \\ c_2 \end{bmatrix} = \begin{bmatrix} 0 \\ 0 \end{bmatrix} \implies \begin{bmatrix} \mp i(k \pm \lambda) & ia \\ ia & \mp i(k \mp \lambda) \end{bmatrix} \begin{bmatrix} c_1 \\ c_2 \end{bmatrix} = \begin{bmatrix} 0 \\ 0 \end{bmatrix}.$$

In other words,

$$c_2 = \frac{\pm(k \pm \lambda)}{a} c_1 = \frac{\pm a e^{\mp ip}}{a} c_1 = \pm e^{\mp ip} c_1,$$

Which gives us the eigenfunctions

$$\psi^{\pm}(\lambda) = \frac{i}{2k} e^{\mp i\frac{\pi}{4}} e^{\pm i\frac{p}{2}} \begin{bmatrix} a e^{ia^2 t} \\ \pm a e^{\mp ip} e^{-ia^2 t} \end{bmatrix} e^{\pm i(kx + 2k\lambda t)} \tag{1.2.9}$$

where the real value p is defined by

$$k \pm \lambda = a e^{\mp ip} \tag{1.2.10}$$

for any purely imaginary or purely real eigenvalue λ.

1.3 Linear Instability of the Stokes wave for NLS

In this section we show that the plane-wave is unstable for both the periodic and infinite line boundary conditions in x [10] [12].

Let q_s satisfy

$$i(q_s)_t + (q_s)_{xx} + 2\left(|q_s|^2 - a^2\right) q_s = 0 \tag{1.3.1}$$

and define $q(x,t) = q_s(x,t) + v(x,t)$, where v is a perturbation to the solution q_s. We are interested in the behavior of the perturbation. In order to claim u is stable, we must have that u stays near u_s. In other words, v cannot grow without bound. With this in mind, we want to analyze the behavior of the perturbation, v.

For (1.3.1), the constant amplitude solution is $u_s = a$, where $a > 0$. Beginning with this solution, we examine the perturbed solution $q(x,t) = a + v(x,t)$. Keeping only the first order terms in v we see that

$$\begin{aligned} q_t &= v_t, \\ q_{xx} &= v_{xx}, \\ \left(|q|^2 - a^2\right) u &= \left[(a+v)(a+v^*) - a^2\right] u \\ &= \left[a(v+v^*) + \mathcal{O}\left(v^2\right)\right](a+v) \\ &= a^2(v+v^*) + \mathcal{O}\left(v^2\right). \end{aligned}$$

Substituting the quantities into (1.3.1) we have linearized the equation about the solution a

$$iv_t + iv_{xx} + 2a^2(v+v^*) = 0. \tag{1.3.2}$$

To determine the behavior of v, we consider two related real-valued functions. Recall that for any $z \in \mathbb{C}$, $z + z^* = 2\,\mathrm{Re}(z)$ and $z - z^* = 2\,\mathrm{Im}(z)$, so if we define r and s as

$$r = v + v^*, \qquad\qquad is = v - v^*, \tag{1.3.3}$$

then we can reconstruct v as

$$v = \tfrac{1}{2}(r + is). \tag{1.3.4}$$

The linear differential equations that these functions satisfy is based on (1.3.2) and its complex conjugate. If we sum the equation and its conjugate, we arrive at

$$i(v_t - v_t^*) + v_{xx} + v_{xx}^* + 4a^2(v+v^*) = 0 \implies i(is_t) + r_{xx} + 4a^2 r = 0.$$

If we subtract the conjugate of (1.3.2) from the equation, we see that

$$i(v_t + v_t^*) + v_{xx} - v_{xx}^* = 0 \implies ir_t + is_{xx} = 0.$$

The two linear differential equations that define the relationship between r and s are

$$\begin{cases} s_t & -r_{xx} - 4a^2 r = 0, \\ r_t & +s_{xx} = 0. \end{cases} \tag{1.3.5}$$

Next, we assume that r and s have Fourier series expansions in x and take the series expansion of both equations.

For the purposes of this section, we define the Fourier Transform of a function f on a domain D as $\widehat{f}$, where

$$\begin{aligned} \widehat{f}(k) &= \mathcal{F}_k[f] = \int_D e^{-ikx} f(x)\, dx, \\ f(x) &= \mathcal{F}_x^{-1}[f] = \frac{1}{2\pi} \int_D e^{ikx} \widehat{f}(k)\, dk. \end{aligned}$$

These are spatial transforms, so the temporal information is not being altered by the transformation. Note that

$$\begin{aligned} \mathcal{F}[f_{xx}] &= \int_D e^{-ikx} f_{xx}(x)\, dx \\ &= \left[e^{-ikx} f_{xx}(x)\right] \Big|_D + ik \int_D e^{-ikx} f_x(x)\, dx \\ &= \left[e^{-ikx} f_x(x) + ikf\right] \Big|_D - k^2 \int_D e^{-ikx} f(x)\, dx \\ &= -k^2 \widehat{f}, \end{aligned} \tag{1.3.6}$$

given appropriate boundary conditions that the boundary terms are zero. In the context of this problem we consider periodic boundary conditions in section 1.3.1 and infinite line boundary conditions in 1.3.2.

We can now transform the system (1.3.5) into

$$\begin{cases} \widehat{s}_t &= -(k^2 - 4a^2)\widehat{r} \\ \widehat{r}_t &= k^2\widehat{s} \end{cases} \implies \begin{bmatrix} \widehat{r}_t \\ \widehat{s}_t \end{bmatrix} = \begin{bmatrix} 0 & k^2 \\ -k^2 + 4a^2 & 0 \end{bmatrix} \begin{bmatrix} \widehat{r} \\ \widehat{s} \end{bmatrix}.$$

This defines an autonomous (no explicit dependence on time in the coefficients) system of first order differential equations. We seek solutions of the form $\exp(i\Omega t)$, which allows us to transform the system into an eigenvalue problem in terms of Ω. To have linearly independent solutions $\widehat{r}$ and $\widehat{s}$ we must have that the following determinant is zero:

$$\begin{vmatrix} -i\Omega & k^2 \\ -k^2 + 4a^2 & -i\Omega \end{vmatrix} = -\Omega^2 - k^2(-k^2 + 4a^2) = 0$$

$$\implies \Omega^2 = -k^2(4a^2 - k^2)$$

$$\Omega = \pm ik\sqrt{4a^2 - k^2}. \tag{1.3.7}$$

Note that when Ω is real, the solutions to $e^{i\Omega t}$ are periodic functions, but when Ω is imaginary, $e^{i\Omega t}$ grows without bound for either $t \to \infty$ or $t \to -\infty$. Since $k \in \mathbb{R}$, the only way for $\Omega \notin \mathbb{R}$ is if it is purely imaginary, which occurs when $\sqrt{4a^2 - k^2} \in \mathbb{R}$. This is only possible when

$$4a^2 - k^2 > 0 \implies -2a < k < 2a.$$

Finally, we determine which wavenumber k results in the largest growth rate by determining the maximum $|\Omega(k)|$ when $\Omega \notin \mathbb{R}$. In this case,

$$\Omega_k = \sqrt{k^2 - 4a^2} + k^2(k^2 - 4a^2)^{-1/2} = \frac{2k^2 - 4a^2}{\sqrt{k^2 - 4a^2}} = \frac{2(k^2 - 2a^2)}{\sqrt{k^2 - 4a^2}},$$

which is zero when $k = \pm\sqrt{2}a$, with $|\Omega(\pm\sqrt{2}a)| = 2a^2$, so the maximum growth rate of the system is $\exp(2a^2t)$.

The work in this section allows us to conclude that for $a > 0$ there are potentially wavenumbers where the constant amplitude solution is unstable in time.

1.3.1 Periodic spatial interval

In this subsection we will confirm (1.3.6) and which wave numbers leave to instabilities in the case where q is periodic in space. Note that if a function is periodic with period L, then its derivatives are also periodic with period L. If $u = u_s + v$ is periodic, then v is also periodic. Furthermore, since r and s are multiples of the real and imaginary components of the perturbation, v, they are also periodic.

Furthermore, if $f(x)$ is periodic, so is $f'(x)$ since

$$f'(x + L) = \lim_{h \to 0} \frac{f(x + L + h) - f(x + L)}{h} = \lim_{h \to 0} \frac{f(x + h) - f(x)}{h} = f'(x).$$

In this case, $u(x + L, t) = u(x, t)$ and thus $u_x(x + L, t) = u_x(x, t)$, so the conditions in (1.3.6) are

$$\left[e^{-ikx} r_x(x, t) + ikr(x, t)\right] \Big|_0^L = e^{-ikL} r_x(L, t) + ikr(L, t) - r_x(0, t) - ikr(0, t)$$

$$= e^{-ikL} r_x(L,t) - r_x(0,t) = 0,$$

if, and only if, $k = 2j\pi/L$ where j is an integer. Under the same conditions on k,

$$\begin{aligned}\left[e^{-ikx} s_x(x,t) + iks(x,t)\right]\Big|_0^L &= e^{-ikL} s_x(L,t) + iks(L,t) - s_x(0,t) - iks(0,t) \\ &= e^{-ikL} s_x(L,t) - s_x(0,t) = 0.\end{aligned}$$

Combining this with the conclusion that the solution is unstable when $-2a < k < 2a$, we conclude that

$$-2a < \frac{2j\pi}{L} < 2a \implies -\frac{aL}{\pi} < j < \frac{aL}{\pi}. \tag{1.3.8}$$

The combined requirements that j is an integer and j satisfy (1.3.8) mean that there are a finite number of nonnegative j values (and thus modes in the Fourier expansion) that are unstable for a fixed pair of a and L.

1.3.2 Infinite spatial interval

In this subsection we examine which wavenumbers lead to instability in the case where u decays to a as $x \to \pm\infty$. Since v is the perturbation from the constant background state, in this case, $v \to 0$ as $x \to \pm\infty$. Since r and s are the real and imaginary components of v, respectively, then we also have that r and s decay to 0 as $x \to \pm\infty$, and their derivatives also go to 0 as $x \to \pm\infty$.

Hence, (1.3.6) becomes

$$\left[e^{-ikx}r_x(x,t) + ikr(x,t)\right]\Big|_{-\infty}^{\infty} = 0,$$
$$\left[e^{-ikx}s_x(x,t) + iks(x,t)\right]\Big|_{-\infty}^{\infty} = 0.$$

The wave numbers $-2a < k < 2a$ correspond to unbounded growth of the perturbation in the infinite line case.

1.4 Periodic spectral theory

If we impose periodic boundary conditions we can determine the conditions under which the plane wave is unstable in terms of the Floquet spectral theory of the NLS equation [13].

Defining the spectrum of the spatial part of the Lax pair as the set of eigenvalues for which the eigenvector remains bounded for all x, i.e.

$$\sigma = \left\{ \lambda \in \mathbb{C} \;\middle|\; L\vec{v} = 0,\ |\vec{v}| \text{ bounded } \forall x \right\}.$$

We calculate the fundamental matrix $\Phi(x; x_0, \lambda)$, where if $\vec{c} \in \mathbb{R}^2$ is a vector of arbitrary constants, any solution of $\phi_x = U\phi$ can be written as $\Phi\vec{c}$ and $\det\{\Phi\} = 1$. Note that because of the structure of the fundamental matrix, the chosen base point, x_0, does not change the determinant, i.e. $\det[\Phi(x; \widehat{x}_0, \lambda)] = \det[\Phi(x; x_0, \lambda)]$ [14], so we will use $x_0 = 0$.

We define the Monodromy matrix as

$$M(\lambda) = \Phi(L; 0, \lambda), \tag{1.4.1}$$

and the Floquet discriminant as

$$\Delta = \mathrm{tr}[M(\lambda)]. \tag{1.4.2}$$

The condition that the eigenvector is bounded for all x can be defined in terms of Δ as

$$\sigma = \left\{ \lambda \in \mathbb{C} \;\middle|\; \Delta(u,\lambda) \in \mathbb{R},\, -2 \leq \Delta(u,\lambda) \leq 2 \right\}. \tag{1.4.3}$$

The continuous spectrum of curves in the complex plane, of particular interest is the discrete periodic/antiperiodic spectrum composed of simple points of the spectrum, σ^s, and double points of the spectrum, σ^d. These sets are countable and defined as

$$\sigma^s = \left\{ \lambda_j^s \;\middle|\; \Delta(u,\lambda) = \pm 2,\, \frac{d\Delta}{d\lambda} \neq 0 \right\}, \tag{1.4.4}$$

$$\sigma^d = \left\{ \lambda_j^d \;\middle|\; \Delta(u,\lambda) = \pm 2,\, \frac{d\Delta}{d\lambda} = 0,\, \frac{d^2\Delta}{d\lambda^2} \neq 0 \right\}. \tag{1.4.5}$$

The remainder of this section uses this methodology to determine the spectrum for the plane-wave.

The plane wave, q_a, is isospectral, meaning the spectrum does not change as the solution evolves. Assume the solution ϕ of $\phi_x = U(q_a(0))\phi$ has the form $\phi = \vec{c}e^{\mu x}$. Substituting this assumption into the equation we arrive at

$$\frac{\partial}{\partial x}\begin{bmatrix} \phi_1 \\ \\ \phi_2 \end{bmatrix} = \mu \begin{bmatrix} \phi_1 \\ \\ \phi_2 \end{bmatrix} = \begin{bmatrix} -i\lambda & ia \\ \\ ia & i\lambda \end{bmatrix} \begin{bmatrix} \phi_1 \\ \\ \phi_2 \end{bmatrix} \quad \text{or,}$$

$$\mu \vec{c} e^{\mu x} = A \vec{c} e^{\mu x}.$$

We have turned this into another eigenvalue problem, this one in terms of μ. First calculating these new eigenvalues, we note that

$$\begin{vmatrix} -i\lambda-\mu & ia \\ ia & i\lambda-\mu \end{vmatrix} = (-i\lambda-\mu)(i\lambda-\mu)-(ia)^2 = \lambda^2+\mu^2+a^2 = 0.$$

Thus $\mu^2 = -(\lambda^2+a^2)$ or $\mu_\pm = \pm i\sqrt{\lambda^2+a^2}$. The form of the two linearly independent solutions are $\phi^+ = \vec{c}e^{\mu_+ x}$ and $\phi^- = \vec{c}e^{\mu_- x}$. So we have that

$$\begin{bmatrix} -i\lambda-\mu_\pm & ia \\ ia & i\lambda-\mu_\pm \end{bmatrix}\begin{bmatrix} c_1 \\ c_2 \end{bmatrix} = 0, \text{ i.e., } c_2 = \frac{(-i\lambda-\mu_\pm)}{ia}c_1.$$

If we choose $c_1 = ia$, then our eigenvectors are

$$\phi^+ = \begin{bmatrix} 1 \\ (-i\lambda-\mu_+) \end{bmatrix}e^{\mu_+ x}, \qquad \phi^- = \begin{bmatrix} 1 \\ (-i\lambda-\mu_-) \end{bmatrix}e^{\mu_- x},$$

which we can represent in matrix form as

$$\begin{bmatrix} iae^{\mu_+ x} & iae^{\mu_- x} \\ (-i\lambda-\mu_+)e^{\mu_+ x} & (-i\lambda-\mu_-)e^{\mu_- x} \end{bmatrix} A = \begin{bmatrix} iae^{\mu x} & iae^{-\mu x} \\ (-i\lambda-\mu)e^{\mu x} & (-i\lambda+\mu)e^{-\mu x} \end{bmatrix} A \equiv \psi A.$$

Since $\mu_- = -\mu_+$ we have simplified the expression by defining $\mu = \mu_+$

If we now consider the solution vector $\vec{x}$, with $\vec{x} = \psi\vec{c}$, where $\vec{c} \in \mathbb{R}^2$ is constant in time, then $\vec{x}(0) = \psi(0)\vec{c}$. We see that we can solve for $\vec{c}$ uniquely, if $\psi(0)$ is invertible. We see that $|\psi| = 2ia\mu$ for all x, thus $\phi(0)$ is invertible for $\mu \neq 0$. Referring back to our definition of μ we see that we require $\lambda \neq \pm ia$. Supposing this criteria has been satisfied, we have $\vec{c} = \psi^{-1}(0)\vec{x}(0)$ thus for any $\vec{x}$ we can write

$$\vec{x} = \psi\psi^{-1}(0)\vec{x}(0) = \Phi\vec{x_0},$$

where

$$\psi(0) = \begin{bmatrix} ia & ia \\ (-i\lambda - \mu) & (-i\lambda + \mu) \end{bmatrix} \text{ so that } \psi^{-1}(0) = \frac{1}{2ia\mu} \begin{bmatrix} (-i\lambda + \mu) & -ia \\ (i\lambda + \mu) & ia \end{bmatrix},$$

and finally, we have our solution $\phi = \Phi\vec{c}$, where $\vec{p}$ is composed of arbitrary constants, and

$$\begin{aligned}
\Phi &= \frac{1}{2ia\mu} \begin{bmatrix} ia(-i\lambda + \mu)e^{\mu x} + ia(i\lambda + \mu)e^{-\mu x} & ia(-ia)e^{\mu x} + ia(ia)e^{-\mu x} \\ -(i\lambda + \mu)(-i\lambda + \mu)e^{\mu x} + (i\lambda + \mu)(-i\lambda + \mu)e^{-\mu x} & ia(i\lambda + \mu)e^{\mu x} + ia(-i\lambda + \mu)e^{-\mu x} \end{bmatrix} \\
&= \frac{1}{2ia\mu} \begin{bmatrix} ia(-i\lambda + \mu)e^{\mu x} + ia(i\lambda + \mu)e^{-\mu x} & ia(-ia)e^{\mu x} + ia(ia)e^{-\mu x} \\ ia(-ia)(e^{\mu x} - e^{-\mu x}) & ia(i\lambda + \mu)e^{\mu x} + ia(-i\lambda + \mu)e^{-\mu x} \end{bmatrix} \\
&= \frac{1}{2\mu} \begin{bmatrix} -i\lambda(e^{\mu x} - e^{-\mu x}) + \mu(e^{\mu x} + e^{-\mu x}) & (-ia)(e^{\mu x} - e^{-\mu x}) \\ (-ia)(e^{\mu x} - e^{-\mu x}) & i\lambda(e^{\mu x} - e^{-\mu x}) + \mu(e^{\mu x} + e^{-\mu x}) \end{bmatrix}.
\end{aligned}$$

Recall that $2\cos(\theta) = (e^{\theta} + e^{-\theta})$ and $2i\sin(\theta) = (e^{\theta} - e^{-\theta})$ for $\theta \in \mathbb{R}$ so if we define $\tilde{\mu} = i\mu$ we have

$$\begin{aligned}
\Phi &= \frac{1}{2\mu} \begin{bmatrix} 2\lambda\sin(\tilde{\mu}x) + 2\mu\cos(\tilde{\mu}x) & 2a\sin(\tilde{\mu}x) \\ 2a\sin(\tilde{\mu}x) & -2\lambda\sin(\tilde{\mu}x) + 2\mu\cos(\tilde{\mu}x) \end{bmatrix} \\
&= \frac{1}{\mu} \begin{bmatrix} \lambda\sin(\tilde{\mu}x) + \mu\cos(\tilde{\mu}x) & a\sin(\tilde{\mu}x) \\ a\sin(\tilde{\mu}x) & -\lambda\sin(\tilde{\mu}x) + \mu\cos(\tilde{\mu}x) \end{bmatrix}.
\end{aligned}$$

Finding the trace of Φ to eventually find the Monodromy matrix, we have

$$\begin{aligned}
\mathrm{tr}\Phi &= \frac{1}{\mu}\Big(\lambda\sin(\tilde{\mu}x) + \mu\cos(\tilde{\mu}x) - \lambda\sin(\tilde{\mu}x) + \mu\cos(\tilde{\mu}x)\Big) \\
&= -\frac{a}{2\mu}\left(2\mu\cos(\tilde{\mu}x)\right) = 2\cos(\tilde{\mu}x).
\end{aligned}$$

For the plane wave, we find that $\Delta = 2\cos(\sqrt{\lambda^2 + a^2}L)$. Since $|\cos(x)| \leq 1$ for $x \in \mathbb{R}$, so we require $\sqrt{\lambda^2 + a^2} \in \mathbb{R}$, which occurs when $\lambda \in \mathbb{R}$ and on the imaginary axis $\lambda \in [-ia, ia]$.

Taking derivatives with respect to λ we find

$$\frac{d\Delta}{d\lambda} = -2L\lambda \frac{\sin\left(L\sqrt{a^2+\lambda^2}\right)}{\sqrt{a^2+\lambda^2}}, \tag{1.4.6}$$

$$\frac{d^2\Delta}{d\lambda^2} = -\frac{2L^2\lambda^2\cos\left(L\sqrt{a^2+\lambda^2}\right)}{a^2+\lambda^2} + \frac{2L\lambda^2\sin\left(L\sqrt{a^2+\lambda^2}\right)}{(a^2+\lambda^2)^{3/2}} - \frac{2L\sin\left(L\sqrt{a^2+\lambda^2}\right)}{\sqrt{a^2+\lambda^2}}. \tag{1.4.7}$$

Setting (1.4.6) to 0, we find for $\lambda \neq 0$

$$\begin{aligned} \sin(L\sqrt{a^2+\lambda^2}) = 0 &\implies L\sqrt{a^2+\lambda^2} = j\pi \text{ for } j \in \mathbb{Z}^+ \\ &\implies a^2+\lambda^2 = \left(\frac{j\pi}{L}\right)^2 \\ &\implies \lambda^2 = \left(\frac{j\pi}{L}\right)^2 - a^2. \end{aligned} \tag{1.4.8}$$

We see that for eigenvalues where $d\Delta/d\lambda = 0$ and $\lambda \neq 0$,

$$\frac{d^2\Delta}{d\lambda^2} = -\frac{2\left((j\pi)^2 - (aL)^2\right)\cos(j\pi)}{\left(\frac{j\pi}{L}\right)^2} = (-1)^{j+1}2L^2\frac{\left((j\pi)^2 - (aL)^2\right)}{(j\pi)^2}$$

which is nonzero for $\lambda \neq 0$. Thus λ_j^d have algebraic multiplicity exactly 2.

For the plane wave, the single points are the endpoints of continuous bands of spectrum. In the case of the plane wave, $\sigma^s = \{-ia, ia\}$. The double points are discrete points embedded in continuous spectrum. In the case of the plane wave, there are infinitely many on the real axis, and N on the imaginary axis, where $\sqrt{\lambda^2 + a^2} = j\pi/L$ and $N = \lfloor aL/\pi \rfloor$.

An example of the spectrum for $L = 4\sqrt{2}\pi$ and $a = .5$ is shown in Figure 1.2. Notice that there are two double points on the positive imaginary axis (denoted with an "x") and

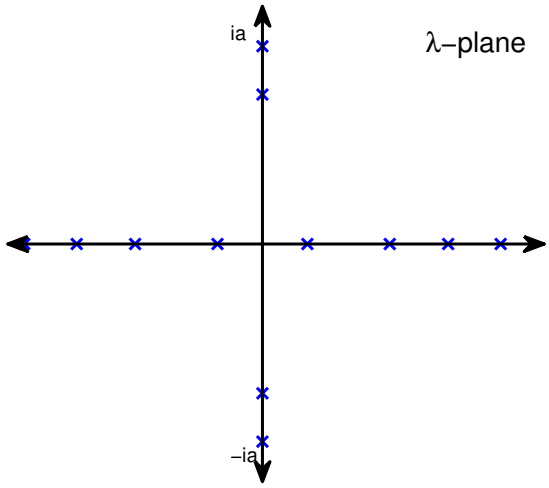

Figure 1.2: The spectrum of the plane wave with $L = 4\sqrt{2}\pi$ and $a = .5$. Double points are indicated by crossess. The simple points of the spectrum are not denoted in this figure.

$N = \lfloor aL/\pi \rfloor = \lfloor 2\sqrt{2} \rfloor \approx \lfloor 2.83 \rfloor = 2$. As L increases, the number of complex double points increases. Figure 1.3 shows the spectrum with $N = 3$ and $N = 4$ on the left and right, respectively. For a fixed amplitude, the number of double points on the imaginary axis increases as L increases. The simple points of the spectrum are not denoted in this figure.

In Figure 1.3 we see that as the length of the spatial period increases (and thus N increases) for a fixed a more double points move onto the imaginary axis and they also move up the imaginary axis closer to ia and $-ia$. For very large L the imaginary axis is densely covered in complex double points.

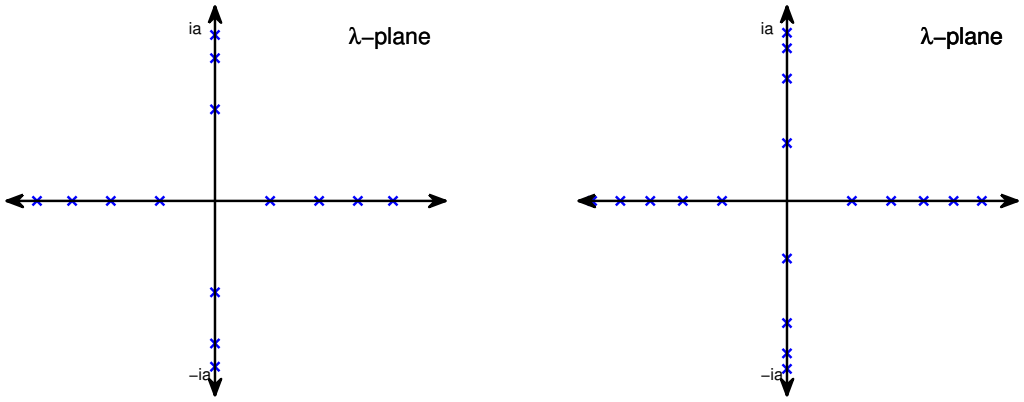

Figure 1.3: The spectrum of the plane wave with $a = .5$ and $L = 5\sqrt{2}\pi$ (left) and $a = .5$ with $L = 6\sqrt{2}\pi$ (right). Double points are indicated by crossess. The simple points of the spectrum are not denoted in this figure.

1.5 Models for rogue waves in NLS

Rogue waves are anomalously large waves. To better define "large" we look to the strength of the wave, which compares the amplitude of the wave at a given point to the other waves occurring at the same time.

The significant wave height (SWH), $H_s(t)$, is is 4 times the standard deviation of the amplitude of the surface at time t. The maximum amplitude is $U_{\max} = \max_{x \in D} |u(x,t)|$. The ratio of these quantities is defined the strength of the waves,

$$S(t) = \frac{U_{\max}(t)}{H_s(t)}. \tag{1.5.1}$$

If $S(t^*) > 2.2$, a rogue wave occurs at time t^*. Depending on the method of calculating the SWH, some researchers use criteria as low as a strength of 1.8 to determine rogue waves.

For a solution u of (1.1.7) on spatial domain D, we define the amplification factor as

$$A_f = \frac{\max\limits_{x\in D, t\in\mathbb{R}} |u(x,t)|}{\lim\limits_{t\to\pm\infty} |u(x,t)|}. \tag{1.5.2}$$

In the case of an analytical solution, we can use the amplification factor to quantify the extent of the growth of the instabilities that solution permits to compare to other solutions. The amplification factor has been used to quantify an analytical solution as a model for rogue waves.

Although the plane wave is a solution to NLS it is not a candidate for a rogue wave solution because it does not have the features we know rogue waves possess from real-world observation. In this section we discuss two classes of solutions commonly used as models for rogue waves: the spatially periodic breathers and the rational solutions.

1.5.1 Single mode spatially periodic breathers

Breather-type solutions of NLS are commonly used to model rogue wave behavior (see, for example [15], [16], [17], [18]) because they have many of the desired features of rogue waves. The single mode spatially periodic breather is a single-parameter solution that "breathes" only once in time. The solution was discovered independently by Akhmediev *et al.* in 1987 and Ablowitz and Herbst in 1990 [15].

The spatially periodic breather is obtained in section 2.2 by applying the Bäklund transformation to an unstable plane-wave with amplitude a and spatial period L. Recall

from section 1.2 that such a solution has M unstable modes, where $M = \lfloor aL/\pi \rfloor$ is the largest integer less than or equal to aL/π. The formula for the single mode SPB associated with the j-th UM of the plane-wave (for $1 \leq j \leq M$) is

$$U^{(j)}(x,t) = ae^{i(2a^2t+\phi)} \frac{\cos 2p_j - \sin p_j \operatorname{sech}(\rho - \sigma_j t)\cos(2\pi jx/L + \alpha) + i \sin 2p_j \tanh(\rho - \sigma_j t)}{1 + \sin p_j \operatorname{sech}(\rho - \sigma_j t)\cos(2\pi jx/L + \alpha)}, \tag{1.5.3}$$

where $\cos p_j = \pi j/aL$ and ρ and α are real phase parameters for time and space, respectively, $k_j = \pi j/L$, and $\sigma_j = 2k_j\sqrt{a^2 - k_j^2}$.

Note that as $t \to \infty$, $\operatorname{sech}(\rho - \sigma_j t) \to 0$ and $\tanh(\rho - \sigma_j t) \to -1$, and

$$U^{(j)}(x,t) \to ae^{i(2a^2t+\phi)}\left(\cos 2p_j - i \sin 2p_j\right) = ae^{i(2a^2t+\phi)}e^{-2ip_j} = ae^{i(2a^2t+\phi-2p_j)}.$$

Similarly, as $t \to -\infty$, $U^{(j)}(x,t) \to ae^{i(2a^2t+\phi+2p_j)}$. Thus the breather decays to the original plane wave that has a different phase shift. So the breather is localized in time and periodic in space.

Figure 1.4 shows the amplitude of the single mode SPB, $U^{(1)}(x,t;\rho)$, over the plane wave with one UM for $a = .5$ and $L = 2\sqrt{2\pi}$. The figure shows that the amplitude of the solution is decaying exponentially quickly to the amplitude of the original plane-wave, $a = .5$. The amplification factor of the amplitude for $U^{(1)}(x,t;\rho)$ in the figure, as defined in (1.5.2) is $A_f \approx 2.4$.

The single mode SPB retains the same structure for various L, but as L increases the number of unstable modes in the underlying plane-wave increases. This causes $2\pi j/L$ to decrease, and allows the amplification factor to increase to $A_{f,\max} \approx 3.1$.

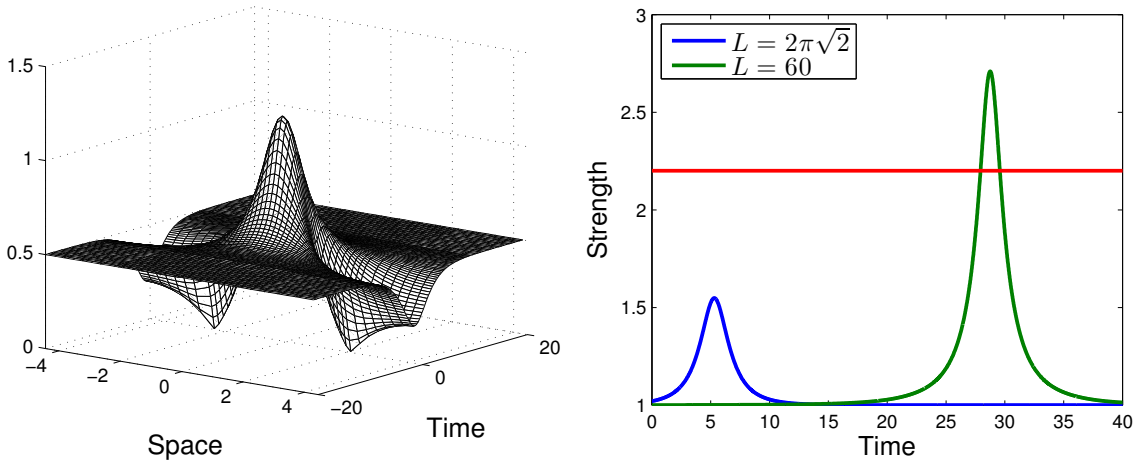

Figure 1.4: (a) Amplitude of the single mode SPB $U^{(1)}(x,t;\rho)$ over an unstable plane wave with one UM: $a = 0.5$, $L = 2\sqrt{2}\pi$. Strength of $|U^{(1)}(x,t;-3)|$ with $a = .5$ for $L = 2\sqrt{2}\pi$, and $L = 60$.

If we calculate the strength (1.5.1) of the single mode SPB for a fixed amplitude but different interval lengths, we see that the strength increases as L increases. Based on the criteria that $S(t^*) > 2.2$, the growth of the solution for $L = 2\sqrt{2}\pi$ does not constitute a rogue wave, whereas the solution for $L = 60$ does satisfy the criteria for a rogue wave.

1.5.2 Two mode spatially periodic breathers

We can generate a higher-order spatially periodic breather by iterating the Bäklund transformation at a second double point of the periodic spectrum (see Chapter 2). Once there are two unstable modes the separation in time of the two has a considerable impact on the overall strength and steepness of the solution.

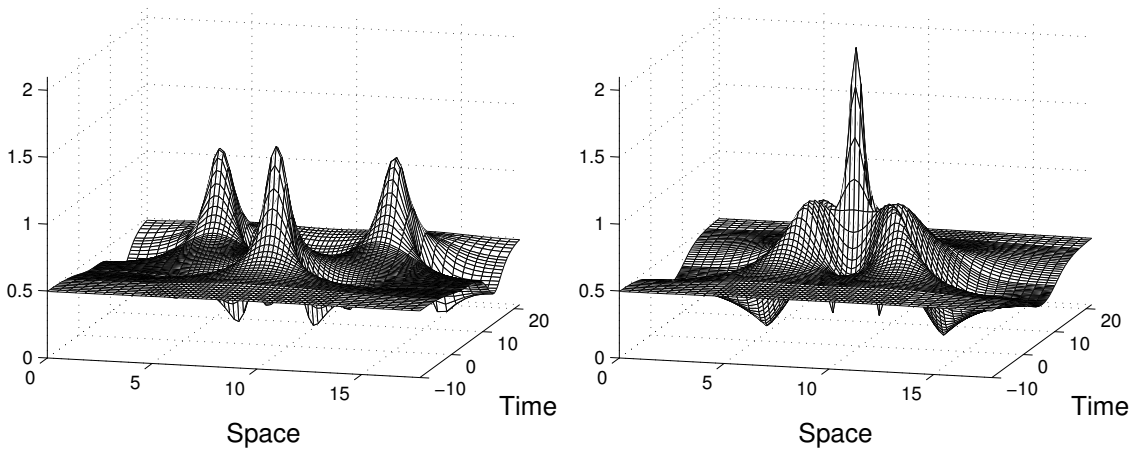

Figure 1.5: The amplitude of $U^{(1,2)}(x,t;-2,\tau)$ with $a=.5$, $L=4\sqrt{2}\pi$, where (a) the modes are well separated ($\tau=-6$), and (b) the modes are coalesced ($\tau=-3$).

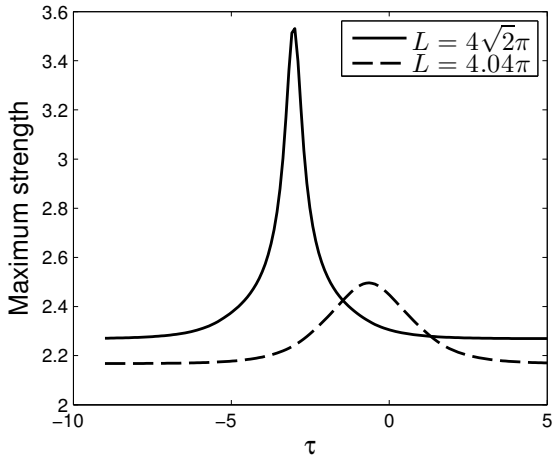

Figure 1.6: Plots of the maximum strength of $U^{(1,2)}(x,t;-2,\tau)$, as a function of τ with $a=.5$, $L=4\sqrt{2}\pi$ [solid line], and $L=4(1+.01)\pi$ [dashed line].

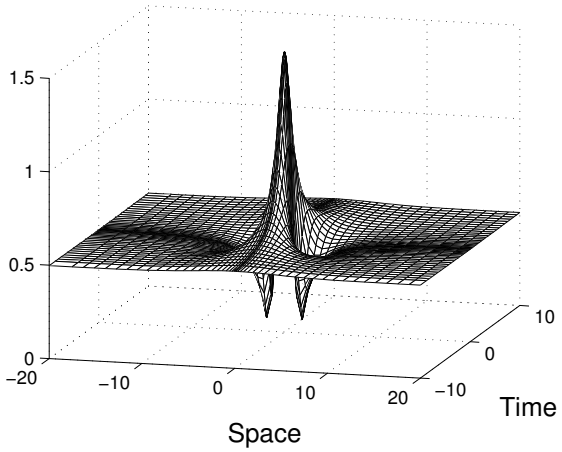

Figure 1.7: The amplitude of $U_P(x,t)$ with $a = .5$, on the region $-10 \leq x \leq 10$ $-20 \leq t \leq 20$.

1.5.3 Peregrine solution

The Peregrine solution

$$u_P(x,t) = ae^{2ia^2t+\gamma}\left(-1 + \frac{16ia^2t+4}{4a^2x^2+16a^4t^2+1}\right), \tag{1.5.4}$$

which is the lowest-order rational solution of the NLS on the infinite line. The Peregrine solution was first derived as taking the temporal period of the Ma soliton to be infinitely large [19], [18], or by taking the spatial period of the spatially periodic breather to be infinitely large [20]. We will only discuss this rational solution in this dissertation, so the phrase "rational solution" will be specifically the Peregrine solution.

Because the solution does not depend on a spatial period, neither does the strength nor the amplification factor of the solution.

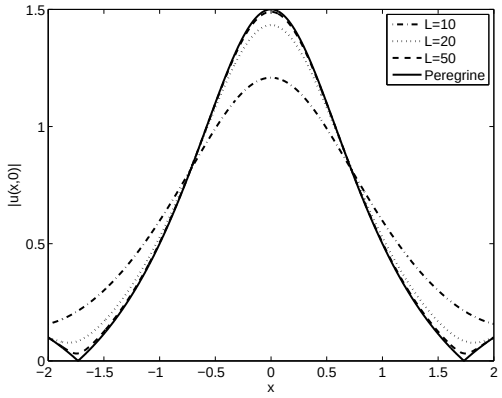

Figure 1.8: Comparison of the single-mode SPB solution for various L to the Peregrine solution at $t = 0$ where $a = .5$ in all cases.

For $\gamma = 0$ the maximum of u_P occurs at $x = t = 0$, which is $u_P(0, 0) = 3a$. Also note that as $t \to \pm\infty$, $u_P \to ae^{2ia^2t+\gamma+i\pi}$, so $A_f = 3$ regardless of the amplitude of the underlying plane-wave.

In Figure 1.8 we see a comparison of the amplitude of the Peregrine solution compared to some spatially periodic breathers for different periods. Even though the amplitude of the underlying plane wave is the same for all four curves, the maximum amplitude is much higher for the Peregrine than for the SPB on a small period. We see that at L increases, however, the single-mode SPB solution becomes closer to the Peregrine solution. In fact, the curve for the $L = 50$ SPB is nearly indistinguishable from that of the Peregrine away from the maximum and minimum points.

CHAPTER 2

CONSTRUCTING THE SPB AND RATIONAL SOLUTIONS

2.1 Bäklund-Gauge transformation for the NLS equation

We derive the Bäklund transformation (BT) by changing the scattering problem into a pair of Riccati equations following the work of [21]. The BT transforms a known solution q with eigenvectors $\phi^{\pm}$ of a Lax pair into another solution, Q. Using the Lax pair (1.2.1) we can write two systems of equations for the components ϕ_i of the eigenfunction $\vec{\phi}$. Beginning with the spatial part we have

$$\begin{cases} \phi_{1x} &= -i\lambda\phi_1 + iq\phi_2 \\ \phi_{2x} &= iq^*\phi_1 + i\lambda\phi_2 \end{cases} \Longrightarrow \begin{cases} \phi_{1x}\phi_2 &= -i\lambda\phi_1\phi_2 + iq\phi_2^2 \\ \phi_1\phi_{2x} &= iq^*\phi_1^2 + i\lambda\phi_1\phi_2 \end{cases}.$$

Subtracting the second equation from the first we have

$$\phi_{1x}\phi_2 - \phi_1\phi_{2x} = -2i\lambda\phi_1\phi_2 + iq\phi_2^2 - iq^*\phi_1^2$$

and scaling by ϕ_2^2 yields

$$\frac{\phi_{1x}\phi_2 - \phi_1\phi_{2x}}{\phi_2^2} = -2i\lambda\frac{\phi_1}{\phi_2} + iq - iq^*\left(\frac{\phi_1}{\phi_2}\right)^2. \tag{2.1.1}$$

Similarly, if we let $V_{11} = -2i\lambda^2 + i|q|^2$, $V_{12} = -q_x + 2i\lambda q$, and $V_{21} = q_x^* + 2i\lambda q^*$, then the temporal part of the Lax pair gives us the system of equations

$$\begin{cases} \phi_{1t} &= V_{11}\phi_1 + V_{12}\phi_2 \\ \phi_{2t} &= V_{21}\phi_1 - V_{11}\phi_2 \end{cases} \implies \begin{cases} \phi_{1t}\phi_2 &= V_{11}\phi_1\phi_2 + V_{12}\phi_2^2 \\ \phi_1\phi_{2t} &= V_{21}\phi_1^2 - V_{11}\phi_1\phi_2 \end{cases}.$$

Subtracting the second equation from the first we have

$$\phi_{1t}\phi_2 - \phi_1\phi_{2t} = 2V_{11}\phi_1\phi_2 + V_{12}\phi_2^2 - V_{21}\phi_1^2$$

and scaling by ϕ_2^2 yields

$$\frac{\phi_{1t}\phi_2 - \phi_1\phi_{2t}}{\phi_2^2} = 2V_{11}\frac{\phi_1}{\phi_2} + V_{12} - V_{21}\left(\frac{\phi_1}{\phi_2}\right)^2. \tag{2.1.2}$$

Let $\xi = \phi_1/\phi_2$, then

$$\xi_x = \frac{d}{dx}\left[\frac{\phi_1}{\phi_2}\right] = \frac{\phi_{1x}\phi_2 - \phi_1\phi_{2x}}{\phi_2^2} \qquad \text{and} \qquad \xi_t = \frac{\phi_{1t}\phi_2 - \phi_1\phi_{2t}}{\phi_2^2}.$$

With this definition we can write (2.1.1) and (2.1.2) as

$$\begin{aligned} \xi_x &= iq - 2i\lambda\xi - iq^*\xi^2, \\ \xi_t &= V_{12} + 2V_{11}\xi - V_{21}\xi^2, \end{aligned} \tag{2.1.3}$$

thus the ratio of the components of any eigenfunction with potential q and eigenvalue λ must satisfy both of these Riccati equations.

We seek a new potential and a new eigenfunction based on the current ones. Let

$$\hat{\xi} = -\frac{1}{\xi^*} \qquad \text{and} \qquad \hat{u} = -u + 2i\frac{\xi^2\xi_x^* - \xi_x}{1 - |\xi|^4}.$$

If these constitute a new potential and eigenfunction pair at the same λ we must have

$$\begin{aligned}
\hat{\xi}_x &= i\hat{q} - 2i\lambda\hat{\xi} - i\hat{q}^*\hat{\xi}^2, \\
\frac{\xi_x^*}{(\xi^*)^2} &= i\left(-q + 2i\frac{\xi^2\xi_x^* - \xi_x}{1-|\xi|^4}\right) + 2i\lambda\frac{1}{\xi^*} - i\left(-q^* - 2i\frac{(\xi^*)^2\xi_x - \xi_x^*}{1-|\xi|^4}\right)\frac{1}{(\xi^*)^2}, \\
\xi_x^* &= -iq(\xi^*)^2 + 2i\lambda\xi^* + iq^* - 2\frac{|\xi|^4\xi_x^* - (\xi^*)^2\xi_x + (\xi^*)^2\xi_x - \xi_x^*}{1-|\xi|^4} \\
\xi_x^* &= -iq(\xi^*)^2 + 2i\lambda\xi^* + iq^* + 2\xi_x^* \\
\xi_x^* &= iq(\xi^*)^2 - 2i\lambda\xi^* - iq^*, \qquad (2.1.4)
\end{aligned}$$

which is the conjugate of (2.1.3) if $\lambda^* = -\lambda$. So we can transform the eigenfunction and potential at any purely imaginary eigenvalue.

We would like to write the equation for the new potential in terms of the existing eigenfunction, $\vec{\phi}$. Using (2.1.3) and (2.1.4) we see that

$$\begin{aligned}
\xi^2\xi_x^* - \xi_x &= \xi^2\left(iq(\xi^*)^2 - 2i\lambda\xi^* - iq^*\right) - \left(iq - 2i\lambda\xi - iq^*\xi^2\right) \\
&= iq|\xi|^4 - 2i\lambda|\xi|^2\xi - iq^*\xi^2 - iq + 2i\lambda\xi + iq^*\xi^2 \\
&= -iq(1-|\xi|^4) + 2i\lambda\xi(1-|\xi|^2), \\
\hat{q} &= -q + 2i\left[\frac{-iq(1-|\xi|^4) + 2i\lambda\xi(1-|\xi|^2)}{1-|\xi|^4}\right] \\
&= -q + 2q - 4\lambda\xi\frac{1-|\xi|^2}{(1-|\xi|^2)(1+|\xi|^2)} = q - 4\lambda\frac{\xi}{1+|\xi|^2}.
\end{aligned}$$

Recall that $\xi = \phi_1/\phi_2$, so we have

$$\hat{q} = q - 4\lambda\frac{\frac{\phi_1}{\phi_2}}{1+\frac{|\phi_1|^2}{|\phi_2|^2}} = q - 4\lambda\frac{\phi_1\phi_2\phi_2^*}{\phi_2(|\phi_1|^2+|\phi_2|^2)} = q - 4\lambda\frac{\phi_1\phi_2}{|\phi_1|^2+|\phi_2|^2}.$$

Using the Bäcklund transformation we can get a new potential by building at the complex double-point ν_1 of the spectrum

$$Q(x,t) = q(x,t) - 2(\nu_1 - \nu_1^*)\frac{\phi_1\phi_2^*}{|\phi_1|^2 + |\phi_2|^2},$$

where $\phi = [\phi_1, \phi_2]^T$ is the general linear combination of the eigenfunctions at ν_1: $\phi = c_+\psi^+(\nu_1) + c_-\psi^-(\nu_1)$.

To prove this transformation gives a new potential and eigenfunction we must substitute these quantities into the Lax pair and show that both the spatial and temporal equations are satisfied for all λ. We define the following quantities for convenience:

$$f(\phi) = \frac{|\phi_1|^2}{|\phi_1|^2 + |\phi_2|^2}, \quad g(\phi) = \frac{|\phi_2|^2}{|\phi_1|^2 + |\phi_2|^2}, \quad h(\phi) = \frac{\phi_1\phi_2^*}{|\phi_1|^2 + |\phi_2|^2}.$$

Note that $f(\phi)$ and $g(\phi)$ are real-valued functions. There are also some quantities that we will find useful in the future:

$$f(\phi)g(\phi) = \frac{|\phi_1|^2|\phi_2|^2}{|\phi_1|^2 + |\phi_2|^2} = \frac{(\phi_1\phi_2^*)(\phi_1^*\phi_2)}{|\phi_1|^2 + |\phi_2|^2} = \frac{\phi_1\phi_2^*}{|\phi_1|^2 + |\phi_2|^2}\frac{(\phi_1\phi_2^*)(\phi_1\phi_2^*)^*}{|\phi_1|^2 + |\phi_2|^2} = h(\phi)h^*(\phi) = |h(\phi)|^2$$

$$f(\phi) + g(\phi) = \frac{|\phi_1|^2}{|\phi_1|^2 + |\phi_2|^2} + \frac{|\phi_2|^2}{|\phi_1|^2 + |\phi_2|^2} = \frac{|\phi_1|^2 + |\phi_2|^2}{|\phi_1|^2 + |\phi_2|^2} = 1$$

Combining these facts we have

$$\begin{aligned}(f+g)^2 &= f^2 + 2fg + g^2,\\ 1 &= f^2 - 2fg + g^2 + 4fg\\ &= (f-g)^2 + 4fg,\\ (f-g)^2 &= 1 - 4fg = 1 - 4|h|^2 \end{aligned} \tag{2.1.5}$$

Lemma 2.1.1. *If $\phi = [\phi_1, \phi_2]^T$ is a solution of (1.2.1) with potential q at eigenvalue ν and*

$$f(\phi) = \frac{|\phi_1|^2}{|\phi_1|^2 + |\phi_2|^2}, \quad g(\phi) = \frac{|\phi_2|^2}{|\phi_1|^2 + |\phi_2|^2}, \quad h(\phi) = \frac{\phi_1 \phi_2^*}{|\phi_1|^2 + |\phi_2|^2}, \tag{2.1.6}$$

the following equations are satisfied:

$$\begin{cases} f_x &= -2i(\nu - \nu^*)|h|^2 + iqh^* - iq^*h \\ g_x &= -f_x \\ h_x &= -2i(\nu^* f + \nu g)h - iqf + iqg \end{cases} . \tag{2.1.7}$$

Proof. Since ϕ satisfies the Lax pair with eigenvalue ν, we know that

$$\begin{cases} \phi_{1x} = -i\nu\phi_1 + iq\phi_2 \\ \phi_{2x} = iq^*\phi_1 + i\nu\phi_2 \end{cases}$$

Taking the conjugate of these equations we see that ϕ_{1x}^* and ϕ_{2x}^* must satisfy

$$\begin{cases} \phi_{1x}^* = i\nu^*\phi_1^* - iq^*\phi_2^* \\ \phi_{2x}^* = -iq\phi_1^* - i\nu^*\phi_2^*. \end{cases}$$

We will need the derivatives of the following three products to proceed.

$$\begin{aligned} \tfrac{\partial}{\partial x}\left[|\phi_1|^2\right] &= \phi_{1x}\phi_1^* + \phi_1\phi_{1x}^* \\ &= -i\nu|\phi_1|^2 + iq\phi_1^*\phi_2 + i\nu^*|\phi_1|^2 - iq^*\phi_1\phi_2^* \\ &= -i(\nu - \nu^*)|\phi_1|^2 + iq\phi_1^*\phi_2 - iq^*\phi_1\phi_2^*, \\ \tfrac{\partial}{\partial x}\left[|\phi_2|^2\right] &= \phi_{2x}\phi_2^* + \phi_2\phi_{2x}^* \\ &= iq^*\phi_1\phi_2^* + i\nu|\phi_2|^2 - iq\phi_1^*\phi_2 - i\nu^*|\phi_2|^2 \\ &= i(\nu - \nu^*)|\phi_2|^2 + iq^*\phi_1\phi_2^* - iq\phi_1^*\phi_2, \end{aligned}$$

$$\begin{aligned}\tfrac{\partial}{\partial x}\left[\phi_1\phi_2^*\right] &= \phi_{1x}\phi_2^* + \phi_1\phi_{2x}^* \\ &= -i\nu\phi_1\phi_2^* + iq|\phi_2|^2 - iq|\phi_1|^2 - i\nu^*\phi_1\phi_2^* \\ &= -iq(|\phi_1|^2 - |\phi_1|^2) - i(\nu+\nu^*)\phi_1\phi_2^*.\end{aligned}$$

Note that the denominator of each of the functions in (2.1.6) is the same, so we will define a new function $j(\phi) = |\phi_1|^2 + |\phi_2|^2$ for convenience of notation. Furthermore, we see that

$$\begin{aligned}\frac{\partial}{\partial x}[|\phi_1|^2 + |\phi_2|^2] &= -i(\nu-\nu^*)|\phi_1|^2 + iq\phi_1^*\phi_2 - iq^*\phi_1\phi_2^* + i(\nu-\nu^*)|\phi_2|^2 + iq^*\phi_1\phi_2^* - iq\phi_1^*\phi_2 \\ &= -i(\nu-\nu^*)(|\phi_1|^2 - |\phi_2|^2), \\ \frac{j_x}{j} &= -i(\nu-\nu^*)(f-g).\end{aligned}$$

Finally,

$$\begin{aligned}f_x &= -i(\nu-\nu^*)f + iqh^* - iq^*h + i(\nu-\nu^*)f(f-g) \\ &= -i(\nu-\nu^*)f(1-f+g) + iqh^* - iq^*h \\ &= -i(\nu-\nu^*)f(2g) + iqh^* - iq^*h \quad \text{since} \quad f+g=1 \\ &= -2i(\nu-\nu^*)|h|^2 + iqh^* - iq^*h \quad \text{since} \quad fg = |h|^2, \\ g_x &= i(\nu-\nu^*)g + iq^*h - iqh^* + i(\nu-\nu^*)g(f-g) \\ &= i(\nu-\nu^*)g(1+f-g) + iq^*h - iqh^* \\ &= 2i(\nu-\nu^*)|h|^2 + iq^*h - iqh^* \\ &= -\left[-2i(\nu-\nu^*)|h|^2 - iq^*h + iqh^*\right] = -f_x,\end{aligned}$$

and,

$$\begin{aligned} h_x &= -iq(f-g) - i(\nu+\nu^*)h + ih(\nu-\nu^*)(f-g) \\ &= -ih\big[(\nu+\nu^*)(f+g) - (\nu-\nu^*)(f-g)\big] - iq(f-g) \\ &= -ih\big[(\nu+\nu^*-\nu+\nu^*)f + (\nu+\nu^*+\nu-\nu^*)g\big] - iq(f-g) \\ &= -2i(\nu^* f + \nu g)h - iq(f-g). \end{aligned}$$

□

Lemma 2.1.2. *If $\phi = [\phi_1, \phi_2]^T$ is a solution of (1.2.1) with potential q at eigenvalue $\nu = i\alpha$ for $\alpha \in \mathbb{R}$ and f, g, and h are as defined in (2.1.6) the following equations are satisfied:*

$$\begin{cases} f_t &= -2\alpha(q^*h + qh^*) - (q_x^*h + q_x h^*) + 4\alpha f(qh^* + q^*h) \\ g_t &= -2\alpha(q^*h + qh^*) + q_x^*h + q_x h^* + 4\alpha g(qh^* + q^*h) \\ h_t &= 2i(2\alpha^2 + |q|^2)h - 2\alpha q + q_x(f-g) + 4\alpha h(qh^* + q^*h) \end{cases} . \tag{2.1.8}$$

Proof. Since ϕ satisfies the Lax pair with eigenvalue ν, we know that

$$\begin{cases} \phi_{1t} = (-2i\nu^2 + i|q|^2)\phi_1 + (2i\nu q - q_x)\phi_2 \\ \phi_{2t} = (2i\nu q^* + q_x^*)\phi_1 + (2i\nu^2 - i|q|^2)\phi_2 \end{cases} = \begin{cases} \phi_{1t} = (2i\alpha^2 + i|q|^2)\phi_1 - (2\alpha q + q_x)\phi_2 \\ \phi_{2t} = (-2\alpha q^* + q_x^*)\phi_1 - (2i\alpha^2 + i|q|^2)\phi_2. \end{cases}$$

Taking the conjugate of these equations we see that ϕ_{1x}^* and ϕ_{2x}^* must satisfy

$$\begin{cases} \phi_{1t}^* = -(2i\alpha^2 + i|q|^2)\phi_1^* - (2\alpha q^* + q_x^*)\phi_2^* \\ \phi_{2t}^* = (-2\alpha q + q_x)\phi_1^* + (2i\alpha^2 + i|q|^2)\phi_2^*. \end{cases}$$

Note that the denominator of each of the functions in (2.1.6) is the same, so we will define a new function $j(\phi) = |\phi_1|^2 + |\phi_2|^2$ for convenience of notation. To determine f_t, g_t, and h_t

we work out the following derivatives:

$$\begin{aligned}
\frac{\partial}{\partial t}\Big[|\phi_1|^2\Big] &= \phi_{1t}\phi_1^* + \phi_1\phi_{1t}^* \\
&= (2i\alpha^2 + i|q|^2)|\phi_1|^2 - (2\alpha q + q_x)\phi_1^*\phi_2 - (2i\alpha^2 + i|q|^2)|\phi_1|^2 - (2\alpha q^* + q_x^*)\phi_1\phi_2^* \\
&= -(2\alpha q + q_x)\phi_1^*\phi_2 - (2\alpha q^* + q_x^*)\phi_1\phi_2^*, \\
\frac{\partial}{\partial t}\Big[|\phi_2|^2\Big] &= \phi_{2t}\phi_2^* + \phi_2\phi_{2t}^* \\
&= (-2\alpha q^* + q_x^*)\phi_1\phi_2^* - (2i\alpha^2 + i|q|^2)|\phi_2|^2 + (-2\alpha q + q_x)\phi_1^*\phi_2 + (2i\alpha^2 + i|q|^2)|\phi_2|^2 \\
&= (-2\alpha q^* + q_x^*)\phi_1\phi_2^* + (-2\alpha q + q_x)\phi_1^*\phi_2, \\
\frac{\partial}{\partial t}\Big[\phi_1\phi_2^*\Big] &= \phi_{1t}\phi_2^* + \phi_1\phi_{2t}^* \\
&= (2i\alpha^2 + i|q|^2)\phi_1\phi_2^* - (2\alpha q + q_x)|\phi_2|^2 + (-2\alpha q + q_x)|\phi_1|^2 + (2i\alpha^2 + i|q|^2)\phi_1\phi_2^* \\
&= -2\alpha q(|\phi_1|^2 + |\phi_2|^2) - q_x(|\phi_2|^2 - |\phi_1|^2) + 2(2i\alpha^2 + i|q|^2)\phi_1\phi_2^*.
\end{aligned}$$

Furthermore, we see that

$$\begin{aligned}
\frac{\partial}{\partial t}[|\phi_1|^2 + |\phi_2|^2] &= -(2\alpha q + q_x)\phi_1^*\phi_2 - (2\alpha q^* + q_x^*)\phi_1\phi_2^* - (2\alpha q^* - q_x^*)\phi_1\phi_2^* - (2\alpha q - q_x)\phi_1^*\phi_2 \\
&= -4\alpha q\phi_1^*\phi_2 - 4\alpha q^*\phi_1\phi_2^*, \\
\frac{j_t}{j} &= -4\alpha q h^* - 4\alpha q^* h = -4\alpha(qh^* + q^*h).
\end{aligned}$$

Finally, we conclude that

$$\begin{aligned}
f_t &= -(2\alpha q + q_x)h^* - (2\alpha q^* + q_x^*)h - f\frac{j_t}{j} \\
&= -2\alpha(q^*h + qh^*) - (q_x^*h + q_x h^*) + 4\alpha f(qh^* + q^*h), \\
g_t &= (-2\alpha q^* + q_x^*)h + (-2\alpha q + q_x)h^* - g\frac{j_t}{j}
\end{aligned}$$

$$= -2\alpha(q^*h + qh^*) + q_x^*h + q_xh^* + 4\alpha g(qh^* + q^*h),$$

$$h_t = -2\alpha q(f+g) - q_x(g-f) + 2(2i\alpha^2 + i|q|^2)h - h\frac{j_t}{j}$$

$$= -2\alpha q + q_x(f-g) + 2i(2\alpha^2 + |q|^2)h + 4\alpha h(qh^* + q^*h).$$

□

The Gauge matrix for the ϕ at a new eigenvalue λ which is a double point of the spectrum is

$$G(\lambda;\nu,\phi) \equiv N \begin{bmatrix} -\lambda+\nu & 0 \\ 0 & -\lambda+\nu^* \end{bmatrix} N^{-1}, \text{ where } N \equiv \begin{bmatrix} \phi_1 & -\phi_2^* \\ \phi_2 & \phi_1^* \end{bmatrix}, \text{so that}$$

$$\det(N) = \phi_1\phi_1^* + \phi_2^*\phi_2 = |\phi_1|^2 + |\phi_2|^2, \text{ and } N^{-1} = \frac{1}{|\phi_1|^2+|\phi_2|^2} \begin{bmatrix} \phi_1^* & \phi_2^* \\ -\phi_2 & \phi_1 \end{bmatrix}.$$

Then, we can see in this form that if $\nu = i\alpha$ for $\alpha \in \mathbb{R}$,

$$G = \begin{bmatrix} -\lambda + \nu f(\phi) + \nu^* g(\phi) & (\nu-\nu^*)h(\phi) \\ (\nu-\nu^*)h^*(\phi) & -\lambda + \nu g(\phi) + \nu^* f(\phi) \end{bmatrix} = \begin{bmatrix} -\lambda + i\alpha\big(f-g\big) & 2i\alpha h \\ 2i\alpha h^* & -\lambda - i\alpha\big(f-g\big) \end{bmatrix}.$$

Theorem 2.1.3. *Let $\phi = [\phi_1, \phi_2]^T$ be a general linear combination of two linearly independent eigenfunctions ϕ^+ and ϕ^- with potential q at the eigenvalue ν. If ψ is **any** solution to the Lax pair with the potential u and eigenvalue λ, i.e.*

$$\begin{bmatrix} \psi_1 \\ \psi_2 \end{bmatrix}_x = \begin{bmatrix} -i\lambda & iq \\ iq^* & i\lambda \end{bmatrix} \begin{bmatrix} \psi_1 \\ \psi_2 \end{bmatrix} = U(q,\lambda)\psi,$$

$$\begin{bmatrix} \psi_1 \\ \psi_2 \end{bmatrix}_t = \begin{bmatrix} i|q|^2 - 2i\lambda^2 & -q_x + 2i\lambda q \\ q_x^* + 2i\lambda q^* & -i|q|^2 + 2i\lambda^2 \end{bmatrix} = V(q,\lambda)\psi,$$

then $\Psi = G(\lambda;\nu,\phi)\psi$ *is a solution to the Lax pair with the potential* Q *and eigenvalue* λ*, where the new potential* $Q(x,t)$ *is*

$$Q(x,t) = q(x,t) - 2(\nu - \nu^*)\frac{\phi_1\phi_2^*}{|\phi_1|^2 + |\phi_2|^2}. \tag{2.1.9}$$

Proof. Using the definition of h in (2.1.6), the new potential can be written as

$$Q = q - 2(\nu - \nu^*)h(\phi).$$

The new eigenfunction is $\Psi = G(\lambda;\nu,\phi)\psi$, where ψ is a solution to the spatial part of the Lax pair at the potential q and eigenvalue λ, i.e. $\psi_x = U(q;\lambda)\psi$. Thus,

$$\begin{aligned} \Psi_x &= G_x(\nu,\phi)\psi + G(\lambda;\nu,\phi)\psi_x \\ &= G_x(\nu,\phi)\psi + G(\lambda;\nu,\phi)U(q;\lambda)\psi \\ &= \Big(G_x(\nu,\phi) + G(\lambda;\nu,\phi)U(q;\lambda)\Big)\psi \\ U(Q;\lambda)\Psi &= U(Q;\lambda)G(\lambda;\nu,\phi)\psi \end{aligned}$$

$$\Psi_x = U(Q;\lambda)\Psi \iff G_x(\nu,\phi) + G(\lambda;\nu,\phi)U(q;\lambda) = U(Q;\lambda)G(\lambda;\nu,\phi)$$

for all ψ such that $\psi_x = U(q;\nu)\psi$. We temporarily define M as

$$M \equiv U(Q;\lambda)G(\lambda;\nu,\phi) - G(\lambda;\nu,\phi)U(q;\lambda)$$

so we seek to show that $G_x = M$. Because of the structure of the Lax pair, the main diagonal components will end up being of opposite sign, but identical otherwise, and the off diagonal

components will be complex conjugates of each other. For this reason, we only present the verification of the $(1,1)$ and $(1,2)$ components. To simplify the presentation we also only present the case where ν is pure imaginary, i.e. $\nu = i\alpha$ for $\alpha \in \mathbb{R}$.

For the left hand side we have

$$G_x = \begin{bmatrix} \nu f_x(\phi) + \nu^* g_x(\phi) & (\nu - \nu^*)h_x(\phi) \\ (\nu - \nu^*)h_x^*(\phi) & \nu g_x(\phi) + \nu^* f_x(\phi) \end{bmatrix} = 2i\alpha \begin{bmatrix} f_x & h_x \\ h_x^* & -f_x \end{bmatrix},$$

so G_x is not a function of λ (recall that ϕ_1 and ϕ_2 are already evaluated at ν so f, g, and h are independent of λ).

Looking at the (1,1) component of M we see

$$\begin{aligned} M_{(1,1)} &= U(Q)_{(1,1)}G_{(1,1)} + U(Q)_{(1,2)}G_{(2,1)} - U(q)_{(1,1)}G_{(1,1)} - U(q)_{(2,1)}G_{(1,2)} \\ &= \big[U(Q)_{(1,1)} - U(q)_{(1,1)}\big]G_{(1,1)} + U(Q)_{(1,2)}G_{(2,1)} - U(q)_{(2,1)}G_{(1,2)} \\ &= \big[-i\lambda + i\lambda\big]G_{(1,1)} + iQ(2i\alpha h^*) - iq^*(2i\alpha h) \\ &= 2i\alpha\big[i(q - 4i\alpha h)h^* - iq^*h\big] \\ &= 2i\alpha\big[iqh^* - iq^*h + 4\alpha|h|^2\big]. \end{aligned}$$

Using (2.1.7) we see f_x when $\nu = i\alpha$ is

$$f_x = 4i\alpha|h|^2 + iqh^* - iq^*h,$$

so $M_{(1,1)} = 2i\alpha f_x$ as desired.

Proceeding with the off diagonal component, $M_{(1,2)}$ we have

$$M_{(1,2)} = U(Q)_{(1,1)}G_{(1,2)} + U(Q)_{(1,2)}G_{(2,2)} - U(q)_{(1,2)}G_{(1,1)} - U(q)_{(2,2)}G_{(1,2)}$$

$$= \big[U(Q)_{(1,1)} - U(q)_{(2,2)}\big]G_{(1,2)} + U(Q)_{(1,2)}G_{(2,2)} - U(q)_{(1,2)}G_{(1,1)}$$

$$= -2i\lambda(2i\alpha h) + iQ\big[-\lambda - i\alpha(f-g)\big] - iq\big[-\lambda + i\alpha(f-g)\big]$$

$$= -2i\lambda(2i\alpha h) - i\lambda(Q-q) + \alpha(f-g)(Q+q)$$

$$= 4\alpha\lambda h - i\lambda(-4i\alpha h) + \alpha(f-g)(2q - 4i\alpha h)$$

$$= -2i\alpha(f-g)(iq + 2\alpha h)$$

Using (2.1.7) we see h_x when $\nu = i\alpha$ is

$$h_x = -(f-g)(2\alpha h + iq),$$

so $M_{(1,2)} = 2i\alpha h_x$ as desired.

Since the left and right sides are equal, the new potential and eigenfunction pair satisfy $\Psi_x = U(Q,\lambda)\Psi$.

Now for the temporal part we define

$$M \equiv V(Q;\lambda)G(\lambda;\nu,\phi) - G(\lambda;\nu,\phi)V(q;\lambda)$$

and

$$G_t = \begin{bmatrix} \nu f_t(\phi) + \nu^* g_t(\phi) & (\nu - \nu^*)h_t(\phi) \\ (\nu - \nu^*)h_t^*(\phi) & \nu g_t(\phi) + \nu^* f_t(\phi) \end{bmatrix} = 2i\alpha \begin{bmatrix} i\alpha(f_t - g_t) & 2i\alpha h_t \\ 2i\alpha h_t^* & -i\alpha(f_t - g_t) \end{bmatrix}.$$

Looking at the (1,1) component we have

$$M_{(1,1)} = V(Q)_{(1,1)}G_{(1,1)} + V(Q)_{(1,2)}G_{(2,1)} - V(q)_{(1,1)}G_{(1,1)} - V(q)_{(2,1)}G_{(1,2)}$$

$$= \big[V(Q)_{(1,1)} - V(q)_{(1,1)}\big]G_{(1,1)} + V(Q)_{(1,2)}G_{(2,1)} - V(q)_{(2,1)}G_{(1,2)}$$

$$
\begin{aligned}
&= (-\lambda + i\alpha(f-g))(-2i\lambda^2 + i|Q|^2 + 2i\lambda^2 - i|q|^2) \\
&\quad + 2i\alpha\left(2i\lambda h^* Q - h^* Q_x - 2i\lambda h q^* + h q_x^*\right) \\
&= (-i\lambda - \alpha(f-g))\left(|Q|^2 - |q|^2\right) - 4\alpha\lambda\left(h^* Q - h q^*\right) - 2i\alpha\left(h^* Q_x + h q_x^*\right) \\
&= -[i\lambda + \alpha(f-g)]\left[4i\alpha(q h^* - q^* h) + 16\alpha^2 |h|^2\right] - 4\alpha\lambda\left(h^* q - 4i\alpha|h|^2 - h q^*\right) \\
&\quad - 2i\alpha\left(h^* q_x - 4i\alpha h^* h_x + h q_x^*\right) \\
&= 4\alpha\lambda(q h^* - q^* h) - 16i\alpha^2|h|^2\lambda - 16\alpha^3(f-g)|h|^2 - 4\alpha\lambda(q h^* - q^* h) + 16i\alpha^2|h|^2\lambda \\
&\quad - 2i\alpha(h^* q_x + h q_x^*) - 8\alpha^2 h^* h_x - 4i\alpha^2(f-g)(q h^* - q^* h) \\
&= -16\alpha^3(f-g)|h|^2 - 2i\alpha(h^* q_x + h q_x^*) + 8\alpha^2(f-g)(2\alpha|h|^2 + i q h^*) \\
&\quad - 4i\alpha^2(f-g)(q h^* - q^* h) + 4i\alpha^2(f-g)(q^* h - q h^*) \\
&= -2i\alpha(h^* q_x + h q_x^*) + 4i\alpha^2(f-g)(q^* h + q h^*) \\
&= i\alpha\left[4\alpha(f-g)(q^* h + q h^*) - 2(h^* q_x + h q_x^*)\right].
\end{aligned}
$$

We need to show that this matches $i\alpha\left[f_t - g_t\right]$. Indeed, using Lemma 2.1.2 we see

$$
\begin{aligned}
f_t - g_t &= -2\alpha(q^* h + q h^*) - (q_x^* h + q_x h^*) + 4\alpha f(q h^* + q^* h) \\
&\quad + 2\alpha(q^* h + q h^*) - (q_x^* h + q_x h^*) - 4\alpha g(q h^* + q^* h) \\
&= 4\alpha(f-g)(q h^* + q^* h) - 2(q_x^* h + q_x h^*).
\end{aligned}
$$

So we have $M_{(1,1)} = i\alpha\left[f_t - g_t\right]$.

Looking at the (1,2) component we have

$$
M_{(1,2)} = V(Q)_{(1,1)} G_{(1,2)} + V(Q)_{(1,2)} G_{(2,2)} - \left(G_{(1,1)} V(q)_{(1,2)} + G_{(1,2)} V(q)_{(2,2)}\right)
$$

$$
\begin{aligned}
&= G_{(1,2)}\left(V(Q)_{(1,1)} - V(q)_{(2,2)}\right) + V(Q)_{(1,2)}G_{(2,2)} - V(q)_{(1,2)}G_{(1,1)} \\
&= 2i\alpha h\left(-2i\lambda^2 + i|Q|^2 - 2i\lambda^2 + i|q|^2\right) + (2i\lambda Q - Q_x)\left(-\lambda - i\alpha(f-g)\right) \\
&\quad - (2i\lambda q - q_x)\left(-\lambda + i\alpha(f-g)\right) \\
&= -2\alpha h\left(-4\lambda^2 + |Q|^2 + |q|^2\right) - \lambda\left(2i\lambda Q - Q_x - 2i\lambda q + q_x\right) \\
&\quad - i\alpha(f-g)\left(2i\lambda Q - Q_x + 2i\lambda q - q_x\right) \\
&= 8\alpha\lambda^2 h - 2\alpha h\left[2|q|^2 + 4i\alpha(qh^* - q^*h) + 16\alpha^2|h|^2\right] - \lambda\left[2i\lambda(-4i\alpha h) - (-4i\alpha h_x)\right] \\
&\quad - i\alpha(f-g)\left[4i\lambda q + 2\lambda(4\alpha h) - 2q_x - (-4i\alpha h_x)\right] \\
&= 8\alpha\lambda^2 h - 4\alpha|q|^2 h - 8i\alpha^2 h(qh^* - q^*h) - 32\alpha^3 h|h|^2 - 8\lambda^2\alpha h - 4i\alpha\lambda h_x \\
&\quad + 4\alpha\lambda(f-g)q - 8i\alpha^2\lambda h(f-g) + 2i\alpha(f-g)q_x + 4\alpha^2(f-g)h_x \\
&= 8\alpha\lambda^2 h - 4\alpha|q|^2 h - 8i\alpha^2 h(qh^* - q^*h) - 32\alpha^3 h|h|^2 - 8\lambda^2\alpha h + 4i\alpha\lambda(f-g)(2\alpha h + iq) \\
&\quad + 4\alpha\lambda(f-g)q - 8i\alpha^2\lambda h(f-g) + 2i\alpha(f-g)q_x - 4\alpha^2(f-g)^2(2\alpha h + iq) \\
&= 8\alpha\lambda^2 h - 4\alpha|q|^2 h - 8i\alpha^2(qh^* - q^*h)h - 32\alpha^3 h|h|^2 - 8\lambda^2\alpha h + 8i\alpha^2\lambda(f-g)h \\
&\quad - 4\alpha\lambda(f-g)q + 4\alpha\lambda(f-g)q - 8i\alpha^2\lambda h(f-g) + 2i\alpha(f-g)q_x \\
&\quad - 4\alpha^2\left((1 - 4|h|^2\right)(2\alpha h + iq) \\
&= -4\alpha|q|^2 h - 8i\alpha^2(qh^* - q^*h)h - 32\alpha^3 h|h|^2 + 2i\alpha(f-g)q_x - 8\alpha^3 h \\
&\quad + 32\alpha^3 h|h|^2 - 4i\alpha^2 q + 16i\alpha^2|h|^2 q \\
&= -4\alpha|q|^2 h + 8i\alpha^2(qh^* + q^*h)h + 2i\alpha(f-g)q_x - 8\alpha^3 h - 4i\alpha^2 q.
\end{aligned}
$$

Furthermore, from Lemma 2.1.2 we have

$$
2i\alpha h_t = 2i\alpha\Big[2i(2\alpha^2 + |q|^2)h - 2\alpha q + q_x(f-g) + 4\alpha h(qh^* + q^*h)\Big]
$$

$$= 2\alpha\Big[-2(2\alpha^2 + |q|^2)h - 2i\alpha q + iq_x(f-g) + 4i\alpha h(qh^* + q^*h)\Big]$$

$$= -8\alpha^3 h - 4\alpha|q|^2 h - 4i\alpha^2 q + 2i\alpha(f-g) + 8i\alpha^2 h(qh^* + q^*h)$$

so we have shown $2i\alpha h_t = M_{(1,2)}$ as desired. Since the left and right sides are equal, the new potential and eigenfunction pair satisfy $\Psi_t = V(Q,\lambda)\Psi$.

The work in this proof shows that the eigenfunction Ψ satisfies the Lax pair (1.2.1) with eigenvalue λ and solution Q. □

2.2 Bäcklund-Gauge transformation for spatially periodic boundary conditions

Let ν be a purely imaginary point of the spectrum. We define the relationship between ν and the wave number k as $\pm k - \nu = \pm a e^{\mp ip}$. The arbitrary linear combination of the eigenfunctions evaluated at ν is ϕ, i.e.

$$\phi = \begin{bmatrix} \phi_1 \\ \\ \phi_2 \end{bmatrix} = c_+\phi^+(\nu) + c_-\phi^-(\nu) \tag{2.2.1}$$

$$= c_-\left(e^{\rho}e^{i\beta}\phi^+(\nu) + \phi^-(\nu)\right)$$

$$= \frac{iac_-}{2k}\begin{bmatrix} \left(e^{\rho}e^{i\beta}e^{-i\frac{\pi}{4}}e^{i\frac{p}{2}}e^{i(kx+2k\nu t)} + e^{i\frac{\pi}{4}}e^{-i\frac{p}{2}}e^{-i(kx+2k\nu t)}\right)e^{ia^2t} \\ \\ \left(e^{\rho}e^{i\beta}e^{-i\frac{\pi}{4}}e^{-i\frac{p}{2}}e^{i(kx+2k\nu t)} - e^{i\frac{\pi}{4}}e^{i\frac{p}{2}}e^{-i(kx+2k\nu t)}\right)e^{-ia^2t} \end{bmatrix}$$

The Gauge matrix is

$$G(\lambda;\nu,\phi) = \begin{bmatrix} -\lambda + \nu\frac{|\phi_1|^2}{|\phi_1|^2+|\phi_2|^2} + \nu^*\frac{|\phi_2|^2}{|\phi_1|^2+|\phi_2|^2} & (\nu-\nu^*)\frac{\phi_1\phi_2^*}{|\phi_1|^2+|\phi_2|^2} \\ \\ (\nu-\nu^*)\frac{\phi_1^*\phi_2}{|\phi_1|^2+|\phi_2|^2} & -\lambda + \nu\frac{|\phi_2|^2}{|\phi_1|^2+|\phi_2|^2} + \nu^*\frac{|\phi_1|^2}{|\phi_1|^2+|\phi_2|^2} \end{bmatrix}$$

$$= \begin{bmatrix} -\lambda + i\alpha\frac{|\phi_1|^2-|\phi_2|^2}{|\phi_1|^2+|\phi_2|^2} & i\alpha\frac{2\phi_1\phi_2^*}{|\phi_1|^2+|\phi_2|^2} \\ i\alpha\frac{2\phi_1^*\phi_2}{|\phi_1|^2+|\phi_2|^2} & -\lambda - i\alpha\frac{|\phi_1|^2-|\phi_2|^2}{|\phi_1|^2+|\phi_2|^2} \end{bmatrix} \quad \text{since } \nu = i\alpha \text{ is purely imaginary,}$$

If we define A and B as

$$A = \frac{|\phi_1|^2 - |\phi_2|^2}{|\phi_1|^2 + |\phi_2|^2} = f - g \qquad \text{and} \qquad B = \frac{2\phi_1\phi_2^*}{|\phi_1|^2 + |\phi_2|^2} = 2h \tag{2.2.2}$$

then we can rewrite the Gauge matrix as

$$G(\lambda;\nu,\phi) = \begin{bmatrix} -\lambda + i\alpha A & i\alpha B \\ i\alpha B^* & -\lambda - i\alpha A \end{bmatrix} \tag{2.2.3}$$

Recall that ϕ_1 and ϕ_2 are already evaluated at ν so they are independent of λ. Let $\sigma = -4ik\nu$. Since $k \in \mathbb{R}$ and ν is purely imaginary, $\sigma \in \mathbb{R}$. We need to compute the sum and difference of $|\phi_1|^2$ and $|\phi_2|^2$ to proceed. First, we calculate $|\phi_1|^2$.

$$\begin{aligned}
\phi_1 &= \frac{iac_-}{2k}\left(e^{\rho}e^{i\beta}e^{-i\frac{\pi}{4}}e^{i\frac{p}{2}}e^{i(kx+2k\nu t)} + e^{i\frac{\pi}{4}}e^{-i\frac{p}{2}}e^{-i(kx+2k\nu t)}\right)e^{ia^2t} \\
\phi_1^* &= \frac{-iac_-^*}{2k}\left(e^{\rho}e^{-i\beta}e^{i\frac{\pi}{4}}e^{-i\frac{p}{2}}e^{-i(kx-2k\nu t)} + e^{-i\frac{\pi}{4}}e^{i\frac{p}{2}}e^{i(kx-2k\nu t)}\right)e^{-ia^2t} \\
|\phi_1|^2 &= \frac{a^2|c_-|^2}{4k^2}\left(e^{2\rho}e^{4ik\nu t} + e^{\rho}e^{i\beta}e^{-i\frac{\pi}{2}}e^{ip}e^{2ikx} + e^{\rho}e^{-i\beta}e^{i\frac{\pi}{2}}e^{-ip}e^{-2ikx} + e^{-4ik\nu t}\right) \\
&= \frac{a^2|c_-|^2}{4k^2}e^{\rho}\left(e^{\rho}e^{4ik\nu t} + e^{ip}e^{i(2kx+\beta-\frac{\pi}{2})} + e^{-ip}e^{-i(2kx+\beta-\frac{\pi}{2})} + e^{-\rho}e^{-4ik\nu t}\right) \\
&= \frac{a^2|c_-|^2}{4k^2}e^{\rho}\left(e^{\rho-\sigma t} + e^{ip}e^{i(2kx+\beta-\frac{\pi}{2})} + e^{-ip}e^{-i(2kx+\beta-\frac{\pi}{2})} + e^{-(\rho-\sigma t)}\right).
\end{aligned}$$

Next, we follow the same method but construct $|\phi_2|^2$.

$$\begin{aligned}
\phi_2 &= \frac{iac_-}{2k}\left(e^{\rho}e^{i\beta}e^{-i\frac{\pi}{4}}e^{-i\frac{p}{2}}e^{i(kx+2k\nu t)} - e^{i\frac{\pi}{4}}e^{i\frac{p}{2}}e^{-i(kx+2k\nu t)}\right)e^{-ia^2t} \\
\phi_2^* &= \frac{-iac_-^*}{2k}\left(e^{\rho}e^{-i\beta}e^{i\frac{\pi}{4}}e^{i\frac{p}{2}}e^{-i(kx-2k\nu t)} - e^{-i\frac{\pi}{4}}e^{-i\frac{p}{2}}e^{i(kx-2k\nu t)}\right)e^{ia^2t}
\end{aligned}$$

$$
\begin{aligned}
|\phi_2|^2 &= \frac{a^2|c_-|^2}{4k^2}\left(e^{2\rho}e^{4ik\nu t} - e^{\rho}e^{i\beta}e^{-i\frac{\pi}{2}}e^{-ip}e^{2ikx} - e^{\rho}e^{-i\beta}e^{i\frac{\pi}{2}}e^{ip}e^{-2ikx} + e^{-4ik\nu t}\right) \\
&= \frac{a^2|c_-|^2}{4k^2}e^{\rho}\left(e^{\rho}e^{4ik\nu t} - e^{-ip}e^{i(2kx+\beta-\frac{\pi}{2})} - e^{ip}e^{-i(2kx+\beta-\frac{\pi}{2})} + e^{-\rho}e^{-4ik\nu t}\right) \\
&= \frac{a^2|c_-|^2}{4k^2}e^{\rho}\left(e^{\rho-\sigma t} - e^{-ip}e^{i(2kx+\beta-\frac{\pi}{2})} - e^{ip}e^{-i(2kx+\beta-\frac{\pi}{2})} + e^{-(\rho-\sigma t)}\right).
\end{aligned}
$$

Looking at the sum of these two quantities we have

$$
\begin{aligned}
|\phi_1|^2 + |\phi_2|^2 &= \frac{a^2|c_-|^2}{4k^2}e^{\rho}\left[2e^{\rho-\sigma t} + \left(e^{ip} - e^{-ip}\right)\left(e^{i(2kx+\beta-\frac{\pi}{2})} - e^{-i(2kx+\beta-\frac{\pi}{2})}\right) + 2e^{-(\rho-\sigma t)}\right] \\
&= \frac{a^2|c_-|^2}{4k^2}e^{\rho}\left[2\left(e^{\rho-\sigma t} + e^{-(\rho-\sigma t)}\right) + 2i\sin(p)\left(e^{i(2kx+\beta-\frac{\pi}{2})} - e^{i(2kx+\beta-\frac{\pi}{2})}\right)\right] \\
&= \frac{a^2|c_-|^2}{k^2}e^{\rho}\left[\cosh\left(\rho-\sigma t\right) + \sin(p)\cos(2kx+\beta)\right].
\end{aligned}
$$

The difference of the two quantities is

$$
\begin{aligned}
|\phi_1|^2 - |\phi_2|^2 &= \frac{a^2|c_-|^2}{4k^2}e^{\rho}\left[\left(e^{ip} + e^{-ip}\right)\left(e^{i(2kx+\beta-\frac{\pi}{2})} + e^{i(2kx+\beta-\frac{\pi}{2})}\right)\right] \\
&= \frac{a^2|c_-|^2}{k^2}e^{\rho}\cos(p)\cos\left(2kx+\beta-\frac{\pi}{2}\right) \\
&= \frac{a^2|c_-|^2}{k^2}e^{\rho}\cos(p)\sin\left(2kx+\beta\right).
\end{aligned}
$$

To compute B we need to know $\phi_1\phi_2^*$. This product evaluates to

$$
\begin{aligned}
2\phi_1\phi_2^* &= \frac{a^2|c_-|^2}{2k^2}e^{\rho}\left[e^{\rho}e^{ip}e^{4ik\nu t} - e^{i\beta}e^{-i\frac{\pi}{2}}e^{2ikx} + e^{-i\beta}e^{i\frac{\pi}{2}}e^{-2ikx} - e^{-\rho}e^{-ip}e^{-4ik\nu t}\right] \\
&= \frac{a^2|c_-|^2}{k^2}e^{\rho}\left[\sinh\left(\rho-\sigma t+ip\right) - i\sin\left(2kx+\beta-\frac{\pi}{2}\right)\right] \\
&= \frac{a^2|c_-|^2}{k^2}e^{\rho}\left[\cosh\left(\rho-\sigma t\right)\sinh(ip) + \sinh\left(\rho-\sigma t\right)\cosh(ip) + i\cos\left(2kx+\beta\right)\right] \\
&= \frac{a^2|c_-|^2}{k^2}e^{\rho}\left[i\sin(p)\cosh\left(\rho-\sigma t\right) + \cos(p)\sinh\left(\rho-\sigma t\right) + i\cos\left(2kx+\beta\right)\right]
\end{aligned}
$$

We can now construct both A and B from these pieces of information as follows:

$$
A = \frac{|\phi_1|^2 - |\phi_2|^2}{|\phi_1|^2 + |\phi_2|^2}
$$

$$= \frac{\cos(p)\sin(2kx+\beta)}{\cosh(\rho-\sigma t)+\sin(p)\cos(2kx+\beta)} \tag{2.2.4}$$

$$B = \frac{2\phi_1\phi_2^*}{|\phi_1|^2+|\phi_2|^2}$$

$$= e^{2ia^2t}\frac{i\sin(p)\cosh(\rho-\sigma t)+\cos(p)\sinh(\rho-\sigma t)+i\cos(2kx+\beta)}{\cosh(\rho-\sigma t)+\sin(p)\cos(2kx+\beta)} \tag{2.2.5}$$

So the new eigenfunctions are

$$\chi^{\pm}(\lambda;\nu,\phi) = G(\lambda;\nu,\phi)\phi^{\pm}(\lambda) \tag{2.2.6}$$

$$= \frac{ia}{2\hat{k}}e^{\mp i\frac{\pi}{4}}e^{\pm i\frac{\hat{p}}{2}}\begin{bmatrix} -\lambda+\nu A & \nu B \\ \nu B^* & -\lambda-\nu A \end{bmatrix}\begin{bmatrix} e^{ia^2t} \\ \pm e^{\mp i\hat{p}}e^{-ia^2t} \end{bmatrix}e^{\pm i(\hat{k}x+2\hat{k}\lambda t)} \tag{2.2.7}$$

where $\hat{k}(\lambda)\pm\lambda = ae^{\pm i\hat{p}}$.

We now construct the new solution. First, note that

$$\nu-\nu^* = (k+\nu)-(k+\nu^*) = (k+\nu)-(k-\nu) = ae^{-ip}-ae^{ip} = -a(e^{ip}-e^{-ip}) = -2ia\sin(p),$$

we have

$$\begin{aligned}
Q(x,t) &= q(x,t)-2(\nu-\nu^*)\frac{\phi_1\phi_2^*}{|\phi_1|^2+|\phi_2|^2} \\
&= q(x,t)+2ia\sin(p)B \\
&= ae^{2ia^2t}+2ia\sin(p)e^{2ia^2t}\frac{\cos p\sinh(\tau)+i\sin p\cosh(\tau)+i\cos(2kx+\beta)}{\cosh(\tau)+\sin p\cos(2kx+\beta)} \\
&= ae^{2ia^2t}\left(1+\frac{2i\sin p\cos p\sinh(\tau)-2\sin^2 p\cosh(\tau)-2\sin p\cos(2kx+\beta)}{\cosh(\tau)+\sin p\cos(2kx+\beta)}\right) \\
&= ae^{2ia^2t}\left(\frac{2i\sin p\cos p\sinh(\tau)+(1-2\sin^2 p)\cosh(\tau)-\sin p\cos(2kx+\beta)}{\cosh(\tau)+\sin p\cos(2kx+\beta)}\right) \\
&= ae^{2ia^2t}\left(\frac{i\sin(2p)\sinh(\tau)+\cos(2p)\cosh(\tau)-\sin p\cos(2kx+\beta)}{\cosh(\tau)+\sin p\cos(2kx+\beta)}\right),
\end{aligned}$$

where the trig identities $2\sin(x)\cos(x) = \sin(2x)$ and $1 - \sin^2(x) = \cos(2x)$ have been used.

Dividing by $\cosh(\tau)$ in the numerator and denominator we arrive at

$$Q(x,t) = ae^{2ia^2t}\left(\frac{i\sin(2p)\tanh(\tau) + \cos(2p) - \sin p\cos(2kx+\beta)\operatorname{sech}(\tau)}{1 + \sin p\cos(2kx+\beta)\operatorname{sech}(\tau)}\right), \tag{2.2.8}$$

which is precisely the form of the spatially periodic breather in [20] and [22].

2.3 Deriving the Peregrine Solution from the breather

To analyze the infinite line case in the same manner as the periodic case, we need the eigenfunctions and new potential for the infinite line boundary conditions. We acquire these elements by allowing the spatial period to become infinite for a fixed background amplitude.

Although a single eigenfunction at a fixed eigenvalue has been calculated for the Peregrine solution in [18], the method used in that work does not allow for multiple eigenfunctions nor eigenfunctions at any other eigenvalue. We derive a family of eigenfunctions dependent on λ that are linearly independent for $\lambda \neq \pm ia$.

2.3.1 Function expansions

We will expand in the case where $\rho = \beta = 0$. But, because $\dfrac{c_+}{c_-} = e^{\rho}e^{i\beta}$, $\rho = \beta = 0$ occurs if, and only if, $c_+ = c_-$, which does not allow ϕ to be an arbitrary linear combination of

the eigenfunctions, but rather a very specific one. Then, $\widetilde{\chi}^{\pm}$ will be eigenfunctions with the Peregrine solution as the potential.

Let $k_j = 2\pi j/L$. Then when $L \to \infty$, $k_j \to 0$ and $\nu_j \to ic$. Expansions for the terms in the expressions for A and B as $k_j \to 0$ are:

$$\begin{aligned}
\cos(p_j) &= \frac{k_j}{2a}, \\
\sigma_j &= 2ak_j - k_j^2 + \ldots, \\
\cos(2p_j) &= 2\cos^2(p_j) - 1 = -1 + \frac{k_j^2}{2a^2} + \ldots, \\
\sin(2p_j) &= 2\sin(p_j)\cos(p_j) = -\frac{k_j}{a} + \ldots, \\
\sin(p_j) &= -\sqrt{1 - \cos^2(p_j)} = -1 + \frac{k_j^2}{8a^2} + \ldots, \\
\sin(k_j x) &= k_j x + \ldots, \\
\cos(k_j x) &= 1 - \frac{k_j^2 x^2}{2} + \ldots, \\
\operatorname{sech}(\sigma_j t) &= 1 - 2k_j^2 a^2 t^2 + \ldots, \\
\tanh(\sigma_j t) &= 2k_j a t + \ldots,
\end{aligned}$$

which leads to

$$\begin{aligned}
\sin p_j \cos(k_j x)\operatorname{sech}(\sigma_j t) &= \left(-1 + \frac{k_j^2}{8a^2}\right)\left(1 - \frac{k_j^2 x^2}{2}\right)\left(1 - 2k_j^2 a^2 t^2\right) + \ldots \\
&= \left(-1 + \frac{k_j^2 x^2}{2} + 2k_j^2 a^2 t^2 + \frac{k_j^2}{8a^2}\right) + \ldots \\
&= -1 + \left(\frac{x^2}{2} + 2a^2 t^2 + \frac{1}{8a^2}\right) k_j^2 + \ldots \\
&= -1 + \left(4a^2 x^2 + 16a^4 t^2 + 1\right)\frac{k_j^2}{8a^2} + \ldots, \\
\sin(2p_j)\tanh(\sigma_j t) &= \left(-\frac{k_j}{a}\right)(2k_j a t) + \ldots = -2tk_j^2 + \ldots,
\end{aligned}$$

$$\cos(p_j)\sin(k_jx)\operatorname{sech}(\sigma_j t) = \frac{k_j}{2a}(k_jx)\left(1-2k_j^2a^2t^2\right)+\ldots = \frac{x}{2a}k_j^2+\ldots.$$

Dividing by $\cosh(\rho-\sigma t)$ and setting $\rho=\beta=0$ in (2.2.4), we have

$$A = \frac{\cos p_j \sin(k_jx)\operatorname{sech}(\sigma_j t)}{1+\sin p_j\cos(k_jx)\operatorname{sech}(\sigma_j t)}.$$

Letting $k_j \to 0$ we arrive at

$$\widetilde{A} = \lim_{k_j\to 0}\left[\frac{\frac{x}{2a}k_j^2}{\left(4a^2x^2+16a^4t^2+1\right)\frac{k_j^2}{8a^2}}+\ldots\right] = \frac{4ax}{4a^2x^2+16a^4t^2+1}. \tag{2.3.1}$$

Similarly, dividing by $\cosh(\rho-\sigma t)$ and setting $\rho=\beta=0$ in (2.2.5)

$$B = e^{2ia^2t}\frac{-\cos(p_j)\tanh(\sigma_j t)+i\sin(p_j)+i\cos(k_jx)\operatorname{sech}(\sigma_j t)}{1+\sin p_j\cos(k_jx)\operatorname{sech}(\sigma_j t)}.$$

Letting $k_j\to 0$ we obtain the expression

$$\begin{aligned}\widetilde{B} &= e^{2ia^2t}\lim_{k_j\to 0}\left[\frac{-\frac{k_j}{2a}(2k_jat)+i\left(-1+\frac{k_j^2}{8a^2}\right)+i\left(1-\frac{k_j^2x^2}{2}-2k_j^2a^2t^2\right)}{\left(4a^2x^2+16a^4t^2+1\right)\frac{k_j^2}{8a^2}}+\ldots\right]\\ &= e^{2ia^2t}\frac{-8a^2t+i\left(1-4a^2x^2-16a^4t^2\right)}{4a^2x^2+16a^4t^2+1} = e^{2ia^2t}\left(\frac{-8a^2t+2i}{4a^2x^2+16a^4t^2+1}-i\right).\end{aligned} \tag{2.3.2}$$

Recall the spatially periodic breather (1.5.3)

$$\begin{aligned}Q &= ae^{2ia^2t}\left(\frac{-i\sin(2p_j)\tanh(\sigma_j t)+\cos(2p_j)-\sin p_j\cos(k_jx)\operatorname{sech}(\sigma_j t)}{1+\sin p_j\cos(k_jx)\operatorname{sech}(\sigma_j t)}\right)\\ \widetilde{Q} &= ae^{2ia^2t}\lim_{k_j\to 0}\left[\frac{2itk_j^2+\left(-1+\frac{k_j^2}{2a^2}\right)-\left(-1+\left(4a^2x^2+16a^4t^2+1\right)\frac{k_j^2}{8a^2}\right)}{\left(4a^2x^2+16a^4t^2+1\right)\frac{k_j^2}{8a^2}}+\ldots\right]\\ &= ae^{2ia^2t}\frac{2it+\frac{1}{2a^2}-\left(4a^2x^2+16a^4t^2+1\right)\frac{1}{8a^2}}{\left(4a^2x^2+16a^4t^2+1\right)\frac{1}{8a^2}}\\ &= ae^{2ia^2t}\frac{16ia^2t+4-\left(4a^2x^2+16a^4t^2+1\right)}{\left(4a^2x^2+16a^4t^2+1\right)}\end{aligned}$$

$$= ae^{2ia^2t}\left(-1+\frac{16ia^2t+4}{4a^2x^2+16a^4t^2+1}\right). \tag{2.3.3}$$

Note that λ and k do not depend on L, so taking the limit as $L\to\infty$ (which is to say $k_j\to 0$) changes only A and B in the eigenfunctions. Thus, the limit eigenfunctions are

$$\begin{aligned}
\widetilde{\chi}^{\pm} &= \frac{i}{2k}e^{\mp i\frac{\pi}{4}}e^{\pm i\frac{p}{2}}\begin{bmatrix} \lambda+ia\widetilde{A} & ia\widetilde{B} \\ ia\widetilde{B^*} & \lambda-ia\widetilde{A}\end{bmatrix}\begin{bmatrix} ae^{ia^2t} \\ \pm ae^{\mp ip}e^{-ia^2t}\end{bmatrix}e^{\pm i(kx+2k\lambda t)} \\
&= \frac{i}{2k}e^{\mp i\frac{\pi}{4}}e^{\pm i\frac{p}{2}}\begin{bmatrix} ae^{ia^2t}\left(\lambda+ia\widetilde{A}\right)\pm ae^{\mp ip}e^{-ia^2t}\left(ia\widetilde{B}\right) \\ ae^{ia^2t}\left(ia\widetilde{B^*}\right)\pm ae^{\mp ip}e^{-ia^2t}\left(\lambda-ia\widetilde{A}\right)\end{bmatrix}e^{\pm i(kx+2k\lambda t)} \\
&= \frac{ia}{2k}e^{\mp i\frac{\pi}{4}}e^{\pm i\frac{p}{2}}\begin{bmatrix} \lambda e^{ia^2t}+iae^{ia^2t}\widetilde{A}\pm iae^{\mp ip}e^{-ia^2t}\widetilde{B} \\ \pm\lambda e^{\mp ip}e^{-ia^2t}+iae^{ia^2t}\widetilde{B^*}\mp iae^{\mp ip}e^{-ia^2t}\widetilde{A}\end{bmatrix}e^{\pm i(kx+2k\lambda t)} \\
&= \frac{ia}{2k}e^{\mp i\frac{\pi}{4}}e^{\pm i\frac{p}{2}}\begin{bmatrix} e^{ia^2t}\left(\lambda+ia\frac{4cx}{m}\pm iae^{\mp ip}\frac{-8a^2t+i\left(1-4a^2x^2-16a^4t^2\right)}{m}\right) \\ e^{-ia^2t}e^{\mp ip}\left(\pm\lambda+iae^{\pm ip}\frac{-8a^2t-i\left(1-4a^2x^2-16a^4t^2\right)}{m}\mp ia\frac{4ax}{m}\right)\end{bmatrix}e^{\pm i(kx+2k\lambda t)},
\end{aligned} \tag{2.3.4}$$

where p and a are real constants, and $m=4a^2x^2+16a^4t^2+1$.

2.4 Eigenfunction verification

Although we have previously verified the limit of the single-mode SPB is the rational solution, it remains to be shown that the limit eigenfunctions satisfy the Lax pair (1.2.1) at the limited potential.

2.4.1 Temporal component of the Lax pair

In this section we show that the eigenfunction $\widetilde{\chi}^{+}$ satisfies the time portion of the Lax pair (1.2.1). Recall the following definitions from earlier sections:

$$\widetilde{\chi}_t^{\pm} = V(Q,\lambda)\widetilde{\chi}^{\pm}, \quad \text{where} \quad V(Q,\lambda) = \begin{bmatrix} i|Q|^2 - 2i\lambda^2 & 2i\lambda Q - Q_x \\ Q_x^* + 2i\lambda Q^* & 2i\lambda^2 - i|Q|^2 \end{bmatrix},$$

$$\begin{aligned} Q &= ae^{2ia^2t}\left(-1 + \frac{16ia^2t+4}{m}\right) \\ &= \bar{Q}e^{2ia^2t}, \text{ where } \bar{Q} = -a + \frac{16ia^3t+4a}{m}, \\ k \pm \lambda &= ae^{\mp ip}, \end{aligned}$$

where p and a are real constants, and $m = 4a^2x^2 + 16a^4t^2 + 1$.

We rewrite the components of the eigenfunction in the following manner to simplify the portions that need to be carried around for the rest of the calculation.

$$\begin{aligned} \widetilde{\chi}^{+} &= \frac{ia}{2k}e^{-i\frac{\pi}{4}}e^{i\frac{p}{2}} \begin{bmatrix} e^{ia^2t}\left(-\lambda + ia\frac{4ax}{m} + iae^{-ip}\frac{-8a^2t+i\left(1-4a^2x^2-16a^4t^2\right)}{m}\right) \\ e^{-ia^2t}e^{-ip}\left(-\lambda + iae^{ip}\frac{-8a^2t-i\left(1-4a^2x^2-16a^4t^2\right)}{m} - ia\frac{4ax}{m}\right) \end{bmatrix} e^{i(kx+2k\lambda t)} \\ &\equiv \frac{ia}{2k}e^{-i\frac{\pi}{4}}e^{i\frac{p}{2}} \begin{bmatrix} e^{ia^2t}Y_1 \\ e^{-ia^2t}Y_2 \end{bmatrix} e^{i(kx+2k\lambda t)}, \end{aligned}$$

where,

$$\begin{aligned} Y_1 &= -\lambda + \frac{4ia^2x}{m} + e^{-ip}\left(\frac{-8ia^3t-2a}{m} + a\right) \\ Y_2 &= e^{-ip}\left[-\lambda - \frac{4ia^2x}{m} + e^{ip}\left(\frac{-8ia^3t+2a}{m} - a\right)\right] \end{aligned}$$

$$= e^{-ip}\left(-\lambda - \frac{4ia^2x}{m}\right) + \frac{-8ia^3t + 2a}{m} - a. \tag{2.4.1}$$

With these new definitions we see that the left hand side of the equation is

$$\left(\widetilde{\chi}^{+}\right)_t = \frac{ia}{2k}e^{-i\frac{\pi}{4}}e^{i\frac{p}{2}}\begin{bmatrix} \left(ia^2Y_1 + 2ik\lambda Y_1 + Y_{1t}\right)e^{ia^2t} \\ \left(-ia^2Y_2 + 2ik\lambda Y_2 + Y_{2t}\right)e^{-ia^2t} \end{bmatrix} e^{i(kx+2k\lambda t)}, \tag{2.4.2}$$

and the right hand side is

$$\begin{aligned} V(Q,\lambda)\widetilde{\chi}^{+} &= \frac{ia}{2k}e^{-i\frac{\pi}{4}}e^{i\frac{p}{2}}\begin{bmatrix} i|Q|^2 - 2i\lambda^2 & 2i\lambda Q - Q_x \\ Q_x^* + 2i\lambda Q^* & 2i\lambda^2 - i|Q|^2 \end{bmatrix}\begin{bmatrix} Y_1 \\ Y_2 \end{bmatrix} e^{i(kx+2k\lambda t)} \\ &= \frac{ia}{2k}e^{-i\frac{\pi}{4}}e^{i\frac{p}{2}}\begin{bmatrix} \left\{\left(i|\bar{Q}|^2 - 2i\lambda^2\right)Y_1 + \left(2i\lambda\bar{Q} - \bar{Q}_x\right)Y_2\right\}e^{ia^2t} \\ \left\{\left(\bar{Q}_x^* + 2i\lambda\bar{Q}^*\right)Y_1 + \left(2i\lambda^2 - i|\bar{Q}|^2\right)Y_2\right\}e^{-ia^2t} \end{bmatrix} e^{i(kx+2k\lambda t)}. \end{aligned} \tag{2.4.3}$$

We see that the constants, $\exp\{\pm ia^2t\}$, and $\exp\{i(kx + 2k\lambda t)\}$ are common to both (2.4.2) and (2.4.3), so they are equal if and only if

$$\begin{bmatrix} ia^2Y_1 + 2ik\lambda Y_1 + Y_{1t} \\ -ia^2Y_2 + 2ik\lambda Y_2 + Y_{2t} \end{bmatrix} = \begin{bmatrix} i|\bar{Q}|^2Y_1 - 2i\lambda^2Y_1 + 2i\lambda\bar{Q}Y_2 - \bar{Q}_xY_2 \\ 2i\lambda\bar{Q}^*Y_1 + \bar{Q}_x^*Y_1 + 2i\lambda^2Y_2 - i|\bar{Q}|^2Y_2 \end{bmatrix}.$$

We need $|\bar{Q}|^2$ and $\bar{Q}_x$ before we start multiplying things out.

$$|\bar{Q}|^2 = a^2\left[\left(-1 + \frac{4}{m}\right)^2 + \left(\frac{16a^2t}{m}\right)^2\right] = a^2 - \frac{8a^2}{m} + \frac{16a^2}{m^2} + \frac{256a^6t^2}{m^2},$$

and

$$\bar{Q}_x = \left(-\frac{16ia^3t + 4a}{m^2}m_x\right) = -\frac{128ia^5xt}{m^2} - \frac{32a^3x}{m^2}.$$

Next, we consider the derivative of Y_1 with respect to t:

$$\begin{aligned} Y_{1t} &= \frac{\partial}{\partial t}\left[\lambda + \frac{4ia^2x}{m} + e^{-ip}\left(\frac{-8ia^3t - 2a}{m} + a\right)\right] \\ &= -\frac{4ia^2x}{m^2}m_t + e^{-ip}\left(-\frac{8ia^3}{m} - \frac{-8ia^3t - 2a}{m^2}m_t\right) \\ &= -\frac{128ia^4xt}{m^2} + e^{-ip}\left(-\frac{8ia^3}{m} + \frac{256ia^5t^2 + 64a^3t}{m^2}\right). \end{aligned} \tag{2.4.4}$$

The following products are length, but necessary for the remainder of the work.

$$\begin{aligned} i|\bar{Q}|^2Y_1 &= i\left(a^2 - \frac{8a^2}{m} + \frac{16a^2}{m^2} + \frac{256a^6t^2}{m^2}\right)Y_1 \\ &= ia^2Y_1 - \lambda\left[-\frac{8ia^2}{m} + \frac{16ia^2}{m^2} + \frac{256ia^6t^2}{m^2}\right] + \frac{32a^4x}{m^2} - \frac{64a^4x}{m^3} - \frac{1024a^8xt^2}{m^3} \\ &\quad + e^{ip}\left(-\frac{64a^5t}{m^2} + \frac{32ia^3}{m^2} - \frac{16ia^3}{m} + \frac{128a^5t}{m^3} - \frac{32ia^3}{m^3} - \frac{256ia^7t^2}{m^3}\right). \end{aligned}$$

Next, we look at the $2ik\lambda Y_1$ term, but since we need ikY_1 for the spatial verification as well, we work that separately. Note that both $k = ae^{-ip} - \lambda$ and $k = ae^{ip} + \lambda$ are used to avoid introducing new powers of e^{ip} while clearing the factor of k that appears on the left hand side, but not the right hand side.

$$\begin{aligned} kY_1 &= k\left(-\lambda + \frac{4ia^2x}{m}\right) + ake^{-ip}\left(-\frac{8ia^2t}{m} - \frac{2}{m} + 1\right) \\ &= \left(ae^{-ip} - \lambda\right)\left(-\lambda + \frac{4ia^2x}{m}\right) + \left(ae^{ip} + \lambda\right)ae^{-ip}\left(-\frac{8ia^2t}{m} - \frac{2}{m} + 1\right) \\ &= -\lambda\left(-\lambda + \frac{4ia^2x}{m}\right) + ae^{-ip}\left(-\lambda + \frac{4ia^2x}{m}\right) \\ &\quad + a^2\left(-\frac{8ia^2t}{m} - \frac{2}{m} + 1\right) + \lambda ae^{-ip}\left(-\frac{8ia^2t}{m} - \frac{2}{m} + 1\right) \\ &= -\lambda Y_1 + ae^{-ip}\left[\lambda + \frac{4ia^2x}{m} - \lambda\frac{16ia^2t}{m} - \lambda\frac{4}{m}\right] + a^2\left(-\frac{8ia^2t}{m} - \frac{2}{m} + 1\right), \end{aligned} \tag{2.4.5}$$

$$2ik\lambda Y_1 = -2i\lambda^2 Y_1 + ae^{-ip}\left[2i\lambda^2 + 2i\lambda\frac{4ia^2x}{m} - 2i\lambda^2\frac{16ia^2t}{m} - 2i\lambda^2\frac{4}{m}\right] + 2ia^2\lambda\left(-\frac{8ia^2t}{m} - \frac{2}{m} + 1\right). \tag{2.4.6}$$

Because only the denominator of Q depends on x, $\bar{Q}_x$ is two terms and consequently $\bar{Q}_x Y_2$ is one of the shortest products we require for this verification.

$$\begin{aligned}
-\bar{Q}_x Y_2 &= -\left(-\frac{128ia^5xt}{m^2} - \frac{32a^3x}{m^2}\right)\left(e^{-ip}\left[-\lambda - \frac{4ia^2x}{m}\right] - \frac{8ia^3t}{m} + \frac{2a}{m} - a\right) \\
&= -e^{-ip}\left[-\lambda\left(-\frac{128ia^5xt}{m^2} - \frac{32a^3x}{m^2}\right) - \frac{512a^7x^2t}{m^3} + \frac{128ia^5x^2}{m^3}\right] \\
&\quad + \frac{1024a^8xt^2}{m^3} - \frac{32a^4x}{m^2} + \frac{64a^4x}{m^3} - \frac{128ia^6xt}{m^2} \\
&= e^{-ip}\left[\lambda\left(-\frac{128ia^5xt}{m^2} - \frac{32a^3x}{m^2}\right) + \frac{512a^7x^2t}{m^3} - \frac{128ia^5x^2}{m^3}\right] \\
&\quad + \frac{1024a^8xt^2}{m^3} - \frac{32a^4x}{m^2} + \frac{64a^4x}{m^3} - \frac{128ia^6xt}{m^2}
\end{aligned}$$

We will use $\bar{Q}Y_2$ for both the spatial and temporal verification, so we solve it separately and then multiply by the appropriate coefficient of $2i\lambda$ for the temporal part.

$$\begin{aligned}
\bar{Q}Y_2 &= a\left(-1 + \frac{16ia^2t}{m} + \frac{4}{m}\right)\left[e^{-ip}\left(-\lambda - \frac{4ia^2x}{m}\right) + a\left(-\frac{8ia^2t}{m} + \frac{2}{m} - 1\right)\right] \\
&= ae^{-ip}\left(-1 + \frac{16ia^2t}{m} + \frac{4}{m}\right)\left(-\lambda - \frac{4ia^2x}{m}\right) \\
&\quad + a^2\left(-1 + \frac{16ia^2t}{m} + \frac{4}{m}\right)\left(-\frac{8ia^2t}{m} + \frac{2}{m} - 1\right) \\
&= ae^{-ip}\left[\lambda\left(1 - \frac{16ia^2t}{m} - \frac{4}{m}\right) + \frac{4ia^2x}{m} + \frac{64a^4xt}{m} - \frac{16ia^2x}{m}\right] \\
&\quad + a^2\left[-\frac{8ia^2t}{m} - \frac{6}{m} + 1 + \frac{128a^4t^2}{m^2} + \frac{8}{m^2}\right], \qquad (2.4.7) \\
2i\lambda\bar{Q}Y_2 &= ae^{-ip}\left[2i\lambda^2\left(1 - \frac{16ia^2t}{m} - \frac{4}{m}\right) + 2i\lambda\left(\frac{64a^4xt}{m} - \frac{12ia^2x}{m}\right)\right]
\end{aligned}$$

$$+ 2ia^2\lambda\left[-\frac{8ia^2t}{m} - \frac{6}{m} + 1 + \frac{128a^4t^2}{m^2} + \frac{8}{m^2}\right].$$

Summing (2.4.4) and (2.4.6) we have

$$LHS = e^{-ip}\left(\lambda^2\left\{\frac{-32a^3t + 8ia}{m} - 2ia\right\} - \lambda\frac{8a^3x}{m} - \frac{8ia^3}{m} + \frac{256ia^5t^2 + 64a^3t}{m^2}\right)$$
$$+ ia^2Y_1 + 2i\lambda^2Y_1 + \lambda\left(\frac{16a^4t - 4ia^2}{m} + 2ia^2\right) - \frac{128ia^4xt}{m^2}.$$

The λ and λ^2 terms on both side of the equation match, and the λ^0 terms are verified similarly.

2.4.2 Spatial component of the Lax pair

In this section we show that the eigenfunction $\widetilde{\chi}^+$ satisfies the time portion of the Lax pair (1.2.1). We seek to show that $\widetilde{\chi}^+$ satisfies

$$\widetilde{\chi}^{\pm}_x = U(Q,\lambda)\widetilde{\chi}^{\pm}, \quad \text{where} \quad U(Q,\lambda) = \begin{bmatrix} -i\lambda & iQ \\ iQ^* & i\lambda \end{bmatrix}$$

Using the definitions of Y_1 and Y_2 from (2.4.1) the two sides of the equation can be formulated as

$$\left(\widetilde{\chi}^+\right)_x = \frac{ia}{2k}e^{-i\frac{\pi}{4}}e^{i\frac{p}{2}}\begin{bmatrix} ikY_1 + Y_{1x} \\ ikY_2 + Y_{2x} \end{bmatrix} e^{i(kx+2k\lambda t)}, \tag{2.4.8}$$

and

$$U(Q,\lambda)\widetilde{\chi}^+ = \frac{ia}{2k}e^{-i\frac{\pi}{4}}e^{i\frac{p}{2}}\begin{bmatrix} -i\lambda & iQ \\ iQ^* & i\lambda \end{bmatrix}\begin{bmatrix} Y_1 \\ Y_2 \end{bmatrix} e^{i(kx+2k\lambda t)}$$

$$= \frac{ia}{2k} e^{-i\frac{\pi}{4}} e^{i\frac{p}{2}} \begin{bmatrix} -i\lambda Y_1 + iQY_2 \\ iQ^* Y_1 + i\lambda Y_2 \end{bmatrix} e^{i(kx+2k\lambda t)}. \tag{2.4.9}$$

We see that the constants and $\exp\{i(kx + 2k\lambda t)\}$ are common to both (2.4.8) and (2.4.9), so they are equal if and only if

$$\begin{bmatrix} ikY_1 + Y_{1x} \\ ikY_2 + Y_{2x} \end{bmatrix} = \begin{bmatrix} -i\lambda Y_1 + iQY_2 \\ iQ^* Y_1 + i\lambda Y_2 \end{bmatrix}$$

$$\begin{aligned} Y_{1x} &= \left(ia\frac{d}{dx}\left[\frac{4ax}{m}\right] + iae^{-ip}\frac{d}{dx}\left[\frac{-8a^2t + 2i}{m} - i\right]\right) \\ &= ia\left(\frac{4a}{m} - \frac{32a^3x^2}{m^2} + e^{-ip}\left[\frac{64a^4xt}{m^2} - \frac{16ia^2x}{m^2}\right]\right) \end{aligned}$$

Using (2.4.5) we see that

$$ikY_1 = -i\lambda Y_1 + ia\left\{e^{-ip}\left[\lambda\left(1 - \frac{16ia^2t}{m} - \frac{4}{m}\right) + \frac{4ia^2x}{m}\right] + a\left(-\frac{8ia^2t}{m} - \frac{2}{m} + 1\right)\right\}$$

$$\begin{aligned} Y_{1x} + ikY_1 &= -i\lambda Y_1 + iae^{-ip}\left[\lambda\left(1 - \frac{16ia^2t}{m} - \frac{4}{m}\right) + \frac{64a^4xt}{m^2} - \frac{16ia^2x}{m^2} + \frac{4ia^2x}{m}\right] \\ &\quad + ia^2\left[1 - \frac{2}{m} - \frac{8iat}{m} + \frac{4}{m} - \frac{32a^2x^2}{m^2}\right] \\ &= -i\lambda Y_1 + ia\left[\lambda\left(1 - \frac{16ia^2t}{m} - \frac{4}{m}\right) + \frac{64a^4xt}{m^2} - \frac{16ia^2x}{m^2} + \frac{4ia^2x}{m}\right] \\ &\quad + ia^2\left[1 - \frac{6}{m} - \frac{8ia^2t}{m} + \frac{8(m - 4a^2x^2)}{m^2}\right] \\ &= -i\lambda Y_1 + ia\left[\lambda\left(1 - \frac{16ia^2t}{m} - \frac{4}{m}\right) + \frac{64a^4xt}{m^2} - \frac{16ia^2x}{m^2} + \frac{4ia^2x}{m}\right] \\ &\quad + ia^2\left[1 - \frac{6}{m} - \frac{8ia^2t}{m} + \frac{8(1 + 16a^4t^2)}{m^2}\right] \end{aligned}$$

$$= -i\lambda Y_1 + i\bar{Q}Y_2 \text{ by (2.4.7)}$$

Now that we have the transformed eigenfunctions and potential for the infinite line case we can proceed to determining the stability for both solutions.

CHAPTER 3

STABILITY

In this chapter we study the stability of the classes of solutions we have chosen as rogue wave models as discussed in section 1.5. We have already considered the linear instability of the Stokes' wave in section 1.3. Recall that we linearized about the solution and we were able to determine the growth rates of the instabilities. With more complicated solutions that technique and determining the growth rate of the instabilities precisely are much more difficult. Instead, we now look at the behavior of certain quantities related to the scattering problem as they are evolved by the linearized PDE.

Using this technique we show that the single-mode SPB is stable if it is on an interval that only allows one complex double point, but that any solution with a (a, L) combination that permits two or more complex double points has a λ which allows for unbounded growth of the perturbation, so the solution is unstable. Recall that for a fixed a, as the length of the period increases the number of complex double points increases. From this, we conjecture that the rational solution is unstable, and in fact we show this is true in the final section of the chapter.

3.1 Squared eigenfunctions and linearized stability

Rather than solving the linearized NLS (3.1.2) directly, which can be challenging with more complicated solutions, we exploit the connection between the solutions of the linearized NLS and the squared components of the eigenfunctions of the Lax pair [23] [24]. We use the transformed eigenfunctions to construct squared eigenfunctions that satisfy the linearized NLS. Since we know the perturbation to the solution solves the linearized NLS the growth of the squared eigenfunctions, or lack thereof, tells us the instability or stability of the perturbed solution.

Let $u = u_a(1+\epsilon)$, where $\epsilon(x,t)$ is a complex-valued function with small magnitude. We are interested in determining the behavior of this perturbation to the solution u_a. If ϵ stays small for all t, then the perturbed solution is near to the original solution, so we say the original solution is stable to small perturbations. If the perturbation is initially small but grows as t changes, we say the original solution is unstable.

Note that if we substitute $u = u_a(1+\epsilon)$ into (1.1.7) and keeping only the linear terms in ϵ we see that the required terms in the equation are

$$\begin{aligned} u_t &= (u_a)_t(1+\epsilon) + u_a\epsilon_t \\ &= 2ia^2u_a(1+\epsilon) + u_a\epsilon_t \\ u_{xx} &= (u_a)_{xx}(1+\epsilon) + 2(u_a)_x\epsilon_x + u_a\epsilon_{xx} \\ &= u_a\epsilon_{xx} \text{ since } u_a \text{ is independent of } x, \end{aligned}$$

$$|u|^2u = |u_a|^2u_a(1+\epsilon+\epsilon^*)(1+\epsilon)$$

$$= u_a(a^2 + 2a^2\epsilon + a^2\epsilon^* + \mathcal{O}\left(\epsilon^2\right))$$

Substituting these into NLS we have

$$u_a(-2a^2 - 2a^2\epsilon + i\epsilon_t + \epsilon_{xx} + 2a^2 + 4a^2\epsilon + 2a^2\epsilon^*) = 0 \tag{3.1.1}$$

$$i\epsilon_t + \epsilon_{xx} + 2a^2(\epsilon + \epsilon^*), \tag{3.1.2}$$

which is the linearized NLS equation.

$$\begin{cases} iu_t &= -u_{xx} + 2u^2r \\ ir_t &= r_{xx} - 2r^2u \end{cases}. \tag{3.1.3}$$

Notice that in order to make the first equation match the form of NLS we are using (1.1.7) we need to have $r = -u^*$. In this case, a Lax pair for NLS can be rewritten as a Lax pair for the system of equations as

$$U(u,r,\lambda) = \begin{bmatrix} -i\lambda & u \\ r & i\lambda \end{bmatrix} \qquad V(u,r,\lambda) = \begin{bmatrix} -iur - 2i\lambda^2 & -u_x + 2i\lambda u \\ -r_x - 2i\lambda r & iur + 2i\lambda^2 \end{bmatrix}. \tag{3.1.4}$$

We say that ϕ is an eigenfunction associated with λ if $\phi_x = U(u,r,\lambda)\phi$ and $\phi_t = V(u,r,\lambda)\phi$.

Let $\tilde{u} = u + w$ and $\tilde{r} = r + v$, where u and r satisfy the NLS system. Substituting this into (3.1.3) and keeping only the first order terms in v and w we have

$$\begin{cases} iw_t &= -w_{xx} + 2u^2v + 4urw \\ iv_t &= v_{xx} - 2r^2w - 4urv \end{cases} \tag{3.1.5}$$

Next, we define the squared components of interest. Let $\phi = [\phi_1, \phi_2]^T$ and $\psi = [\psi_1, \psi_2]^T$ be eigenfunctions associated with the eigenvalue λ. These two solutions do not have to be distinct.

We define f, g, and h as

$$\begin{bmatrix} f \\ g \\ h \end{bmatrix} = \begin{bmatrix} \frac{1}{2}(\phi_1\psi_2 + \phi_2\psi_1) \\ \phi_1\psi_1 \\ -\phi_2\psi_2 \end{bmatrix}$$

and we translate the coupled Lax pair (3.1.4) to a system in terms of the squared components of the eigenfunctions. We begin by examining the behavior of the spatial derivatives of f, g, and h.

$$\begin{aligned}
2f_x &= \phi_{1x}\psi_2 + \phi_1\psi_{2x} + \phi_{2x}\psi_1 + \phi_2\psi_{1x} \\
&= (-i\lambda\phi_1 + iu\phi_2)\psi_2 + \phi_1(-ir\psi_1 + i\lambda\psi_2) + (-ir\phi_1 + i\lambda\phi_2)\psi_1 + \phi_2(-i\lambda\psi_1 + iu\psi_2) \\
&= -i\lambda\phi_1\psi_2 + iu\phi_2\psi_2 - ir\phi_1\psi_1 + i\lambda\phi_1\psi_2 - ir\phi_1\psi_1 + i\lambda\phi_2\psi_1 - i\lambda\phi_2\psi_1 + iu\phi_2\psi_2 \\
&= 2iu\phi_2\psi_2 - 2ir\phi_1\phi_2 = -2iuh - 2irg \\
f_x &= -irg - iuh \\
g_x &= \phi_{1x}\psi_1 + \phi_1\psi_{1x} \\
&= -i\lambda\phi_1\psi_1 + iu\phi_2\psi_1 - i\lambda\phi_1\psi_1 + iu\phi_1\psi_2 \\
&= -2i\lambda\phi_1\psi_1 + 2iu\left[\tfrac{1}{2}(\phi_1\psi_2 + \phi_2\psi_1)\right] \\
&= -2i\lambda g + 2iuf \\
-h_x &= \phi_{2x}\psi_2 + \phi_2\psi_{2x}
\end{aligned}$$

$$= -ir\phi_1\psi_2 + i\lambda\phi_2\psi_2 - ir\phi_2\psi_1 + i\lambda\phi_2\psi_2$$

$$= 2i\lambda\phi_2\psi_2 - 2ir\left[\tfrac{1}{2}(\phi_1\psi_2 + \phi_2\psi_1)\right]$$

$$h_x = 2irf + 2i\lambda h$$

So that

$$\begin{bmatrix} f \\ g \\ h \end{bmatrix}_x = \begin{bmatrix} 0 & -ir & -iu \\ 2iu & -2i\lambda & 0 \\ 2ir & 0 & 2i\lambda \end{bmatrix} \begin{bmatrix} f \\ g \\ h \end{bmatrix}.$$

We follow the same procedure for the time derivatives.

$$2f_t = \phi_{1t}\psi_2 + \phi_1\psi_{2t} + \phi_{2t}\psi_1 + \phi_2\psi_{1t}$$

$$= -i(ur + 2\lambda^2)\phi_1\psi_2 - (u_x - 2i\lambda u)\phi_2\psi_2 + (-2i\lambda r - r_x)\phi_1\psi_1 + i(2\lambda^2 + ur)\phi_1\psi_2$$

$$+ (-2i\lambda r - r_x)\phi_1\psi_1 + i(2\lambda^2 + ur)\phi_2\psi_1 - i(ur + 2\lambda^2)\phi_2\psi_1 - (u_x - 2i\lambda u)\phi_2\psi_2$$

$$= 2(-2i\lambda r - r_x)\phi_1\psi_1 - 2(u_x - 2i\lambda u)\phi_2\psi_2$$

$$= 2(-2i\lambda r - r_x)g + 2(u_x - 2i\lambda u)h$$

$$f_t = (-2i\lambda r - r_x)g + (u_x - 2i\lambda u)h$$

$$g_t = \phi_{1t}\psi_1 + \phi_1\psi_{1t}$$

$$= -i(2\lambda^2 + ur)\phi_1\psi_1 - (u_x - 2i\lambda u)\phi_2\psi_1 - i(2\lambda^2 + ur)\phi_1\psi_1 - (u_x - 2i\lambda u)\phi_1\psi_2$$

$$= -(u_x - 2i\lambda u)(\phi_1\psi_2 + \phi_2\psi_1) - 2i(2\lambda^2 + ur)\phi_1\psi_1$$

$$= -2(u_x - 2i\lambda u)f - 2i(2\lambda^2 + ur)g$$

$$-h_t = \phi_{2t}\psi_2 + \phi_2\psi_{2t}$$

$$= -(r_x + 2i\lambda r)\phi_1\psi_2 + i(2\lambda^2 + ur)\phi_2\psi_2 - (r_x + 2i\lambda r)\phi_2\psi_1 + i(2\lambda^2 + ur)\phi_2\psi_2$$

$$= -(r_x + 2i\lambda r)(\phi_1\psi_2 + \phi_2\psi_1) - 2i(2\lambda^2 + ur)(-\phi_2\psi_2)$$

$$h_t = 2(r_x + 2i\lambda r)f + 2i(2\lambda^2 + ur)h$$

Collecting these into a system, the time derivatives of the squared eigenfunctions form the linear system of differential equations

$$\begin{bmatrix} f \\ g \\ h \end{bmatrix}_t = \begin{bmatrix} 0 & -(2i\lambda r + r_x) & (u_x - 2i\lambda u) \\ 2(2i\lambda u - u_x) & -2i(2\lambda^2 + ur) & 0 \\ 2(r_x + 2i\lambda r) & 0 & 2i(2\lambda^2 + ur) \end{bmatrix} \begin{bmatrix} f \\ g \\ h \end{bmatrix}$$

Lemma 3.1.1. *$w = g$, $v = h$ solves* (3.1.5).

Proof. This claim can be rewritten as a verification that

$$\begin{cases} ig_t + g_{xx} &= 2u^2h + 4urg \\ ih_t - h_{xx} &= -2r^2g - 4urh \end{cases}$$

We know g_t and h_t from the work above. To find g_{xx} and h_{xx} we begin with g_x and h_x and use the other spatial derivatives we have already calculated.

$$ig_t = -2i(u_x - 2i\lambda u)f + 2(2\lambda^2 + ur)g$$

$$= -2iu_xf - 4\lambda uf + 4\lambda^2 g + 2urg$$

$$g_{xx} = \frac{\partial}{\partial x}(-2i\lambda g + 2iuf)$$

$$= -2i\lambda g_x + 2iu_xf + 2iuf_x$$

$$= -2i\lambda(-2i\lambda g + 2iuf) + 2iu_xf + 2iu(-irg - iuh)$$

$$= -4\lambda^2 g + 4\lambda u f + 2iu_x f + 2urg + 2u^2 h$$

$$\implies ig_t + g_{xx} = 4urg + 2u^2 h$$

$$ih_t = 2i(r_x + 2i\lambda r)f - 2(2\lambda^2 + ur)h$$

$$= 2ir_x f - 4\lambda r f - 4\lambda^2 h - 2urh$$

$$h_{xx} = \tfrac{\partial}{\partial x}\left(2i\lambda h + 2irf\right)$$

$$= 2i\lambda h_x + 2ir_x f + 2irf_x$$

$$= 2i\lambda(2irf + 2i\lambda h) + 2ir_x f + 2ir(-irg - iuh)$$

$$= -4\lambda r f - 4\lambda^2 h + 2ir_x f + 2r^2 g + 2urh$$

$$\implies ih_t - h_{xx} = -2urh - (2r^2 g + 2urh) = -2r^2 g - 4urh$$

Hence, both equations are satisfied, so $w = g$, $v = h$ solves (3.1.5). □

Lemma 3.1.2. *Let u be one of the following particular sums of the squared components of the eigenfunctions: $q = \phi_1\psi_1 + \phi_2^*\psi_2^*$, or $q = i\left(\phi_1\psi_1 - \phi_2^*\psi_2^*\right)$. Then q solves*

$$iq_t + q_{xx} + 2u^2 q^* + 4|u|^2 q = 0.$$

Proof. To use the work in Lemma 3.1.1, we translate this problem into the variables we have been using. Recall that $r = -u^*$, so $r^* = -u$, $(r^*)^2 = u^2$ and $(ur)^* = u^*(-u) = u(-u^*) = ur$. The equation we seek to verify is $iq_t + q_{xx} + 2u^2 q^* - 4urq = 0$, and the first claim is that

$q = g - h^*$ is a solution. Note that

$$\begin{aligned} iq_t + q_{xx} &= ig_t - ih_t^* + g_{xx} - h_{xx}^* \\ &= (ig_t + g_{xx}) + (-ih_t^* - h_{xx}^*) \\ &= (ig_t + g_{xx}) + (ih_t - h_{xx})^* \\ &= 4urg + 2u^2h + (-2r^2g - 4urh)^* \\ &= 4urg + 2u^2h - 2u^2g^* - 4urh^* \\ &= -2u^2(g - h^*)^* + 4ur(g - h^*) \\ &= -2u^2q^* + 4urq. \end{aligned}$$

The other solution we seek to verify is $q = i(g + h^*)$. Note that

$$\begin{aligned} iq_t + q_{xx} &= i\left[ig_t + ih_t^* + g_{xx} + h_{xx}^*\right] \\ &= i\left[(ig_t + g_{xx}) - (-ih_t^* - h_{xx}^*)\right] \\ &= i\left[(ig_t + g_{xx}) - (ih_t - h_{xx})^*\right] \\ &= i\left[4urg + 2u^2h - (-2r^2g - 4urh)^*\right] \\ &= i\left[4urg + 2u^2h + 2u^2g^* + 4urh^*\right] \\ &= -2iu^2(g + h^*)^* + 4iur(g + h^*) \\ &= -2u^2q^* + 4urq. \end{aligned}$$

In both cases the proposed solution solves the linearized NLS equation. □

3.2 Investigating the stability of the single-mode SPB

The work on squared eigenfunctions for the single-mode SPB has been done in [6] for the NLS, albeit for a different Lax pair. Let ν be an imaginary double point of the spectrum of the plane-wave, i.e. $\nu = j\pi/L$ for some $j \in \mathbb{Z}$. We examine the transformed eigenfunctions built at ν and as a function of another complex double point of the spectrum of the plane-wave, λ. We consider two distinct cases: (i) $\lambda = \nu$, and (ii) $\lambda \neq \nu$. We define the relationship between ν and the wave number k as $\pm k - \lambda = \pm a e^{\mp ip}$. The arbitrary linear combination of the eigenfunctions evaluated at ν is ϕ, i.e.

$$\begin{aligned}
\phi = \begin{bmatrix} \phi_1 \\ \\ \phi_2 \end{bmatrix} &= c_+\phi^+(\nu) + c_-\phi^-(\nu) \qquad (3.2.1)\\
&= c_- \left(e^{\rho}e^{i\beta}\phi^+(\nu) + \phi^-(\nu)\right) \\
&= \frac{iac_-}{2k} \begin{bmatrix} \left(e^{\rho}e^{i\beta}e^{-i\frac{\pi}{4}}e^{i\frac{p}{2}}e^{i(kx-2k\nu t)} + e^{i\frac{\pi}{4}}e^{-i\frac{p}{2}}e^{-i(kx-2k\nu t)}\right)e^{ia^2t} \\ \left(e^{\rho}e^{i\beta}e^{-i\frac{\pi}{4}}e^{-i\frac{p}{2}}e^{i(kx-2k\nu t)} - e^{i\frac{\pi}{4}}e^{i\frac{p}{2}}e^{-i(kx-2k\nu t)}\right)e^{-ia^2t} \end{bmatrix}.
\end{aligned}$$

The Gauge matrix,

$$\begin{aligned}
G(\lambda;\nu,\phi) &= \begin{bmatrix} \lambda - \nu\frac{|\phi_1|^2}{|\phi_1|^2+|\phi_2|^2} - \nu^*\frac{|\phi_2|^2}{|\phi_1|^2+|\phi_2|^2} & -(\nu-\nu^*)\frac{\phi_1\phi_2^*}{|\phi_1|^2+|\phi_2|^2} \\ -(\nu-\nu^*)\frac{\phi_1^*\phi_2}{|\phi_1|^2+|\phi_2|^2} & \lambda - \nu\frac{|\phi_2|^2}{|\phi_1|^2+|\phi_2|^2} - \nu^*\frac{|\phi_1|^2}{|\phi_1|^2+|\phi_2|^2} \end{bmatrix} \\
&= \begin{bmatrix} \lambda - \nu\frac{|\phi_1|^2-|\phi_2|^2}{|\phi_1|^2+|\phi_2|^2} & -\frac{2\nu\phi_1\phi_2^*}{|\phi_1|^2+|\phi_2|^2} \\ -\frac{2\nu\phi_1^*\phi_2}{|\phi_1|^2+|\phi_2|^2} & \lambda + \nu\frac{|\phi_1|^2-|\phi_2|^2}{|\phi_1|^2+|\phi_2|^2} \end{bmatrix},
\end{aligned}$$

transforms the eigenfunctions $\phi^{\pm}$ for the solution q into the new eigenfunctions, $\chi^{\pm}$ for the new solution Q found by using the Bäcklund transformation. If we define A and B as in

(2.2.2) then we can rewrite the Gauge matrix as

$$G(\lambda;\nu,\phi) = \begin{bmatrix} \lambda - \nu A & -\nu B \\ -\nu B^* & \lambda + \nu A \end{bmatrix}. \tag{3.2.2}$$

Recall that ϕ_1 and ϕ_2 are already evaluated at ν so they are independent of λ.

We now construct the new eigenfunctions for the spatially periodic breather solution using the eigenfunctions of the plane-wave. To do so, we need to evaluate the Gauge matrix so we must find A and B. To do so, we need the components $|\phi_1|^2$, $|\phi_2|^2$, and $\phi_1\phi_2^*$. Let $\sigma = -4ik\nu$. Since $k \in \mathbb{R}$ and ν is purely imaginary, $\sigma \in \mathbb{R}$. Then,

$$\begin{aligned}
\phi_1 &= \frac{iac_-}{2k}\left(e^{\rho}e^{i\beta}e^{-i\frac{\pi}{4}}e^{i\frac{p}{2}}e^{i(kx-2k\nu t)} + e^{i\frac{\pi}{4}}e^{-i\frac{p}{2}}e^{-i(kx-2k\nu t)}\right)e^{ia^2t},\\
\phi_1^* &= \frac{-iac_-^*}{2k}\left(e^{\rho}e^{-i\beta}e^{i\frac{\pi}{4}}e^{-i\frac{p}{2}}e^{-i(kx+2k\nu t)} + e^{-i\frac{\pi}{4}}e^{i\frac{p}{2}}e^{i(kx+2k\nu t)}\right)e^{-ia^2t},\\
|\phi_1|^2 &= \frac{a^2|c_-|^2}{4k^2}\left(e^{2\rho}e^{-4ik\nu t} + e^{\rho}e^{i\beta}e^{-i\frac{\pi}{2}}e^{ip}e^{2ikx} + e^{\rho}e^{-i\beta}e^{i\frac{\pi}{2}}e^{-ip}e^{-2ikx} + e^{4ik\nu t}\right).
\end{aligned}$$

Next,

$$\begin{aligned}
\phi_2 &= \frac{iac_-}{2k}\left(e^{\rho}e^{i\beta}e^{-i\frac{\pi}{4}}e^{-i\frac{p}{2}}e^{i(kx-2k\nu t)} - e^{i\frac{\pi}{4}}e^{i\frac{p}{2}}e^{-i(kx-2k\nu t)}\right)e^{-ia^2t},\\
\phi_2^* &= \frac{-iac_-^*}{2k}\left(e^{\rho}e^{-i\beta}e^{i\frac{\pi}{4}}e^{i\frac{p}{2}}e^{-i(kx+2k\nu t)} - e^{-i\frac{\pi}{4}}e^{-i\frac{p}{2}}e^{i(kx+2k\nu t)}\right)e^{ia^2t},\\
|\phi_2|^2 &= \frac{a^2|c_-|^2}{4k^2}\left(e^{2\rho}e^{-4ik\nu t} - e^{\rho}e^{i\beta}e^{-i\frac{\pi}{2}}e^{-ip}e^{2ikx} - e^{\rho}e^{-i\beta}e^{i\frac{\pi}{2}}e^{ip}e^{-2ikx} + e^{4ik\nu t}\right)\\
&= \frac{a^2|c_-|^2}{4k^2}e^{\rho}\left(e^{\rho}e^{-4ik\nu t} - e^{i(2kx+\beta-p-\frac{\pi}{2})} - e^{-i(2kx+\beta-p-\frac{\pi}{2})} + e^{-\rho}e^{4ik\nu t}\right)\\
&= \frac{a^2|c_-|^2}{4k^2}e^{\rho}\left(e^{\rho-\sigma t} - 2\cos(2kx+\beta-p-\tfrac{\pi}{2}) + e^{-(\rho-\sigma t)}\right).
\end{aligned}$$

Now the denominator of both A and B is

$$|\phi_1|^2 + |\phi_2|^2 = \frac{a^2|c_-|^2}{4k^2}\left[2e^{2\rho}e^{-4ik\nu t} + \left(e^{ip} - e^{-ip}\right)e^{\rho}e^{i\beta}e^{-i\frac{\pi}{2}}e^{2ikx}\right.$$

$$
\begin{aligned}
&\quad - \left(e^{ip} - e^{-ip}\right) e^{\rho} e^{-i\beta} e^{i\frac{\pi}{2}} e^{-2ikx} + 2e^{4ik\nu t}\Big] \\
&= \frac{a^2|c_-|^2}{2k^2} e^{\rho} \left[e^{\rho} e^{-4ik\nu t} + e^{-\rho} e^{4ik\nu t} + i\sin(p)\left(e^{i(2kx+\beta-\frac{\pi}{2})} - e^{i(2kx+\beta-\frac{\pi}{2})}\right)\right] \\
&= \frac{a^2|c_-|^2}{2k^2} e^{\rho} \left[e^{\rho-\sigma t} + e^{-(\rho-\sigma t)} - 2\sin(p)\sin(2kx+\beta-\frac{\pi}{2})\right] \\
&= \frac{a^2|c_-|^2}{k^2} e^{\rho} \left[\cosh\left(\rho-\sigma t\right) + \sin(p)\cos(2kx+\beta)\right].
\end{aligned}
$$

For the numerator of A we find

$$
\begin{aligned}
|\phi_1|^2 - |\phi_2|^2 &= \frac{a^2|c_-|^2}{4k^2} \left[e^{\rho} e^{i\beta} e^{-i\frac{\pi}{2}} \left(e^{ip} + e^{-ip}\right) e^{2ikx} + e^{\rho} e^{-i\beta} e^{i\frac{\pi}{2}} \left(e^{ip} + e^{-ip}\right) e^{-2ikx}\right] \\
&= \frac{a^2|c_-|^2}{2k^2} e^{\rho} \cos(p) \left[e^{i\beta} e^{-i\frac{\pi}{2}} e^{2ikx} + e^{-i\beta} e^{i\frac{\pi}{2}} e^{-2ikx}\right] \\
&= \frac{a^2|c_-|^2}{k^2} e^{\rho} \cos(p) \cos\left(2kx+\beta-\frac{\pi}{2}\right) \\
&= \frac{a^2|c_-|^2}{k^2} e^{\rho} \cos(p) \sin\left(2kx+\beta\right),
\end{aligned}
$$

and for the numerator of B we have

$$
\begin{aligned}
2\phi_1\phi_2^* &= \frac{a^2|c_-|^2}{4k^2} \left[e^{2\rho} e^{ip} e^{2ik\nu t} - e^{\rho} e^{i\beta} e^{-i\frac{\pi}{2}} e^{2ikx} + e^{\rho} e^{-i\beta} e^{i\frac{\pi}{2}} e^{-2ikx} - e^{-ip} e^{4ik\nu t}\right] \\
&= \frac{a^2|c_-|^2}{2k^2} e^{\rho} \left[e^{\rho-\sigma t+ip} - e^{i\left(2kx+\beta-\frac{\pi}{2}\right)} + e^{-i\left(2kx+\beta-\frac{\pi}{2}\right)} - e^{-(\rho-\sigma t+ip)}\right] \\
&= \frac{a^2|c_-|^2}{k^2} e^{\rho} \left[\sinh\left(\rho-\sigma t+ip\right) - i\sin\left(2kx+\beta-\frac{\pi}{2}\right)\right] \\
&= \frac{a^2|c_-|^2}{k^2} e^{\rho} \left[\cosh\left(\rho-\sigma t\right)\sinh(ip) + \sinh\left(\rho-\sigma t\right)\cosh(ip) + i\cos\left(2kx+\beta\right)\right] \\
&= \frac{a^2|c_-|^2}{k^2} e^{\rho} \left[i\sin(p)\cosh\left(\rho-\sigma t\right) + \cos(p)\sinh\left(\rho-\sigma t\right) + i\cos\left(2kx+\beta\right)\right].
\end{aligned}
$$

Finally, we construct A and B as

$$
\begin{aligned}
A &= \frac{|\phi_1|^2 - |\phi_2|^2}{|\phi_1|^2 + |\phi_2|^2} \\
&= \frac{\cos(p)\sin\left(2kx+\beta\right)}{\cosh\left(\rho-\sigma t\right) + \sin(p)\cos(2kx+\beta)},
\end{aligned}
$$

$$B = \frac{2\phi_1\phi_2^*}{|\phi_1|^2 + |\phi_2|^2}$$
$$= e^{2ia^2t}\frac{i\sin(p)\cosh(\rho - \sigma t) + \cos(p)\sinh(\rho - \sigma t) + i\cos(2kx + \beta)}{\cosh(\rho - \sigma t) + \sin(p)\cos(2kx + \beta)}.$$

So the new eigenfunctions are

$$\chi^{\pm}(\lambda;\nu,\phi) = G(\lambda;\nu,\phi)\phi^{\pm}(\lambda)$$
$$= \frac{ia}{2\hat{k}}e^{\mp i\frac{\pi}{4}}e^{\pm i\frac{\hat{p}}{2}}\begin{bmatrix} \lambda - \nu A & -\nu B \\ -\nu B^* & \lambda + \nu A \end{bmatrix}\begin{bmatrix} e^{ia^2t} \\ \pm e^{\mp i\hat{p}}e^{-ia^2t} \end{bmatrix}e^{\pm i(\hat{k}x + 2\hat{k}\lambda t)}$$

where $\hat{k}(\lambda) \pm \lambda = ae^{\mp i\hat{p}}$.

3.2.1 Case 1: repeated eigenvalue

Note that when $\lambda = \nu$, the Gauge matrix reduces to

$$G(\nu;\nu,\phi) = \begin{bmatrix} \nu - \nu\frac{|\phi_1|^2 - |\phi_2|^2}{|\phi_1|^2 + |\phi_2|^2} & -\frac{2\nu\phi_1\phi_2^*}{|\phi_1|^2 + |\phi_2|^2} \\ -\frac{2\nu\phi_1^*\phi_2}{|\phi_1|^2 + |\phi_2|^2} & \nu + \nu\frac{|\phi_1|^2 - |\phi_2|^2}{|\phi_1|^2 + |\phi_2|^2} \end{bmatrix}$$
$$= \frac{2\nu}{|\phi_1|^2 + |\phi_2|^2}\begin{bmatrix} |\phi_2|^2 & -\phi_1\phi_2^* \\ -\phi_1^*\phi_2 & |\phi_1|^2 \end{bmatrix}. \tag{3.2.3}$$

When we take the determinant of (3.2.3) we see that

$$\det\Big(G(\nu;\nu,\phi)\Big) = \frac{2\nu}{|\phi_1|^2 + |\phi_2|^2}\begin{vmatrix} |\phi_2|^2 & -\phi_1\phi_2^* \\ -\phi_1^*\phi_2 & |\phi_1|^2 \end{vmatrix}$$

$$= \frac{2\nu}{|\phi_1|^2 + |\phi_2|^2} \left(|\phi_1|^2 |\phi_2|^2 - (\phi_1 \phi_2^*)(\phi_1^* \phi_2) \right)$$
$$= \frac{2\nu}{|\phi_1|^2 + |\phi_2|^2} \left(|\phi_1|^2 |\phi_2|^2 - |\phi_1|^2 |\phi_2|^2 \right) = 0.$$

Recall that the new eigenfunctions, $\chi^{\pm}$ are formed as

$$\chi^{\pm}(\nu; \nu, \phi) = G(\nu; \nu, \phi)\phi^{\pm}(\nu).$$

Since $\det\Big(G(\nu; \nu, \phi)\Big) = 0$, χ^+ and χ_- are linearly dependent. Therefore, it is sufficient to examine only one of the eigenfunctions, we look at the behavior of χ^+. In the case of using a repeated eigenvalue we have

$$\chi^+(\nu; \nu, \phi) = \frac{2\nu}{|\phi_1|^2 + |\phi_2|^2} \begin{bmatrix} |\phi_2|^2 & -\phi_1 \phi_2^* \\ -\phi_1^* \phi_2 & |\phi_1|^2 \end{bmatrix} \begin{bmatrix} \phi_1^+ \\ \phi_2^+ \end{bmatrix}$$
$$= \frac{2\nu}{|\phi_1|^2 + |\phi_2|^2} \begin{bmatrix} |\phi_2|^2 \phi_1^+ - \phi_1 \phi_2^* \phi_2^+ \\ -\phi_1^* \phi_2 \phi_1^+ + |\phi_1|^2 \phi_2^+ \end{bmatrix}$$
$$= \frac{2\nu}{|\phi_1|^2 + |\phi_2|^2} \begin{bmatrix} \phi_2^* \left(\phi_2 \phi_1^+ - \phi_1 \phi_2^+ \right) \\ -\phi_1^* \left(\phi_2 \phi_1^+ + \phi_1 \phi_2^+ \right) \end{bmatrix}.$$

Recall that ϕ is the linear combination of ϕ^+ and ϕ^- as formed in (3.2.1), so the quantity in parenthesis above can be rewritten as

$$\phi_2 \phi_1^+ - \phi_1 \phi_2^+ = \left(c_+ \phi_2^+ + c_- \phi_2^- \right) \phi_1^+ - \left(c_+ \phi_1^+ + c_- \phi_1^- \right) \phi_2^+$$
$$= c^+ \phi_1^+ \phi_2^+ + c_- \phi_1^+ \phi_2^- - c_+ \phi_1^+ \phi_2^+ - c_- \phi_1^- \phi_2^+$$
$$= c_- \left(\phi_1^+ \phi_2^- - \phi_1^- \phi_2^+ \right)$$

$$
\begin{aligned}
&= c_{-}\det\left(\begin{bmatrix} \phi_1^{+} & \phi_2^{+} \\ \\ \phi_1^{-} & \phi_2^{-} \end{bmatrix}\right) \\
&= c_{-}\det\left(\begin{bmatrix} \phi_1 & \phi_2 \end{bmatrix}\right) \\
&= c_{-}W[\phi_1, \phi_2],
\end{aligned}
$$

where $W[M]$ is the Wronskian of the matrix M.

Since $\phi^{\pm}$ are the eigenfunctions of the plane wave, we see that

$$
\begin{aligned}
W[\phi_1, \phi_2] &= \phi_1^{+}\phi_2^{-} - \phi_1^{-}\phi_2^{+} \\
&= \left(\frac{ia}{2k}\right)^2 \left[e^{ia^2t}(-e^{ip}e^{-ia^2t}) - (e^{-ip}e^{-ia^2t})e^{ia^2t}\right] \\
&= \frac{a}{4k^2}\left[ae^{ip} + ae^{-ip}\right] \\
&= \frac{a}{4k^2}\left[k + \nu + k - \nu\right] \\
&= \frac{a}{2k}.
\end{aligned}
$$

Namely, $W[\phi_1, \phi_2]$ is constant in space and time, so the effect of this term on the behavior of the eigenfunction remains unchanged.

With this information we can rewrite χ^{+} at ν as

$$
\begin{aligned}
\chi^{+}(\nu; \nu, \phi) &= \frac{2c_{-}\nu W[\phi_1, \phi_2]}{|\phi_1|^2 + |\phi_2|^2} \begin{bmatrix} \phi_2^{*} \\ \\ -\phi_1^{*} \end{bmatrix} \\
&= \frac{a\nu c_{-}}{k} \begin{bmatrix} \frac{\phi_2^{*}}{|\phi_1|^2+|\phi_2|^2} \\ \\ \frac{-\phi_1^{*}}{|\phi_1|^2+|\phi_2|^2} \end{bmatrix}. \qquad (3.2.4)
\end{aligned}
$$

The quantities ϕ_2^* and $|\phi_1|^2 + |\phi_2|^2$ have already been computed for evaluating B, we see that

$$\begin{aligned}\frac{\phi_2^*}{|\phi_1|^2 + |\phi_2|^2} &= -\frac{ik}{ac_-}\frac{e^{\frac{\rho}{2}}\left(e^{-i\beta}e^{i\frac{\pi}{4}}e^{i\frac{p}{2}}e^{-ikx}e^{\frac{\rho}{2}}e^{2ik\nu t} - e^{-i\frac{\pi}{4}}e^{-i\frac{p}{2}}e^{ikx}e^{-\frac{\rho}{2}}e^{-2ik\nu t}\right)}{e^{\rho}\left(e^{\rho}e^{-4ik\nu t} + e^{-\rho}e^{4ik\nu t} + i\sin(p)\sin(2kx+\beta-\frac{\pi}{2}))\right)} \\ &= -\frac{ik}{ac_-}e^{-\frac{\rho}{2}}\frac{e^{-i\beta}e^{i\frac{\pi}{4}}e^{i\frac{p}{2}}e^{-ikx}e^{(\rho-\sigma t)/2} - e^{-i\frac{\pi}{4}}e^{-i\frac{p}{2}}e^{ikx}e^{-(\rho-\sigma t)/2}}{e^{\rho-\sigma t} + e^{-(\rho-\sigma t)} + 2\sin(p)\cos(2kx+\beta)}.\end{aligned}$$

So as $t \to \pm\infty$, the behavior is exponential in both the numerator and denominator, but the denominator grows more quickly, so the function goes to 0 as $t \to \pm\infty$ and the eigenfunction does not have exponential growth.

If the underlying plane-wave has only one unstable mode, $N = 1$, then there are no other potential sources of growth since λ and ν must be chosen to be complex double points and there is only on double point from which to chose. If $N \geq 2$, however, we must separately address the behavior at the other complex double points. We show in section 3.2.2 that the other double points correspond to growth of the perturbation.

3.2.2 Case 2: distinct eigenvalues

In the case that $N \geq 2$ we have shown in the previous case that ν does not contribute growth of the perturbation, but we show in this section that other eigenvalues do cause growth. We are interested in finding the behavior of the bounded functions that form a portion of the components of $\chi^{\pm}$ so we can look at the behavior of the squared eigenfunctions.

Let

$$\chi^{\pm}(\lambda;\nu,\phi) = \frac{ia}{2\hat{k}} e^{\mp i\frac{\pi}{4}} e^{\pm i\frac{\hat{p}}{2}} \begin{bmatrix} B_1^{\pm}(\lambda;\nu,\phi)e^{ia^2t} \\ B_2^{\pm}(\lambda;\nu,\phi)e^{-ia^2t} \end{bmatrix} e^{\pm i(\hat{k}x+2\hat{k}\lambda t)}$$

Then

$$\begin{aligned} B_1^+ = \Bigg[\lambda - \nu e^{-i\hat{p}} \frac{i\sin(p)\cosh(\rho-\sigma t) + \cos(p)\sinh(\rho-\sigma t)}{\cosh(\rho-\sigma t) + \sin(p)\cos(2kx+\beta)} \\ -\nu e^{-i\hat{p}} \frac{\cos(p)\sin(2kx+\beta)e^{i\hat{p}} + i\cos(2kx+\beta)}{\cosh(\rho-\sigma t) + \sin(p)\cos(2kx+\beta)}\Bigg] \\ B_2^+ = e^{-i\hat{p}}\Bigg[\lambda + \nu e^{i\hat{p}} \frac{i\sin(p)\cosh(\rho-\sigma t) - \cos(p)\sinh(\rho-\sigma t)}{\cosh(\rho-\sigma t) + \sin(p)\cos(2kx+\beta)} \\ +\nu \frac{\cos(p)\sin(2kx+\beta) + ie^{i\hat{p}}\cos(2kx+\beta)}{\cosh(\rho-\sigma t) + \sin(p)\cos(2kx+\beta)}\Bigg] \end{aligned}$$

We are interested in behavior for large t, so taking the limit as $t \to \infty$ we find

$$\begin{aligned} \lim_{t\to\infty} B_1^+(\lambda;\nu,\phi) &= \lambda - \nu e^{-i\hat{p}} \lim_{t\to\infty} \left[\frac{i\sin(p) + \cos(p)\tanh(\rho-\sigma t)}{1 + \sin(p)\cos(2kx+\beta)\operatorname{sech}(\rho-\sigma t)}\right] \\ &= \lambda - \nu e^{-i\hat{p}}(\cos(p) + i\sin(p)) \\ &= \lambda - \nu e^{-i(\hat{p}-p)} \\ \lim_{t\to\infty} B_2^+(\lambda;\nu,\phi) &= e^{-i\hat{p}}\left(\lambda + \nu e^{i\hat{p}} \lim_{t\to\infty}\left[\frac{i\sin(p) - \cos(p)\tanh(\rho-\sigma t)}{1 + \sin(p)\cos(2kx+\beta)\operatorname{sech}(\rho-\sigma t)}\right]\right) \\ &= e^{-i\hat{p}}\left(\lambda + \nu e^{i\hat{p}}(i\sin(p) - \cos(p))\right) \\ &= e^{-i\hat{p}}\left(\lambda - \nu e^{i\hat{p}}(\cos(-p) + i\sin(-p))\right) \\ &= e^{-i\hat{p}}\left(\lambda - \nu e^{i(\hat{p}-p)}\right). \end{aligned}$$

Letting $\lambda = \nu$ we have

$$\lim_{t\to\infty} B_1^+(\nu;\nu,\phi) = \nu - \nu e^{-ip}e^{ip} = \nu - \nu = 0,$$

$$\lim_{t\to\infty} B_2^+(\nu;\nu,\phi) = e^{-i\hat{p}}\left(\nu - \nu e^{ip}e^{-ip}\right) = e^{-i\hat{p}}\left(\nu-\nu\right) = 0.$$

Furthermore, one of the squared eigenfunctions we are looking for requires us to examine $(B_1^+)^2 - (B_2^{+*})^2$

$$\begin{aligned}(B_1^+)^2 - (B_2^{+*})^2 &\to \left(\lambda - \nu e^{-i(\hat{p}-p)}\right)^2 - \left(e^{i\hat{p}}\left(\lambda^* + \nu e^{-i(\hat{p}-p)}\right)\right)^2 \\ &= \left(\lambda - \nu e^{-i(\hat{p}-p)}\right)^2 - e^{2i\hat{p}}\left(\lambda - \nu e^{-i(\hat{p}-p)}\right)^2 \\ &= \left(1 - e^{2i\hat{p}}\right)\left(\lambda - \nu e^{-i(\hat{p}-p)}\right)^2,\end{aligned}$$

which is fixed for a fixed λ. Furthermore, this quantity is nonzero for $\lambda \neq \nu$ (and thus $\hat{p} \neq p$). If we let $\phi = \psi = \chi^+$, then one of the squared eigenfunctions is

$$\begin{aligned}g + h^* &= \left(\chi_1^+\right)^2 - \left(\chi_2^{+*}\right)^2 \\ &= -\frac{a^2}{4\hat{k}^2}e^{-i\frac{\pi}{2}}e^{i\hat{p}}e^{2i\hat{k}x}\left[\left(B_1^+(x,t)e^{ia^2t}e^{i2k\lambda t}\right)^2 - \left(B_2^{+*}(x,t)e^{ia^2t}e^{i2k\lambda t}\right)^2\right] \\ &= -\frac{a^2}{4\hat{k}^2}e^{-i\frac{\pi}{2}}e^{i\hat{p}}e^{2i\hat{k}x}\left[\left(B_1^+(x,t)\right)^2 - \left(B_2^{+*}(x,t)\right)^2\right]e^{2ia^2t}e^{4i\hat{k}\lambda t},\end{aligned}$$

which is the product of quantities bounded in x and t for $\lambda \neq \nu$ with the factor $\exp\{4i\hat{k}\lambda t\}$ that grows exponentially in time since $\hat{k} \in \mathbb{R}$ and $\lambda \in \mathbb{C}$ is a complex double point of the spectrum. Because the squared eigenfunctions satisfy the linearized NLS, this exponential growth indicates that the perturbation to the plane wave will grow exponentially in NLS. Note that the limit in t would be indeterminate in the case when $\lambda = \nu$, which is precisely the case in section 3.2.1.

In conclusion, the spatially periodic breather is stable if, and only if, the background plane wave has exactly one unstable mode ($N = 1$).

3.3 Peregrine stability

Recall that we have already determined the behavior of A and B as $L \to \infty$. From equations (2.3.1) and (2.3.2) we know

$$\widetilde{A} = \frac{4cx}{4c^2x^2 + 16c^4t^2 + 1},$$
$$\widetilde{B} = e^{-2ia^2t}\left(\frac{-8c^2t + 2i}{4c^2x^2 + 16c^4t^2 + 1} - i\right) = e^{-2ia^2t}\widetilde{B}.$$

and the new eigenfunctions are constructed as

$$\begin{aligned}
\widetilde{\chi}^{\pm} &= \frac{i}{2k}e^{\mp i\frac{\pi}{4}}e^{\pm i\frac{p}{2}}\begin{bmatrix} \lambda + ia\widetilde{A} & ia\widetilde{B} \\ ia\widetilde{B^*} & \lambda - ia\widetilde{A} \end{bmatrix}\begin{bmatrix} ae^{ia^2t} \\ \pm ae^{\mp ip}e^{-ia^2t} \end{bmatrix} e^{\pm i(kx+2k\lambda t)} \\
&= \frac{ia}{2k}e^{\mp i\frac{\pi}{4}}e^{\pm i\frac{p}{2}}\begin{bmatrix} \left(\lambda + ia\widetilde{A}\right) \pm e^{\mp ip}ia\widetilde{B}e^{-ia^2t} \\ ia\widetilde{B^*}e^{-ia^2t} \pm e^{\mp ip}\left(\lambda - ia\widetilde{A}\right)e^{-ia^2t} \end{bmatrix} e^{\pm i(kx+2k\lambda t)} \\
&= \frac{ia}{2k}e^{\mp i\frac{\pi}{4}}e^{\pm i\frac{p}{2}}\begin{bmatrix} \left(\lambda + ia\widetilde{A} \pm e^{\mp ip}ia\widetilde{B}\right)e^{ia^2t} \\ \left(ia\widetilde{B^*} \pm e^{\mp ip}(\lambda - ia\widetilde{A})\right)e^{-ia^2t} \end{bmatrix} e^{\pm i(kx+2k\lambda t)} \\
&= \frac{ia}{2k}e^{\mp i\frac{\pi}{4}}e^{\pm i\frac{p}{2}}\begin{bmatrix} \widetilde{B}_1^{\pm}e^{ia^2t} \\ \widetilde{B}_2^{\pm}e^{-ia^2t} \end{bmatrix} e^{\pm i(kx+2k\lambda t)}.
\end{aligned}$$

Since

$$\lim_{t\to\infty}\widetilde{A} = \lim_{t\to\infty}\frac{4cx}{4c^2x^2 + 16c^4t^2 + 1} = 0,$$
$$\text{and } \lim_{t\to\infty}\widetilde{B} = \left(\frac{-8c^2t + 2i}{4c^2x^2 + 16c^4t^2 + 1} - i\right) = -i,$$

we know that

$$\lim_{t\to\infty}\widetilde{B}_1^{\pm} = \lambda \pm e^{\mp ip}ia(-i) = \lambda \pm ae^{\mp ip},$$

$$\lim_{t\to\infty} \widetilde{B}_2^{\pm} = ia(i) \pm \lambda e^{\mp ip} = -a \pm \lambda e^{\mp ip}.$$

Assume λ is purely imaginary, i.e. $\lambda = i\alpha$ for $\alpha \in \mathbb{R}$. Then as $t \to \infty$,

$$\begin{aligned}
\left(B_{\infty 1}^{+}\right)^2 - \left(B_{\infty 2}^{+*}\right)^2 &\to \left(\lambda + ae^{-ip}\right)^2 - \left(\left(e^{-ip}(\lambda - ae^{ip})\right)^*\right)^2 \\
&= \left(i\alpha + ae^{-ip}\right)^2 - \left(e^{ip}(ia^2 t - ae^{-ip})\right)^2 \\
&= \left(\lambda + ae^{-ip}\right)^2 - e^{2ip}\left(i\alpha + ae^{-ip}\right)^2 \\
&= \left(1 - e^{2ip}\right)\left(i\alpha + ae^{-ip}\right)^2.
\end{aligned}$$

For $\alpha \neq a$, $e^{ip} \neq i$, and this quantity is bounded away from 0.

Looking at one of the squared eigenfunctions,

$$\begin{aligned}
g + h^* &= \left(\chi_{\infty 1}^{+}\right)^2 - \left(\chi_{\infty 2}^{+*}\right)^2 \\
&= -\frac{a^2}{4k^2} e^{-i\frac{\pi}{2}} e^{ip} e^{2ikx} \left[\left(B_{\infty 1}^{+}(x,t) e^{ia^2 t} e^{i2k\lambda t}\right)^2 - \left(B_{\infty 2}^{+*}(x,t) e^{ia^2 t} e^{i2k\lambda t}\right)^2\right] \\
&= -\frac{a^2}{4\hat{k}^2} e^{-i\frac{\pi}{2}} e^{i\hat{p}} e^{2ikx} \left[\left(B_{\infty 1}^{+}(x,t)\right)^2 - \left(B_{\infty 2}^{+*}(x,t)\right)^2\right] e^{2ia^2 t} e^{4ik\lambda t}.
\end{aligned}$$

Since $k \in \mathbb{R}$ is the wave number, the squared eigenfunction grows as $t \to \infty$ for purely imaginary λ. Thus the solution is unstable.

3.3.1 Conclusions

In this chapter we have carried out a comprehensive investigation of the linear stability of the Peregrine solution of the NLS equation. Viewing the Peregrine soliton as the singular limit

of the one mode SPB, we obtained general eigenfunctions of the Peregrine solution by taking the limit of the eigenfunctions for the one mode SPB. We verified the Peregrine solution and corresponding eigenfunctions satisfy the Lax pair. The main theorem used to study stability is that, for a given solution $u(x,t)$ of the NLS equation, its associated squared eigenfunctions satisfy the linearized equation about $u(x,t)$. As a result the question of stability is resolved by examining the behavior in time of the squared eigenfunctions $f(x,t)$ and $g(x,t)$.

Using the squared eigenfunction approach, we constructed a λ-parametrized family of solutions of the linearization of NLS equation about the Peregrine soliton. This produces a fairly general family of such solutions. To satisfy the boundary conditions in the spatial variable x, i.e. the solutions are required to be bounded in x and to decay polynomially as $x \to \pm\infty$, λ is limited to be in the imaginary band [-ia, ia]. Finally, we found that for any such λ there are solutions of the linearization that exhibit exponential in time behavior, thus showing the Peregrine soliton has infinitely many (in fact a continuum of) linear instabilities.

CHAPTER 4

ROGUE WAVES AND DOWNSHIFTING

4.1 Higher order NLS

Recently, Gramstad and Trulsen derived a version of the higher order NLS equation (HONLS) with periodic boundary conditions, i.e. $u(x,t) = u(x+L,t)$ [25]. We add damping and wind effects as follows:

$$iu_t + u_{xx} + 2|u|^2u + i\Gamma u + i\hat{\epsilon}\left(\tfrac{1}{2}u_{3x} - 8|u|^2u_x - 2ui(1+i\beta)\left[\mathcal{H}\left(|u|^2\right)\right]_x\right) = 0, \qquad (4.1.1)$$

where $\mathcal{H}(f)$ is the Hilbert transform of f, and $\beta > 0$ is the nonlinear damping of the mean flow, and Γ is the effect due to wind. When $\beta = \Gamma = 0$, we refer to (4.1.1) as the HONLS equation.

4.2 Wave energy and Flux

The total wave energy, E, and the momentum or total energy flux, P for a solution $u(x,t)$ of the HONLS equation are given by

$$E(t) = \int_0^L |u|^2 \,\mathrm{d}x. \qquad (4.2.1)$$

To examine how the perturbation affects the wave energy, we examine $\frac{dE}{dt}$.

Lemma 4.2.1. *The wave energy changes in time as*

$$\frac{dE}{dt} = -2\int_0^L |u|^2 \left(\Gamma + 2\epsilon\beta\left[\mathcal{H}(|u|^2)\right]_x\right)\, dx. \tag{4.2.2}$$

Proof. Note that the integral in (4.2.1) is with respect to x, so we can pass the time derivative through the integral. Furthermore, (4.1.1) solved for u_t and its conjugate are

$$u_t = iu_{xx} + 2i|u|^2u - \Gamma u - \epsilon\left(\tfrac{1}{2}u_{3x} - 8|u|^2u_x - 2iu(1+i\beta)\left[\mathcal{H}\left(|u|^2\right)\right]_x\right), \tag{4.2.3}$$

$$u_t^* = -iu_{xx}^* - 2i|u|^2u^* - \Gamma u^* - \epsilon\left(\tfrac{1}{2}u_{3x}^* - 8|u|^2u_x^* + 2iu^*(1-i\beta)\left[\mathcal{H}\left(|u|^2\right)\right]_x\right). \tag{4.2.4}$$

Since $|u|^2 = uu^*$, we have

$$\begin{aligned}
\frac{d|u|^2}{dt} &= u_tu^* + uu_t^* \\
&= \left[iu_{xx} + 2i|u|^2u - \Gamma u - \epsilon\left(\tfrac{1}{2}u_{3x} - 8|u|^2u_x - 2iu(1+i\beta)\left[\mathcal{H}\left(|u|^2\right)\right]_x\right)\right]u^* \\
&\quad + \left[-iu_{xx}^* - 2i|u|^2u^* - \Gamma u^* - \epsilon\left(\tfrac{1}{2}u_{3x}^* - 8|u|^2u_x^* + 2iu^*(1-i\beta)\left[\mathcal{H}\left(|u|^2\right)\right]_x\right)\right]u \\
&= iu_{xx}u^* + 2i|u|^2uu^* - \Gamma uu^* - \epsilon\left(\tfrac{1}{2}u_{3x}u^* - 8|u|^2u_xu^* - 2iuu^*(1+i\beta)\left[\mathcal{H}\left(|u|^2\right)\right]_x\right) \\
&\quad - iu_{xx}^*u - 2i|u|^2u^*u - \Gamma u^*u - \epsilon\left(\tfrac{1}{2}u_{3x}^*u - 8|u|^2u_x^*u + 2iu^*u(1-i\beta)\left[\mathcal{H}\left(|u|^2\right)\right]_x\right) \\
&= iu_{xx}u^* + 2i|u|^4 - \Gamma|u|^2 - \epsilon\left(\tfrac{1}{2}u_{3x}u^* - 8|u|^2u_xu^* - 2i|u|^2(1+i\beta)\left[\mathcal{H}\left(|u|^2\right)\right]_x\right) \\
&\quad - iu_{xx}^*u - 2i|u|^4 - \Gamma|u|^2 - \epsilon\left(\tfrac{1}{2}u_{3x}^*u - 8|u|^2u_x^*u + 2i|u|^2(1-i\beta)\left[\mathcal{H}\left(|u|^2\right)\right]_x\right) \\
&= iu_{xx}u^* + 2i|u|^4 - \Gamma|u|^2 - \epsilon\left(\tfrac{1}{2}u_{3x}u^* - 8|u|^2u_xu^* - 2i|u|^2(1+i\beta)\left[\mathcal{H}\left(|u|^2\right)\right]_x\right) \\
&\quad - iu_{xx}^*u - 2i|u|^4 - \Gamma|u|^2 - \epsilon\left(\tfrac{1}{2}u_{3x}^*u - 8|u|^2u_x^*u + 2i|u|^2(1-i\beta)\left[\mathcal{H}\left(|u|^2\right)\right]_x\right) \\
&= -\epsilon\left[\tfrac{1}{2}(u_{3x}u^* + u_{3x}^*u) - 8|u|^2(u_xu^* + u_x^*u) + 4|u|^2\beta\left[\mathcal{H}\left(|u|^2\right)\right]_x\right]
\end{aligned}$$

$$+ iu_{xx}u^* - iu^*_{xx}u - 2\Gamma|u|^2$$

$$= -2|u|^2\left(\Gamma + 2\epsilon\beta\left[\mathcal{H}\left(|u|^2\right)\right]_x\right) + r(u(x,t)),$$

where,

$$r(u(x,t)) \equiv iu_{xx}u^* - iu^*_{xx}u - \epsilon\left[\tfrac{1}{2}(u_{3x}u^* + u^*_{3x}u) - 8|u|^2(u_xu^* + u^*_xu)\right].$$

Note that

$$u_{xx}u^* - u^*_{xx}u = \frac{d}{dx}\left[u_xu^* - uu^*_x\right],$$
$$u_xu^* + uu^*_x = \frac{d}{dx}\left[uu^*\right],$$
$$u_{3x}u^* + uu^*_{3x} = \frac{d}{dx}\left[u_{2x}u^* - u_xu^*_x + uu^*_{2x}\right].,$$

so we can rewrite $r(u(x,t))$ as

$$r(u(x,t)) = \frac{d}{dx}\left[i(u_xu^* - uu^*_x) - \tfrac{\epsilon}{2}(u_{2x}u^* - u_xu^*_x + uu^*_{2x}) - 8\epsilon|u|^2(uu^*)\right] = \frac{d}{dx}\left[R(u(x,t))\right].$$

Since u is periodic, so is u^*, u_x, u^*_x, etc. Thus,

$$\int_0^L r(u(x,t))\,dx = \int_0^L \frac{d}{dx}\left[R(u(x,t))\right]\,dx = R(u(L,t)) - R(u(0,t)) = 0.$$

Finally, we can compute

$$\frac{dE}{dt} = \int_0^L \Big(- 2|u|^2\left(\Gamma + 2\epsilon\beta\left[\mathcal{H}\left(|u|^2\right)\right]_x\right) + r(u(x,t))\Big)\,dx$$
$$= \int_0^L -2|u|^2\left(\Gamma + 2\epsilon\beta\left[\mathcal{H}\left(|u|^2\right)\right]_x\right)\,dx + \int_0^L r(u(x,t))\,dx$$
$$= -2\int_0^L |u|^2\left(\Gamma + 2\epsilon\beta\left[\mathcal{H}(|u|^2)\right]_x\right)\,dx.$$

□

When $\frac{dE}{dt} = 0$ for all t, the wave energy remains unchanged from the initial state. Note the wave energy is conserved for the NLS ($\epsilon = \beta = \Gamma = 0$) and the HONLS ($\beta = \Gamma = 0$) equations. To see how the change in the wave energy depends on β and Γ, expand $u(x,t)$ and $|u(x,t)|^2$ in the following Fourier series,

$$u(x,t) = \sum_{k=-\infty}^{\infty} \hat{u}_k(t) e^{ikx} \qquad |u(x,t)|^2 = \sum_{k=0}^{\infty} (\alpha_k(t) e^{ikx} + \alpha_k^*(t) e^{-ikx}), \tag{4.2.5}$$

and substitute these expansions into (4.2.2), to arrive at

$$\frac{dE}{dt} = -2L \left[\Gamma \sum_{k=-\infty}^{\infty} |\hat{u}_k|^2 + 2\epsilon\beta \sum_{k=1}^{\infty} k|\alpha_k|^2 \right]. \tag{4.2.6}$$

Notice that when $\Gamma = 0$, the effect due to β is damping for $\beta > 0$. Similarly, when $\epsilon = 0$ the $\Gamma > 0$ removes energy from the system and $\Gamma < 0$ adds energy to the system.

For $\beta \geq 0$: 1) If $\Gamma \geq 0$ then $\frac{dE}{dt} \leq 0$ for all time and the total energy is dissipated or constant. 2) If the wind is pumping energy into the system, $\Gamma < 0$, then for a given β the total energy can transition in time between being damped and being forced. In this dissertation we only examine damped forced regimes, i.e. (β, Γ) pairs, where damping eventually dominates on the time frame examined, i.e where for $t \geq t^*$ $E(t)/E(0) \leq 1$ and $E(t)$ is generally decreasing.

The Fourier expansion of the momentum can be written as

$$P = -2L \sum_{-\infty}^{\infty} k|\hat{u}_k|^2 = 2L \sum_{k=1}^{\infty} k \left(|\hat{u}_{-k}|^2 - |\hat{u}_k|^2 \right),$$

which measures the asymmetry of the Fourier modes. The evolution of the momentum for the damped forced HONLS is

$$\frac{dP}{dt} = -2i \int_0^L (u^* u_x - u u_x^*) \left[\Gamma + 2\epsilon\beta \left(\mathcal{H} \left(|u|^2 \right) \right)_x \right] \, dx. \tag{4.2.7}$$

The total energy flux, P for a solution $u(x,t)$ of the HONLS equation is given by

$$P(t) = i \int_0^L (u^* u_x - u u_x^*) \, \mathrm{d}x, \tag{4.2.8}$$

and the Hamiltonian is

$$\mathcal{H} = \int_0^L \left\{ -i|u_x|^2 + i|u|^4 - \tfrac{\epsilon}{4} \left(u_x u_{xx}^* - u_x^* u_{xx} \right) + 2\epsilon |u|^2 (u^* u_x - u u_x^*) \right\} \, dx. \tag{4.2.9}$$

It should be noted that the momentum is conserved for the HONLS equation whereas for the HONLS equation, an earlier extensively used higher order NLS equation, the momentum oscillates in time [7]. Thus for the HONLS equation there are three conserved quantities to monitor in the numerical experiments: the wave energy, momentum and Hamiltonian.

4.3 Measuring downshifting: the spectral peak and spectral center

Different diagnostics have been developed to address downshifting of the sea state. Traditionally, downshifting has been considered to be a shift down in the spectral peak, k_{peak}, or dominant mode. Here k_{peak} is defined as the wave number k for which $|\hat{u}_k|$ achieves its maximum.

As an alternative, one may consider the spectral center k_m of the spectrum. In analogy with the analysis of $u(x,t)$ on an infinite domain where Parseval's theorem and generalized mean value theorem yield,

$$E(t) = L\int_0^L |\hat{u}|^2 \,\mathrm{d}k \qquad \text{and } P(t) = -2Lk_m \int_0^L |\hat{u}|^2 \,\mathrm{d}k,$$

Uchiyama and Kawahara [26] defined the spectral center or mean wave number as

$$k_m = -\frac{1}{2}\frac{P}{E} = \frac{\sum_{-\infty}^{\infty} k|\hat{u}_k|^2}{\sum_{-\infty}^{\infty} |\hat{u}_k|^2}. \tag{4.3.1}$$

Note that for the NLS and HONLS equations where the energy and momentum are conserved, k_m is also invariant.

Permanent downshift of a wave train is considered to occur when the spectral peak k_{peak} moves permanently to a lower mode [1]. The spectral center and spectral peak can be different. When the Fourier coefficients are sufficiently concentrated about k_{peak}, then $k_m \approx k_{peak}$ and in this case the condition $\dot{k}_m < 0$ has been used to indicate downshifting. In all the numerical experiments we monitor both the spectral peak and the spectral center. We use the spectral center to provide a qualitative understanding of the downshifting mechanism and a necessary condition for permanent downshift, i.e. $\dot{k}_m < 0$. Examining the spectral center alone does not yield information on the time at which the downshift becomes permanent. As a result, the time at which permanent downshifting occurs is determined using k_{peak}. Although temporary downshifts occur in the NLS and HONLS numerical experiments (see sec 5.2), a permanent downshift does not occur since k_m is constant.

k_{asym}	N		
	1	2	3
-1	100%	0	13%
-2	0	100%	0
-3	0	0	83%
-4	0	0	4%

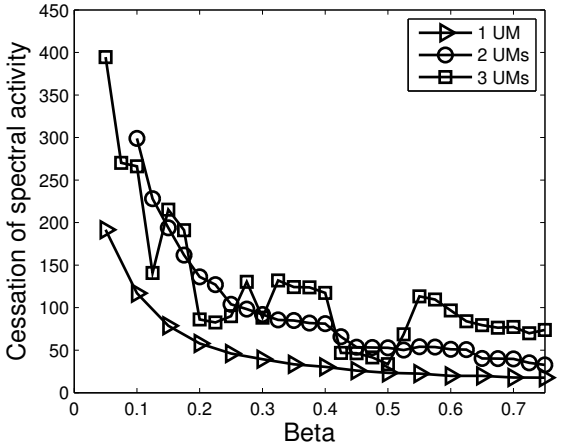

Figure 4.1: The percentage of experiments with asymptotic k_{peak} listed in the first column for experiments with nonlinear damping that settled into a single mode by the end of the experiment (table, left). The average time that settled experiments ceased exhibiting spectral activity (figure, right). The experiments presented are for the data in earlier experiments.

The downshifting mechanism for solutions with both nonlinear damping and linear damping or linear forcing behaves similarly to those without a linear term. As shown in section 5.5, if the experiment has linear forcing, the energy may increase early in the timeseries, but in all of the presented cases the nonlinear damping is dominant causing the energy to decrease. At the same time, the momentum is increasing so the spectral center decreases in a manner similar to the cases with no linear term. We will show the inclusion of linear damping causes the spectral center to decrease less for a given value of β whereas linear forcing causes a larger decrease in the spectral center for a given β value.

We show in section 5.5 that experiments with linear damping or forcing still experience downshifting if the nonlinear term is dominant. Unlike the case with no linear term,

experiments with linear damping or linear forcing have multiple stages of downshifting. After permanent downshift to a lower mode, the spectral peak may continue to move among the lower modes or even move to higher modes (upshift). An experiment may or may not then settle permanently into a single lower mode, which we define as k_{asym} once the ongoing downshifting mechanism ceases.

4.4 Linear Instability of the Stokes wave for nonlinear damped HONLS

In this section we study the stability of the Stokes wave for the nonlinear damped HONLS equation, which is (4.1.1) with $\Gamma = 0$.

Let $A_1, A_2 \in \mathbb{R}$, $u(x,t) = ae^{2ia^2t}$, $\phi(x,t) = \exp i(kx - \Omega t)$, $\phi^*(x,t) = \exp -i(kx - \Omega^* t)$ and construct an ϵ perturbation of the solution u of (4.1.1) as

$$\widetilde{u} = u\left(1 + \epsilon(A_1\phi + A_2\phi^*)\right). \tag{4.4.1}$$

This allows us to expand (4.1.1) about the solution u. With u, ϕ, ϕ^* as given we have

$$\begin{array}{llll} u_t = 2ia^2u & \phi_t = -i\Omega\phi & \phi_t^* = i\Omega^*\phi^* \\ u_x = 0 & \phi_x = ik\phi & \phi_x^* = -ik\phi^* \\ u_{xx} = 0 & \phi_{xx} = -k^2\phi & \phi_{xx}^* = -k^2\phi^* \\ u_{3x} = 0 & \phi_{3x} = -ik^3\phi & \phi_{3x}^* = ik^3\phi^* \end{array}$$

Then we can express each term of (4.1.1) linearly in terms of ϵ as follows:

$$\widetilde{u}_t = u_t\left[1 + \epsilon(A_1\phi + A_2\phi^*)\right] + u\left[\epsilon(A_1\phi_t + A_2\phi_t^*)\right]$$

$$= 2ia^2u\left[1+\epsilon(A_1\phi+A_2\phi^*)\right]+u\left[\epsilon(A_1\phi_t+A_2\phi_t^*)\right]$$

$$= 2ia^2u+\epsilon u\left[A_1(2ia^2\phi+\phi_t)+A_2(2ia^2\phi^*+\phi_t^*)\right]$$

$$\widetilde{u}_x = u_x\left[1+\epsilon(A_1\phi+A_2\phi^*)\right]+u\left[\epsilon(A_1\phi_x+A_2\phi_x^*)\right]$$

$$= \epsilon u\left[A_1\phi_x+A_2\phi_x^*\right]$$

$$\widetilde{u}_{xx} = u_x\left[1+\epsilon(A_1\phi_x+A_2\phi_x^*)\right]+u\left[\epsilon(A_1\phi_{xx}+A_2\phi_{xx}^*)\right]$$

$$= \epsilon u\left[A_1\phi_{xx}+A_2\phi_{xx}^*\right]$$

$$\widetilde{u}_{3x} = u_x\left[1+\epsilon(A_1\phi_{xx}+A_2\phi_{xx}^*)\right]+u\left[\epsilon(A_1\phi_{3x}+A_2\phi_{3x}^*)\right]$$

$$= \epsilon u\left[A_1\phi_{3x}+A_2\phi_{3x}^*\right]$$

$$|\widetilde{u}|^2 = |u|^2\left[1+\epsilon(A_1\phi+A_2\phi^*)\right]\left[1+\epsilon(A_1\phi^*+A_2\phi)\right]$$

$$= a^2\left(1+\epsilon\left[A_1(\phi+\phi^*)+A_2(\phi+\phi^*)\right]\right)$$

$$|\widetilde{u}|^2\widetilde{u} = a^2u\left[1+\epsilon(A_1\phi+A_2\phi^*)\right]\left(1+\epsilon\left[A_1(\phi+\phi^*)+A_2(\phi+\phi^*)\right]\right)$$

$$= a^2u+\epsilon u\left[A_1(2a^2\phi+a^2\phi^*)+A_2(a^2\phi+2a^2\phi^*)\right]$$

$$|\widetilde{u}|^2\widetilde{u}_x = a^2u\left(1+\epsilon\left[A_1(\phi+\phi^*)+A_2(\phi+\phi^*)\right]\right)\left[\epsilon(A_1\phi_x+A_2\phi_x^*)\right]$$

$$= \epsilon ua^2\left[A_1\phi_x+A_2\phi_x^*\right]$$

$$\mathcal{H}\left(|\widetilde{u}|^2\right) = a^2\epsilon(A_1+A_2)\mathcal{H}\left(\phi+\phi^*\right)$$

$$= a^2\epsilon(A_1+A_2)(-i\phi+i\phi^*)$$

$$\widetilde{u}\left[\mathcal{H}\left(|\widetilde{u}|^2\right)\right]_x = \epsilon u\left[a^2(A_1+A_2)(i\phi_x-i\phi_x^*)\right]\left[1+\epsilon(A_1\phi+A_2\phi^*)\right]$$

$$= \epsilon u\left[A_1a^2(-i\phi_x+i\phi_x^*)+A_2a^2(-i\phi_x+i\phi_x^*)\right]$$

Next, the correct coefficients from (4.1.1) are applied to each term.

$$
\begin{aligned}
i\widetilde{u}_t &= -2a^2u + \epsilon u\left[A_1(-2a^2\phi + i\phi_t) + A_2(-2a^2\phi^* + i\phi_t^*)\right] \\
\widetilde{u}_{xx} &= \epsilon u\left[A_1\phi_{xx} + A_2\phi_{xx}^*\right] \\
2|\widetilde{u}|^2\widetilde{u} &= 2a^2u + \epsilon u\left[A_1(4a^2\phi + 2a^2\phi^*) + A_2(2a^2\phi + 4a^2\phi^*)\right] \\
\tfrac{1}{2}i\hat{\epsilon}\widetilde{u}_{3x} &= \epsilon u\left[A_1\tfrac{i}{2}\hat{\epsilon}\phi_{3x} + A_2\tfrac{i}{2}\hat{\epsilon}\phi_{3x}^*\right] \\
-8i\hat{\epsilon}|\widetilde{u}|^2\widetilde{u}_x &= \epsilon u\left[A_1(-8ia^2\hat{\epsilon})\phi_x + A_2(-8ia^2\hat{\epsilon})\phi_x^*\right] \\
2\hat{\epsilon}\widetilde{u}(1+i\beta)\left[\mathcal{H}\left(|\widetilde{u}|^2\right)\right]_x &= \epsilon u\left[A_1 2a^2\hat{\epsilon}(1+i\beta)(-i\phi_x + i\phi_x^*) + A_2 2a^2\hat{\epsilon}(1+i\beta)(-i\phi_x + i\phi_x^*)\right]
\end{aligned}
$$

The two terms without ϵ are opposite, so substituting these expression into (4.1.1) leaves only terms which are multiplied by ϵu. Canceling out this factor and grouping the terms according to A_1, A_2 yields

$$
\begin{aligned}
&i\widetilde{u}_t + \widetilde{u}_{xx} + 2|\widetilde{u}|^2\widetilde{u} + i\hat{\epsilon}\left(\tfrac{1}{2}\widetilde{u}_{3x} - 8|\widetilde{u}|^2\widetilde{u}_x - 2\widetilde{u}i(1+i\beta)\left[\mathcal{H}\left(|\widetilde{u}|^2\right)\right]_x\right) \\
&\quad = i\widetilde{u}_t + \widetilde{u}_{xx} + 2|\widetilde{u}|^2\widetilde{u} + \tfrac{1}{2}i\hat{\epsilon}\widetilde{u}_{3x} - 8i\hat{\epsilon}|\widetilde{u}|^2\widetilde{u}_x + 2\hat{\epsilon}\widetilde{u}(1+i\beta)\left[\mathcal{H}\left(|\widetilde{u}|^2\right)\right]_x \\
&= A_1\left[-2a^2\phi + i\phi_t + \phi_{xx} + 4a^2\phi + 2a^2\phi^* + \tfrac{i}{2}\hat{\epsilon}\phi_{3x} - 8ia^2\hat{\epsilon}\phi_x + 2a^2\hat{\epsilon}(1+i\beta)(-i\phi_x + i\phi_x^*)\right] \\
&\quad + A_2\left[-2a^2\phi^* + i\phi_t^* + \phi_{xx}^* + 2a^2\phi + 4a^2\phi^* + \tfrac{i}{2}\hat{\epsilon}\phi_{3x}^* - 8ia^2\hat{\epsilon}\phi_x^* + 2a^2\hat{\epsilon}(1+i\beta)(-i\phi_x + i\phi_x^*)\right] \\
&= A_1\left[i\phi_t + \phi_{xx} + 2a^2\phi + 2a^2\phi^* + \tfrac{i}{2}\hat{\epsilon}\phi_{3x} - 8ia^2\hat{\epsilon}\phi_x + 2a^2\hat{\epsilon}(1+i\beta)(-i\phi_x + i\phi_x^*)\right] \\
&\quad + A_2\left[i\phi_t^* + \phi_{xx}^* + 2a^2\phi + 2a^2\phi^* + \tfrac{i}{2}\hat{\epsilon}\phi_{3x}^* - 8ia^2\hat{\epsilon}\phi_x^* + 2a^2\hat{\epsilon}(1+i\beta)(-i\phi_x + i\phi_x^*)\right] \\
&= A_1\left[\Omega\phi - k^2\phi + 2a^2\phi + 2a^2\phi^* + \tfrac{1}{2}\hat{\epsilon}k^3\phi + 8a^2\hat{\epsilon}k\phi + 2a^2\hat{\epsilon}(1+i\beta)(k\phi + k\phi^*)\right] \\
&\quad + A_2\left[-\Omega^*\phi^* - k^2\phi^* + 2a^2\phi + 2a^2\phi^* - \tfrac{1}{2}\hat{\epsilon}k^3\phi^* - 8a^2\hat{\epsilon}k\phi^* + 2a^2\hat{\epsilon}(1+i\beta)(k\phi + k\phi^*)\right] \\
&= A_1\left[\left(\Omega - k^2 + 2a^2 + \tfrac{1}{2}\hat{\epsilon}k^3 + 10a^2\hat{\epsilon}k + 2ia^2k\hat{\epsilon}\beta\right)\phi + \left(2a^2 + 2a^2k\hat{\epsilon} + 2ia^2k\hat{\epsilon}\beta\right)\phi^*\right]
\end{aligned}
$$

$$+ A_2 \left[\left(-\Omega^* - k^2 + 2a^2 - \tfrac{1}{2}\hat{\epsilon}k^3 - 6a^2\hat{\epsilon}k + 2ia^2k\hat{\epsilon}\beta \right) \phi^* + \left(2a^2 + 2a^2k\hat{\epsilon} + 2ia^2k\hat{\epsilon}\beta \right) \phi \right]$$

so we can write the linearized equation as

$$A_1 \left[(\Omega + C + B)\, \phi + (D + B)\, \phi^* \right] + A_2 \left[(-\Omega^* + E + B)\, \phi^* + (D + B)\, \phi \right] = 0 \qquad (4.4.2)$$

where

$$B = 2ia^2k\hat{\epsilon}\beta$$

$$C = -k^2 + 2a^2 + \tfrac{1}{2}\hat{\epsilon}k^3 + 10a^2\hat{\epsilon}k$$

$$D = 2a^2 + 2a^2k\hat{\epsilon}$$

$$E = -k^2 + 2a^2 - \tfrac{1}{2}\hat{\epsilon}k^3 - 6a^2\hat{\epsilon}k$$

Noting that $A_1, A_2, C, D, E \in \mathbb{R}$, while $B^* = -B$ we see that the equation conjugate to (4.4.2) is

$$A_1 \left[(\Omega^* + C - B)\, \phi^* + (D - B)\, \phi \right] + A_2 \left[(-\Omega + E - B)\, \phi + (D - B)\, \phi^* \right] = 0. \qquad (4.4.3)$$

Simultaneously satisfying (4.4.2) and (4.4.3) yields the system

$$\begin{bmatrix} (\Omega + C + B)\phi + (D + B)\phi^* & (D + B)\phi + (-\Omega^* + E + B)\phi^* \\ (C + B)\phi + (\Omega^* + C - B)\phi^* & (-\Omega + E - B)\phi + (D - B)\phi^* \end{bmatrix} \begin{bmatrix} A_1 \\ A_2 \end{bmatrix} = \begin{bmatrix} 0 \\ 0 \end{bmatrix}. \qquad (4.4.4)$$

To have a nontrivial solution to (4.4.4), the determinant must be zero, i.e.

$$\left[(\Omega + C + B)\phi + (D + B)\phi^* \right] \left[(-\Omega + E - B)\phi + (D - B)\phi^* \right]$$

$$- [(D-B)\phi + (\Omega^* + C - B)\phi^*] [(D+B)\phi + (-\Omega^* + E + B)\phi^*] = 0$$

$$(\Omega + C + B)(-\Omega + E - B)\phi^2 + [(D-B)(-\Omega + E + B) + (-\Omega + E - B)(D+B)] |\phi|^2$$

$$+ (D+B)(D-B)(\phi^*)^2 - (D-B)(D+B)\phi^2 - (\Omega^* + C - B)(-\Omega^* + E + B)(\phi^*)^2$$

$$- [(D-B)(-\Omega^* + E + B) + (D+B)(\Omega^* + C - B)] |\phi|^2 = 0$$

$$[(\Omega + C + B)(-\Omega + E - B) - (D-B)(D+B)] \phi^2$$

$$+ [(D+B)(D-B) - (\Omega^* + C - B)(-\Omega^* + E + B)] (\phi^*)^2$$

$$+ [(D-B)(-\Omega + \Omega^*) + (-\Omega + \Omega^* + E + C)(D+B)] |\phi|^2 = 0$$

A sufficient condition for the system to have a nontrivial solution is for the coefficients of ϕ^2, $(\phi^*)^2$, and $|\phi|^2 = 1$ to be zero. Isolating just the the ϕ^2 terms we have

$$\begin{aligned}(\Omega + C + B)(-\Omega + E - B) - (D-B)(D+B) \\ &= -\Omega^2 + (E - 2B - C)\Omega + CE - CB + BE - D^2 \\ &= -(\Omega^2 - \hat{B}\Omega - \hat{C}) \end{aligned} \tag{4.4.5}$$

where,

$$\hat{B} = E - 2B - C,$$

$$\hat{C} = (CE - CB + BE - D^2).$$

For the $(\phi^*)^2$ terms, we have

$$\begin{aligned}(D+B)(D-B) - (-\Omega^* + E - B)(\Omega^* + C + B) \\ &= (\Omega^*)^2 - (E + 2B - C)\Omega^* - CE - CB + BE + D^2\end{aligned}$$

$$= (\Omega^*)^2 - (E + 2B - C)\Omega^* - (CE + CB - BE - D^2)$$

$$= (\Omega^*)^2 - \hat{B}^*\Omega^* - \hat{C}^*$$

$$= \left(\Omega^2 - \hat{B}\Omega - \hat{C}\right)^*. \tag{4.4.6}$$

Noting that (4.4.6) is the conjugate of (4.4.5), the conditions on the system(4.4.4) imposed by the $(\phi^*)^2$ terms are consistent with those for the ϕ^2 terms.

Proceeding with the coefficients of (4.4.5) we calculate:

$$\hat{B} = (E - C) - 2B = -k^2 + 2a^2 - \tfrac{1}{2}\hat{\epsilon}k^3 - 10a^2\hat{\epsilon}k + 4ia^2k\hat{\epsilon}\beta + k^2 - 2a^2 - \tfrac{1}{2}\hat{\epsilon}k^3 - 6a^2k\hat{\epsilon}$$

$$= -\hat{\epsilon}k^3 - 16a^2\hat{\epsilon}k - 4ia^2k\hat{\epsilon}\beta$$

$$= -2k\hat{\epsilon}(\tfrac{1}{2}k^2 + 8a^2 + 2ia^2\beta)$$

$$\hat{B}^2 = (E - 2B - C)^2 = (\hat{\epsilon}k)^2(k^2 + 16a^2 + 4ia^2\beta)(k^2 + 16a^2 + 4ia^2\beta)$$

$$= 4(\hat{\epsilon}k)^2\left[\tfrac{1}{4}k^4 + 8a^2k^2 + 2ia^2k^2\beta + 64a^4 + 32ia^4\beta - 4a^4\beta^2\right]$$

Calculating the components of $\hat{C}$ we have

$$CE = (-k^2 + 2a^2 + \tfrac{1}{2}\hat{\epsilon}k^3 + 10a^2\hat{\epsilon}k)(-k^2 + 2a^2 - \tfrac{1}{2}\hat{\epsilon}k^3 - 6a^2\hat{\epsilon}k)$$

$$= k^4 - 4a^2k^3\hat{\epsilon} + 4a^4 + 8a^4k\hat{\epsilon} - \tfrac{1}{4}\hat{\epsilon}^2k^6 - 8a^2k^4\hat{\epsilon}^2 - 60a^4k^2\hat{\epsilon}^2 - 4a^2k^2$$

$$B(E - C) = -2ia^2k\hat{\epsilon}\beta(\hat{\epsilon}k^3 + 16a^2\hat{\epsilon}k)$$

$$-D^2 = -(2a^2 - 2a^2k\hat{\epsilon})(2a^2 - 2a^2k\hat{\epsilon})$$

$$= -4a^4 - 8a^4k\hat{\epsilon} - 4a^4k^2\hat{\epsilon}^2$$

$$CE - D^2 = k^4 - 4a^2k^3\hat{\epsilon} - \tfrac{1}{4}\hat{\epsilon}^2k^6 - 8a^2k^4\hat{\epsilon}^2 - 64a^4k^2\hat{\epsilon}^2 - 4a^2k^2$$

$$\hat{C} = CE - D^2 + B(C - E)$$
$$= k^4 - 4a^2k^2 - 4a^2k^3\hat{\epsilon} + (\hat{\epsilon}k)^2\left[-\tfrac{1}{4}k^4 - 8a^2k^2 - 2ia^2k^2\beta - 64a^4 - 32ia^4\beta\right]$$

So that

$$\hat{B}^2 + 4\hat{C} = 4\left[-4a^4\hat{\epsilon}^2k^2\beta^2 + k^4 - 4a^2k^2 - 4a^2k^3\hat{\epsilon}\right]$$
$$= -4k^2\left[4a^4\hat{\epsilon}^2\beta^2 - k^2 + 4a^2 + 4a^2k\hat{\epsilon}\right]$$

Since (4.4.5) is quadratic in Ω, we have

$$\Omega = \tfrac{1}{2}\left(\hat{B} \pm \sqrt{\hat{B}^2 + 4\hat{C}}\right)$$
$$= \hat{\epsilon}(-\tfrac{1}{2}k^3 - 8a^2k - 2ia^2k\beta) \pm ik\sqrt{4a^2 - k^2 + 4a^4\hat{\epsilon}^2\beta^2 + 4a^2k\hat{\epsilon}}$$

In Figure 4.2 we see the growth rates of the sidebands for the NLS, HONLS, and nonlinear damped HONLS. In particular, we see that the nonlinear damped HONLS has growth rates similar to that of HONLS without damping, and the largest k_j that grows is nearly indistinguishable for the two equations. The HONLS equation, both with and without nonlinear damping, has a larger growth rate for many of the k_j that grow than the NLS equation. There are also more k_j that correspond to growth for HONLS than for NLS.

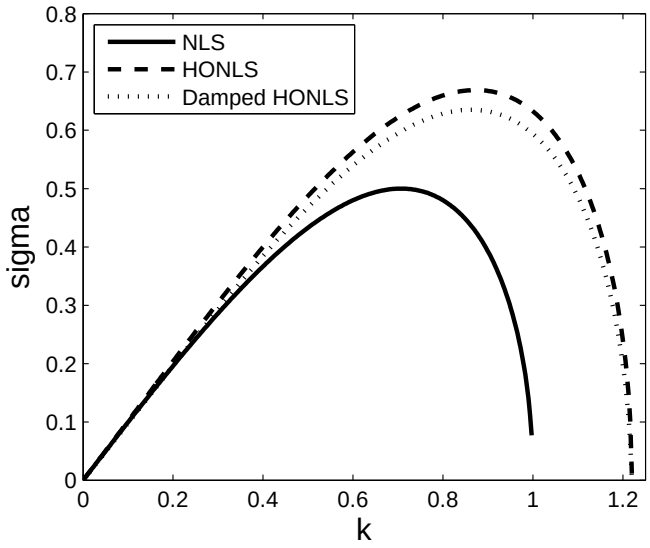

Figure 4.2: Growth rates, σ_j, of the sidebands for the NLS ($\epsilon = \beta = 0$), HONLS ($\epsilon = 0.05$, $\beta = 0$), and nonlinear damped HONLS ($\epsilon = 0.05$, $\beta = .7$) equations as a function of k_j for $a = .5$, $L = 4\sqrt{2}\pi$.

4.5 Linear Instability of the Stokes wave for nonlinear damped HONLS with linear effects

When considering the full equation with linear damping the methodology of determining the stability of the solutions stays the same, but the Stokes' wave is no longer a solution to (4.1.1). Consequently, we must expand about a solution of the full equation. There is still a solution that is independent of space, so we begin by proving that solution satisfies the PDE with additional linear effects.

Theorem 4.5.1. *NLS with the addition of linear effects,*

$$iu_t + u_{xx} + 2|u|^2u + i\Gamma u = 0, \tag{4.5.1}$$

has the solution

$$u(t) = Ae^{-\Gamma t}\exp\{2i|A|^2\frac{1-e^{-2\Gamma t}}{2\Gamma}\}.$$

Proof. Using the product rule, we have

$$\begin{aligned} u_t &= A\frac{d}{dt}\left(e^{-\Gamma t}\right) + Ae^{-\Gamma t}\frac{d}{dt}\left(\exp\{2i|A|^2\frac{1-e^{-2\Gamma t}}{2\Gamma}\}\right) \\ &= -A\Gamma e^{-\Gamma t}\exp\{2i|A|^2\frac{1-e^{-2\Gamma t}}{2\Gamma}\} + 2i|A|^2Ae^{-\Gamma t}\exp\{2i|A|^2\frac{1-e^{-2\Gamma t}}{2\Gamma}\}\frac{d}{dt}\left(\frac{-e^{-2\Gamma t}}{2\Gamma}\right) \\ &= (-\Gamma + 2i|A|^2e^{-2\Gamma t})u \end{aligned}$$

$$\implies iu_t = -(i\Gamma + 2|A|^2e^{-2\Gamma t})u.$$

Note that u is independent of x, so $u_{xx} = 0$. Next, we examine $|u|^2$.

$$|u|^2 = |Ae^{-\Gamma t}\exp\{2i|A|^2\frac{1-e^{-2\Gamma t}}{2\Gamma}\}|^2$$

$$= |A|^2 |e^{-\Gamma t}|^2 | \exp\{2i|A|^2 \frac{1-e^{-2\Gamma t}}{2\Gamma}\}|$$
$$= |A|^2 e^{-2\Gamma t},$$

since $|e^{i\theta}| = 1$ for $\theta \in \mathbb{R}$. So we have

$$iu_t + u_{xx} + 2|u|^2 u + i\Gamma u = -(i\Gamma + 2|A|^2 e^{-2\Gamma t})u + 0 + 2|A|^2 e^{-2\Gamma t} u + i\Gamma u = 0,$$

as desired. □

Corollary 4.5.2. *The spatially-independent function*

$$u(t) = Ae^{-\Gamma t} \exp\{2i|A|^2 \frac{1-e^{-2\Gamma t}}{2\Gamma}\}$$

is a solution to

$$iu_t + u_{xx} + 2|u|^2 u + i\Gamma u = -i\hat{\epsilon}\left(\frac{1}{2}u_{xxx} - 6|u|^2 u_x + u^2 u_x^* - 2iu(1+i\beta)\left[\mathcal{H}\left(|u|^2\right)\right]_x\right),$$

where $\mathcal{H}(f)$ is the Hilbert transform of the function f.

Proof. Since u is independent of x, $u_{xxx} = u_x = u_x^* = 0$. Additionally,

$$\mathcal{H}(f)(t) = p.v. - \frac{1}{2\pi}\int_{-\infty}^{\infty} \frac{f(\tau)}{t-\tau} d\tau$$

Thus if we take a derivative in space we again get no contribution. So none of the terms on the RHS survive the derivative in space. Hence, by the previous problem $u(t)$ is also a solution to this perturbation of the equation. □

Now that we have a solution to the PDE, we can proceed with linearizing about this solution. To simplify the calculations, we first change variables. Let $\psi(x,t) = \mu(x,t)\exp(-2t)$.

So that

$$i\psi_t = i\mu_t e^{-2t} - 2i\mu e^{-2t}$$

$$\psi_{xx} = \mu_{xx} e^{-2t}$$

$$|\psi|^2\psi = |\mu|^2 e^{-4t}\mu e^{-2t} = |\mu|^2 \mu e^{-6t}$$

$$2i\psi = 2i\mu e^{-2t}$$

$$\psi_{3x} = \mu_{3x} e^{-2t}$$

$$|\psi|^2\psi_x = |\mu|^2 \mu_x e^{-6t}$$

$$\mathcal{H}\left(|\psi|^2\right) = \mathcal{H}\left(|\mu|^2 e^{-4t}\right) = e^{-4t}\mathcal{H}\left(|\mu|^2\right)$$

$$\psi\mathcal{H}\left(|\psi|^2\right)_x = \mu e^{-6t}\mathcal{H}\left((|\mu|^2)_x\right)$$

Canceling the common e^{-2t} in each term, the governing equation becomes

$$i\mu_t + \mu_{xx} + 2|\mu|^2\mu e^{-4t} + i\hat{\epsilon}\left(\frac{1}{2}\mu_{3x} + e^{-4t}\left[-8|\mu|^2\mu_x - 2(1+i\beta)\mu\mathcal{H}\left((|\mu|^2)_x\right)\right]\right) = 0$$

Next, we expand about a solution. Let $\mu_0(t) = \exp\left\{2iA^2\left(\frac{1-e^{-4t}}{4} + i\arg(A)\right)\right\}$, and

$$\begin{aligned}\mu(x,t) &= \exp\left\{2i|A|^2\left(\frac{1-e^{-4t}}{4}\right) + i\arg(A)\right\}\left(|A| + \epsilon u(x,t) + i\epsilon v(x,t) + \mathcal{O}\left(\epsilon^2\right)\right) \\ &= \mu_0\left(|A| + \epsilon u + i\epsilon v + \mathcal{O}\left(\epsilon^2\right)\right)\end{aligned}$$

where u and v are real-valued functions. Then

$$|\mu_0|^2 = 1, \text{ since } \left[2|A|^2\left(\frac{1-e^{-4t}}{4}\right) + \arg(A)\right] \in \mathbb{R}.$$

Also,

$$\frac{d}{dt}(\mu_0) = \frac{d}{dt}\left[2i|A|^2\left(\frac{1-e^{-4t}}{4}\right) + i\arg(A)\right]\mu_0 = 2i|A|^2 e^{-4t}\mu_0.$$

We now substitute our form of μ into the transformed governing equation. We have the following:

$$\begin{aligned}
\mu_t &= \frac{d}{dt}(\mu_0)(|A| + \epsilon u + i\epsilon v) + \mu_0(\epsilon u_t + i\epsilon v_t) \\
&= \mu_0 \left[2i|A|^2 e^{-4t}(|A| + \epsilon u + i\epsilon v) + \epsilon u_t + i\epsilon v_t\right] \\
\mu_{xx} &= \mu_0 \left[\epsilon u_{xx} + i\epsilon v_{xx}\right] \\
|\mu|^2 &= |\mu_0|^2||A| + \epsilon u + i\epsilon v|^2 \\
&= (|A| + \epsilon u + i\epsilon v)(|A| + \epsilon u - i\epsilon v) \\
&= (|A|^2 + |A|\epsilon u - i|A|\epsilon v + |A|\epsilon u + i|A|\epsilon v + \mathcal{O}\left(\epsilon^2\right)) \\
&= (|A|^2 + 2|A|\epsilon u + \mathcal{O}\left(\epsilon^2\right)) \\
|\mu|^2\mu &= \mu_0 \left[(|A|^2 + 2|A|\epsilon u + \mathcal{O}\left(\epsilon^2\right))(|A| + \epsilon u + i\epsilon v)\right] \\
&= \mu_0 \left[|A|^3 + |A|^2\epsilon u + i|A|^2\epsilon v + 2|A|^2\epsilon u + \mathcal{O}\left(\epsilon^2\right)\right] \\
&= \mu_0 \left[|A|^3 + 3|A|^2\epsilon u + i|A|^2\epsilon v + \mathcal{O}\left(\epsilon^2\right)\right] \\
\mu_{3x} &= \mu_0 \left[\epsilon u_{3x} + i\epsilon v_{3x}\right] \\
|\mu|^2\mu_x &= \mu_0 \left(|A|^2\epsilon u_x + i|A|^2\epsilon v_x\right) \\
\mathcal{H}\left((|\mu|^2)_x\right) &= 2|A|^2\epsilon\mathcal{H}\left(u_x\right) \\
\mu\mathcal{H}\left((|\mu|^2)_x\right) &= 2\epsilon|A|^2\mu_0\mathcal{H}\left(u_x\right)
\end{aligned}$$

With the appropriate coefficients we have

$$\begin{aligned}
i\mu_t &= \mu_0 \left[-2e^{-4t}|A|^3 - 2e^{-4t}|A|^2\epsilon u - 2ie^{-4t}|A|^2\epsilon v + i\epsilon u_t - \epsilon v_t\right] \\
\mu_{xx} &= \mu_0 \left[\epsilon u_{xx} + i\epsilon v_{xx}\right]
\end{aligned}$$

$$2e^{-4t}|\mu|^2\mu = \mu_0\left[2e^{-4t}|A|^3 + 6e^{-4t}|A|^2\epsilon u + i2e^{-4t}|A|^2\epsilon v\right]$$

$$-8i\hat{\epsilon}e^{-4t}|\mu|^2\mu_x = \mu_0\left(-8i|A|^2\epsilon\hat{\epsilon}e^{-4t}u_x + 8|A|\epsilon\hat{\epsilon}e^{-4t}v_x\right)$$

$$i\hat{\epsilon}\frac{1}{2}\mu_{3x} = \mu_0\left[\epsilon i\hat{\epsilon}\frac{1}{2}u_{3x} - \epsilon\hat{\epsilon}\frac{1}{2}v_{3x}\right]$$

$$2\hat{\epsilon}(1+i\beta)e^{-4t}\mu\mathcal{H}\left((|\mu|^2)_x\right) = \mu_0 4(1+i\beta)\epsilon\hat{\epsilon}|A|^2e^{-4t}\mathcal{H}\left(u_x\right)$$

Summing these at $\mathcal{O}\left(\epsilon^0\right)$ we have

$$\mu_0\left[-2e^{-4t}|A|^3 + 2e^{-4t}|A|^3\right] = 0$$

which is satisfied because μ_0 is a solution to the equation.

Canceling the common factor of μ_0, at $\mathcal{O}\left(\epsilon\right)$ we have

$$\begin{aligned}-2e^{-4t}|A|^2u - 2ie^{-4t}|A|^2v + iu_t - v_t + u_{xx} + iv_{xx} + 6e^{-4t}|A|^2u + i2e^{-4t}|A|^2v \\ - 8i|A|^2\hat{\epsilon}e^{-4t}u_x + 8|A|^2\hat{\epsilon}e^{-4t}v_x + i\hat{\epsilon}\frac{1}{2}u_{3x} - \hat{\epsilon}\frac{1}{2}v_{3x} \\ + 4i\beta\hat{\epsilon}|A|^2e^{-4t}\mathcal{H}\left(u_x\right) + 4\hat{\epsilon}|A|^2e^{-4t}\mathcal{H}\left(u_x\right) = 0.\end{aligned}$$

Or,

$$\begin{aligned}4e^{-4t}|A|^2u + iu_t - v_t + u_{xx} + iv_{xx} - 8i|A|^2\hat{\epsilon}e^{-4t}u_x + 8|A|^2\hat{\epsilon}e^{-4t}v_x \\ + i\hat{\epsilon}\frac{1}{2}u_{3x} - \hat{\epsilon}\frac{1}{2}v_{3x} + 4i\beta\hat{\epsilon}|A|^2e^{-4t}\mathcal{H}\left(u_x\right) + 4\hat{\epsilon}|A|^2e^{-4t}\mathcal{H}\left(u_x\right) = 0.\end{aligned}$$

We assume that u and v have the form

$$\begin{cases} u(x,t) &= U(k,\omega,t)e^{ikx} + c.c \\ v(x,t) &= V(k,\omega,t)e^{ikx} + c.c \end{cases},$$

where *c.c.* is the complex conjugate of the term, we have

$$\begin{aligned}4e^{-4t}|A|^2Ue^{ikx} + iU_te^{ikx} - V_te^{ikx} + U(ik)^2e^{ikx} + iV(ik)^2e^{ikx} \\ - 8i|A|^2\hat{\epsilon}e^{-4t}(ik)Ue^{ikx} + 8|A|^2\hat{\epsilon}e^{-4t}V(ik)e^{ikx} + i\hat{\epsilon}\frac{1}{2}(ik)^3Ue^{ikx} \\ - \hat{\epsilon}\frac{1}{2}(ik)^3Ve^{ikx} + 4i\beta\hat{\epsilon}|A|^2e^{-4t}kUe^{ikx} + 4\hat{\epsilon}|A|^2e^{-4t}kUe^{ikx} = 0.\end{aligned}$$

Simplifying

$$\begin{aligned}4e^{-4t}|A|^2U + iU_t - V_t - k^2U - ik^2V + 12|A|^2\hat{\epsilon}e^{-4t}kU + i8|A|^2\hat{\epsilon}e^{-4t}kV + \hat{\epsilon}\frac{1}{2}k^3U \\ + i\hat{\epsilon}\frac{1}{2}k^3V + 4i\beta\hat{\epsilon}|A|^2e^{-4t}kU = 0.\end{aligned}$$

Grouping by real and imaginary coefficients we have

$$\begin{cases} 4e^{-4t}|A|^2U - V_t - k^2U + 12|A|^2\hat{\epsilon}e^{-4t}kU + \hat{\epsilon}\frac{1}{2}k^3U = 0 \\ U_t - k^2V + 8|A|^2\hat{\epsilon}e^{-4t}kV + \hat{\epsilon}\frac{1}{2}k^3V + 4\beta\hat{\epsilon}|A|^2e^{-4t}kU = 0 \end{cases}$$

$$\begin{cases} V_t &= 4e^{-4t}|A|^2U - k^2U + 12|A|^2\hat{\epsilon}e^{-4t}kU + \hat{\epsilon}\frac{1}{2}k^3U \\ U_t &= k^2V - 8|A|^2\hat{\epsilon}e^{-4t}kV - \hat{\epsilon}\frac{1}{2}k^3V - 4\beta\hat{\epsilon}|A|^2e^{-4t}kU \end{cases}$$

$$\begin{cases} V_t &= \left[4e^{-4t}|A|^2 - k^2 + 12|A|^2\hat{\epsilon}e^{-4t}k + \hat{\epsilon}\frac{1}{2}k^3\right]U \\ U_t &= \left[k^2 - 8|A|^2\hat{\epsilon}e^{-4t}k - \hat{\epsilon}\frac{1}{2}k^3\right]V - 4\beta\hat{\epsilon}|A|^2e^{-4t}kU \end{cases}.$$

Taking another derivative of U_t and substituting in V_t we arrive at

$$U_{tt} = \left[k^2 - 8|A|^2\hat{\epsilon}e^{-4t}k - \hat{\epsilon}\frac{1}{2}k^3\right]V_t - 4\beta\hat{\epsilon}|A|^2e^{-4t}kU_t$$

$$\begin{aligned}U_{tt} + 4\beta\hat{\epsilon}|A|^2e^{-4t}kU_t \\ - \left[k^2 - 8|A|^2\hat{\epsilon}e^{-4t}k - \hat{\epsilon}\frac{1}{2}k^3\right]\left[4e^{-4t}|A|^2 - k^2 + 12|A|^2\hat{\epsilon}e^{-4t}k + \hat{\epsilon}\frac{1}{2}k^3\right]U = 0\end{aligned}$$

Let

$$\begin{aligned}
B(t) &= 4\beta\hat{\epsilon}|A|^2 e^{-4t}k, \\
C(t) &= C_1(t)C_2(t), \\
C_1(t) &= k^2 - 8|A|^2\hat{\epsilon}e^{-4t}k - \hat{\epsilon}\frac{1}{2}k^3, \\
C_2(t) &= 4e^{-4t}|A|^2 - k^2 + 12|A|^2\hat{\epsilon}e^{-4t}k + \hat{\epsilon}\frac{1}{2}k^3.
\end{aligned}$$

So the differential equation can be rewritten as

$$U_{tt} + B(t)U_t - C(t)U = 0. \tag{4.5.2}$$

An integrating factor is utilized in order to get the differential equation into Sturm-Liouville form. Note that (4.5.2) can be rewritten as

$$\begin{aligned}
&e^{\int B(t)\,dt}U_{tt} + B(t)e^{\int B(t)\,dt}U_t - C(t)e^{\int B(t)\,dt}U = 0. \\
&\implies \frac{d}{dt}\left[e^{\int B(t)\,dt}U_t\right] - C(t)e^{\int B(t)\,dt}U = 0.
\end{aligned}$$

Letting $K(t) = e^{\int B(t)\,dt}$ and $G(t) = C(t)K(t)$, equation (4.5.2) has the Sturm-Liouville form

$$\frac{d}{dt}\left[K\frac{dU}{dt}\right] - GU = 0.$$

Now, we consider the signs of K and G. Since $B(t) \in \mathbb{R}$, and moreover, $B(t) \geq 0$, we have that $K(t) \geq 1$ for all t. The sign of $G(t) = C(t)K(t)$ is determined by the sign of $C(t)$. $G(t) \geq 0$ if $C(t) \geq 0$, so $C_1(t)$ and $C_2(t)$ must have the same sign.

First, we address the case where both functions are negative. If $C_1(t) < 0$ then

$$k^2 - 8|A|^2\hat{\epsilon}e^{-4t}k - \hat{\epsilon}\frac{1}{2}k^3 < 0$$
$$\implies k^2 < \hat{\epsilon}\Big(8|A|^2e^{-4t}k + \frac{1}{2}k^3\Big).$$

However, when $\hat{\epsilon} = 0$, this implies that $k^2 < 0$, which is a contradiction. Hence, the only situation where the function has non-oscillatory solutions is when both $C_1(t)$ and $C_2(t)$ are positive.

If $C_1(t) > 0$, then we have $k^2 > \hat{\epsilon}\Big(8|A|^2e^{-4t}k + \frac{1}{2}k^3\Big)$. We must also have

$$C_2(t) = 4e^{-4t}|A|^2 - k^2 + 12|A|^2\hat{\epsilon}e^{-4t}k + \hat{\epsilon}\frac{1}{2}k^3 > 0$$
$$\implies k^2 < 4e^{-4t}|A|^2 + \hat{\epsilon}\Big(12|A|^2e^{-4t}k + \frac{1}{2}k^3\Big).$$

Notice, that when C_1 and C_2 are evaluated at $\hat{\epsilon} = 0$, our conclusion is consistent with Segur's conclusions for the linearly damped NLS [9]. Nonlinear damping of the mean flow was also not considered in that work.

These requirements mean that we have

$$\hat{\epsilon}\Big(8|A|^2e^{-4t}k + \frac{1}{2}k^3\Big) < k^2 < 4e^{-4t}|A|^2 + \hat{\epsilon}\Big(12|A|^2e^{-4t}k + \frac{1}{2}k^3\Big)$$
$$\hat{\epsilon}\Big(8|A|^2e^{-4t}k + \frac{1}{2}k^3\Big) < k^2 < 4e^{-4t}|A|^2(1+\hat{\epsilon}) + \hat{\epsilon}\Big(8|A|^2e^{-4t}k + \frac{1}{2}k^3\Big).$$

Hence the instability region has width $4e^{-4t}|A|^2(1+\hat{\epsilon})$, and as $t \to \infty$, the width of this region goes to 0.

CHAPTER 5

NUMERICAL EXPERIMENTS

5.1 Setup of numerical experiments

The initial data used in the numerical experiments are small perturbations of the unstable plane wave, i.e.

$$u(x,0) = a\Big(1 + \delta\cos(2\pi x/L)\Big), \tag{5.1.1}$$

where $\delta << 1$ and the amplitude a and period L are chosen so that $\lfloor aL/\pi \rfloor = \mathrm{N} = 1,\, 2,\, 3$.

Initial data (5.1.1) is referred to as the N unstable mode (UM) "regime" as the background plane wave has N unstable modes *initially*. The solutions are approximated numerically using a very accurate smoothing exponential integrator. The integrator combines a Fourier-mode decomposition in space with a fourth-order exponential Runge-Kutta method in time which uses Padé approximations of the matrix exponential terms. The integrator was implmented using 256 Fourier modes for $L = 4\sqrt{2}\pi$ and a time step of $\Delta t = 10^{-3}$ for $9 < t < 200$. Each of the applicable conserved quantities for the HONLS equation are conserved to an order of $\mathcal{O}\left(10^{-4}\right)$ for the experiments presented here. See the Appendix for further details.

5.2 Rogue waves and downshifting in HONLS

In this section we compare the development of rogue waves in the NLS and HONLS equations. We begin with modulated plane wave initial data (5.1.1) in the one UM regime, which can be characterized by fixing $L = 2\sqrt{2}\pi$ and varying the amplitude, $0.4 \leq a \leq .67$, with modulation $\delta = .0001$. Figure 5.1(a) shows the maximum strength, $S_{max}(a)$, attained with the NLS and HONLS equations for $0 \leq t \leq 40$. For all values of a, the maximum strengths of the HONLS waves are greater than those of the NLS waves. Even so, whether using modulated plane wave or single mode SPB initial data, Figures 5.1(a-b) show rogue waves are not obtained in either the NLS or the HONLS experiments in the one UM regime. In general, S_{max} increases with the initial amplitude; close to the upper bound for one UM $S_{max}(.67) \approx 2.15$ for the HONLS equation. As such, it may be possible to obtain rogue waves in the HONLS equation for initial data in the one UM regime by using larger values of ϵ, which would introduce another UM. However, none were observed for the range of ϵ considered in our numerical experiments, ($\epsilon \leq 0.05$) .

Figure 5.2(a) shows the surface amplitude $|u(x,t)|$ for initial data (5.1.1) in the two UMs regime, i.e. $a = 0.5$, $\delta = 0.1$, and $L = 4\sqrt{2}\pi$ for $0 < t < 200$. Shortly after a rogue waves appears at $t \approx 8$ the solution becomes chaotic. The evolution of the strength $S(t)$, Figure 5.2(b), shows rogue waves occur intermittently throughout the time series. The larger rogue waves have strengths, $S(t) > 2.6$ at $t \approx 8$ and at $t \approx 173$, are due to partial coalescence of the modes in the chaotic sea state, and are greater than the strengths of the

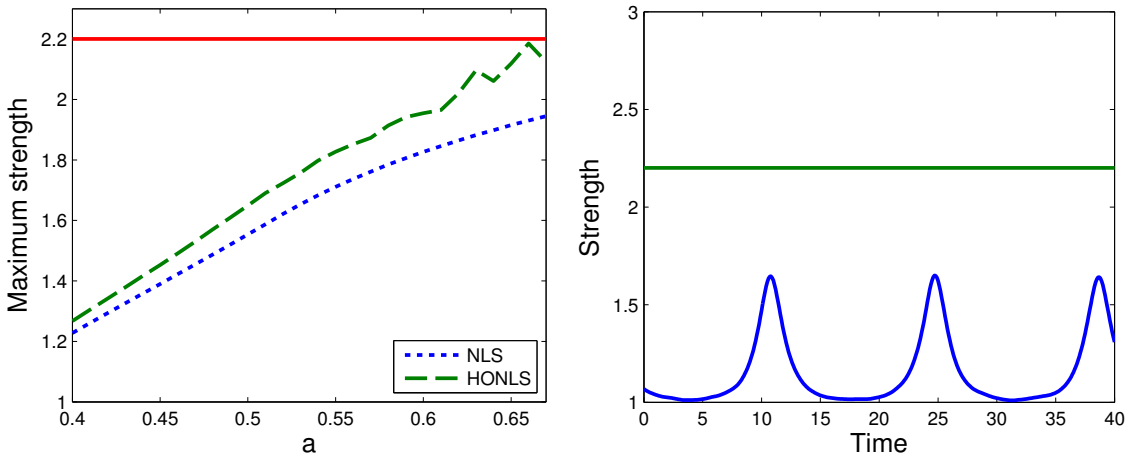

Figure 5.1: (a) $S_{max}(a)$ for the NLS ($\epsilon = 0$) and HONLS ($\epsilon = 0.05$) equations using initial data (5.1.1) with $\delta = .0001$ and $L = 2\sqrt{2}\pi$, (b) HONLS evolution of the single mode SPB initial data, $U^1(x, 0; -2)$, $L = 2\sqrt{2}\pi$, $\epsilon = 0.05$, $\beta = \Gamma = 0$, for $0 \leq t \leq 40$.

well separated two mode SPBs (see Figure 1.6(a)). However, the HONLS wave strengths are typically smaller than S_{max} for the coalesced two mode SPB as the higher order terms in the HONLS equation break symmetry and prevent a complete spatial coalescence of the nonlinear modes.

A temporary downshift in the spectral peak occurs with each large wave. Figure 5.2(c) shows the time evolution of the main Fourier modes $|A_k(t)|$ for $k = 0, \pm 1, \ldots, \pm 4$. During each of the modulation stages the zeroth mode loses energy as the upper and lower higher harmonics become excited. For the HONLS equation the total energy and the total energy flux are constant. This allows the energy to flow back to the zeroth mode keeping the spectral center constant (in the numerical simulation the spectral center was conserved $\mathcal{O}(10^{-12})$).

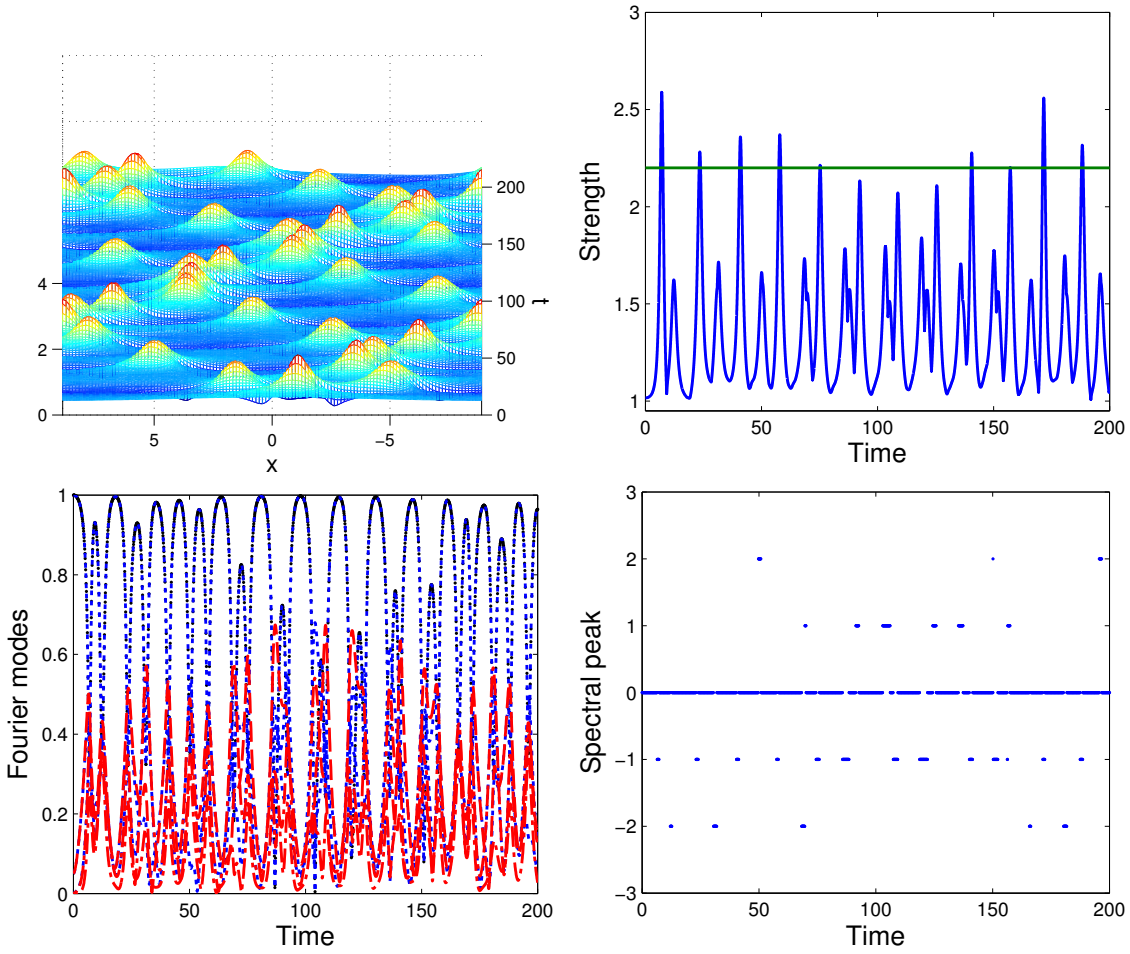

Figure 5.2: HONLS equation with $\epsilon = 0.05$, $\Gamma = \beta = 0$. Evolution of the (a) surface amplitude $|u(x,t)|$, (b) strength $S(t)$, (c) main Fourier modes, and (d) spectral peak using initial data (5.1.1) with $a = 0.5$, $L = 4\sqrt{2}\pi$, $\delta = 0.1$ for $0 < t < 200$.

The plot of k_{peak} in Figure 5.2(d) confirms that a permanent frequency downshift does not occur.

To compare the behavior of the waves for the HONLS ($\epsilon = 0.05, \Gamma = \beta = 0$) and the NLS equations in the two UMs regime, a set of numerical experiments was carried out by varying the amplitude and parameter τ in the two mode SPB initial data $U^{(2)}(x, 0; -5, \tau)$

with $L = 4\sqrt{2}\pi$. For each of the eleven values of a used, $0.4 \leq a \leq 0.5$, twenty one τ values were chosen, $-9 \leq \tau \leq -4$, to include the effects of varying the time difference between the two modes in the SPB. For each value of a, the diagnostics are averaged over τ. The exact two-mode SPBs are evaluated at each (x, t) to provide the NLS solutions.

At most two rogue waves occur in the exact SPB solution depending on whether the modes are coalesced or not. In contrast, rogue waves generically emerge and occur intermittently throughout the entire HONLS time series. Figure 5.3 shows the (a) maximum strength and (b) lifetime of rogue waves for two mode SPB initial data as a function of the amplitude. The exact two mode SPB solutions of the NLS equation are given by the solid line, while HONLS solutions for short times and long times are given by the dashed line $(0 < t < 40)$ and by the dash-dot line $(0 < t < 400)$, respectively.

Figure 5.3(a) shows, on average, the maximum strength of the HONLS waves is larger than for the NLS waves as additional focusing occurs in the HONLS equation. The lifetime and number of rogue waves is greater in the HONLS equation than in the NLS (or the damped HONLS equations). Figure 5.3(b) shows that the difference in lifetime increases as the experiment length is increased. This is to be expected since rogue waves occur throughout the entire HONLS experiment. As a result, the likelihood of obtaining rogue waves with the HONLS equation is greater than with the NLS equation.

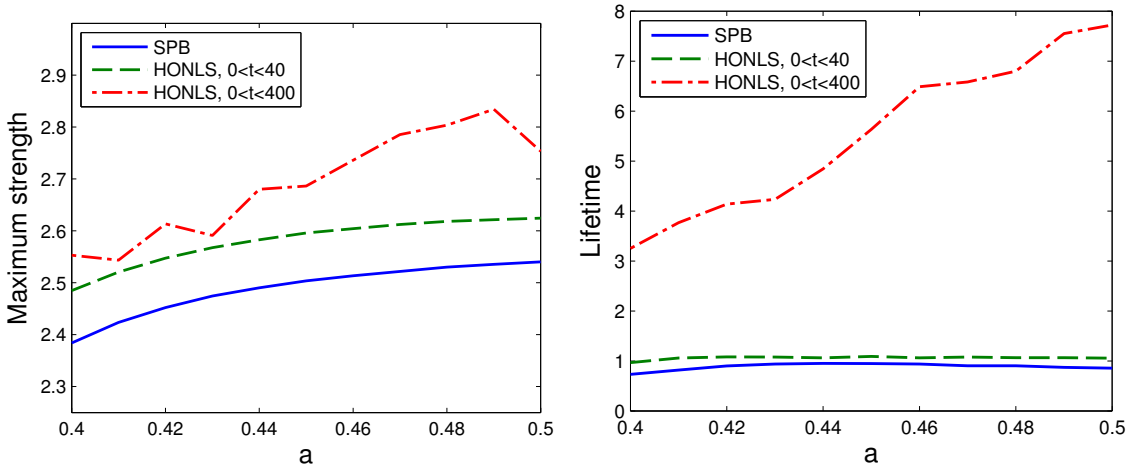

Figure 5.3: The (a) maximum strength and (b) lifetime of rogue waves obtained using two mode SPB initial data $U^{(2)}(x, 0; -5, \tau)$ for the NLS equation (solid line) and HONLS equation for short time, $0 < t < 40$, (dashed line) and long times, $0 < t < 400$, (dash-dot line).

5.3 Rogue waves and downshifting in linear damped HONLS

Equation (4.2.6) for the rate of change of the wave energy clearly shows that linear damping ($\Gamma > 0$ and $\beta = 0$) of the HONLS equation results in a uniform damping of the individual Fourier modes (e.g. see Figure 5.4(c)). Permanent downshifting is not expected for the linear damped HONLS equation since k_m is constant in time. This is confirmed with both k_m and k_{peak} in the numerical experiments. Figure 5.4 shows the evolution of (a) the strength, (b) the spectral peak, and (c) the Fourier modes of the solution of (4.1.1) with $\epsilon = 0.05$, $\Gamma = 0.01$, $\beta = 0$, using initial condition (5.1.1) with $a = .65$, $L = 4\sqrt{2}\pi$ and $\delta = 0.1$. In Figure 5.4(b) k_{peak} continues to return to the original dominant mode throughout the evolution. The

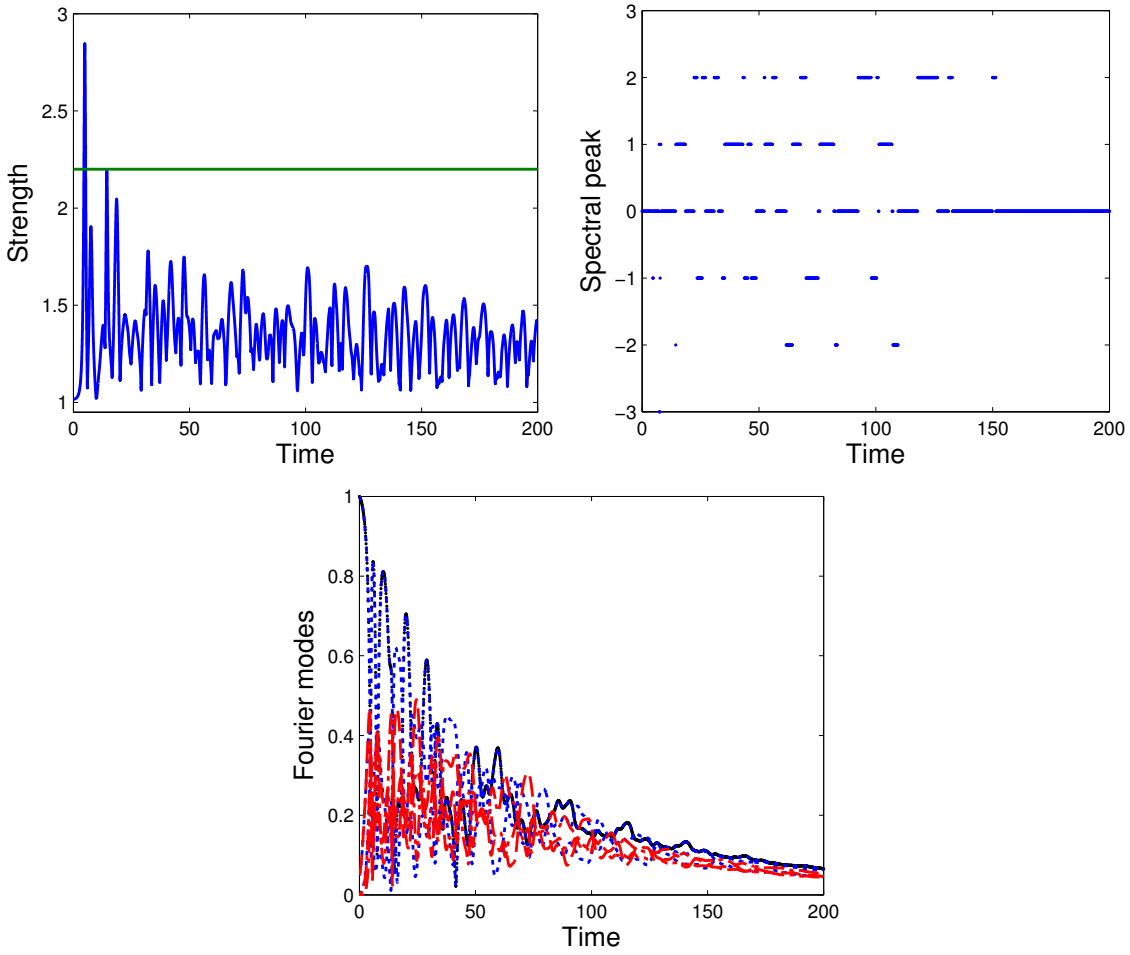

Figure 5.4: HONLS with linear damping, $\epsilon = 0.05$, $\Gamma = 0.01$, $\beta = 0$. Evolution of (a) the strength, (b) the spectral peak, and (c) the Fourier modes using initial condition (5.1.1) with $a = .65$, $L = 4\sqrt{2}\pi$ and $\delta = 0.1$.

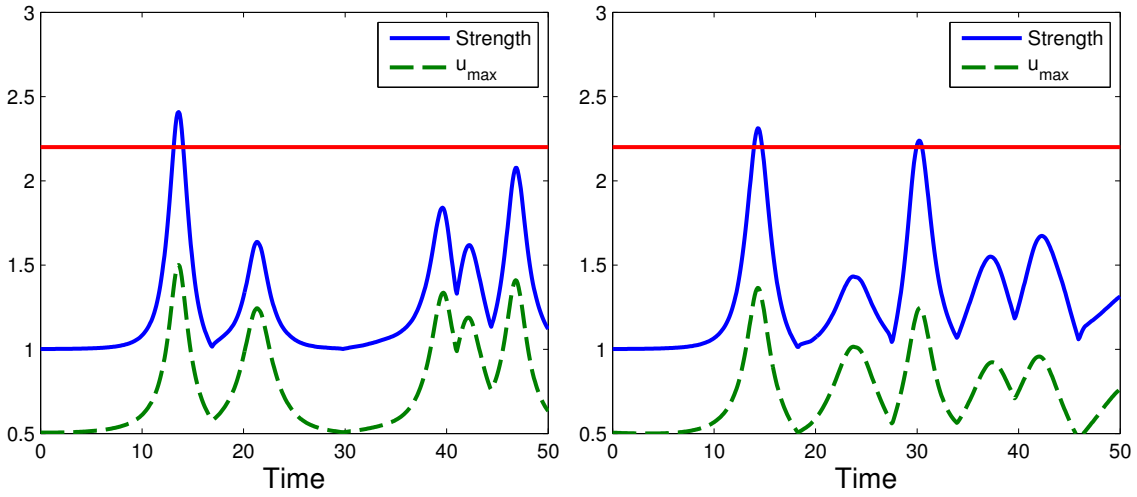

Figure 5.5: Strength $S(t)$ (solid line) and $|u|_{max}$ (dashed line) for (a) HONLS Equation $\epsilon = 0.05$; (b) HONLS Equation with Linear Damping, $\epsilon = 0.05$, $\Gamma = 0.005$, $\beta = 0$, for IC $u_0 = 0.5(1 + 0.01\cos\mu x)$, with $L = 4\sqrt{2}\pi$.

spectral center is conserved within integrator accuracy, $\mathcal{O}(10^{-11})$, of zero (not shown) and a permanent downshift does not occur.

Surprisingly, for short time evolutions, more rogue waves may appear in the damped HONLS equation than in the undamped HONLS equation. Figure 5.5 provides the wave strength $S(t)$ (solid line) and $|U|_{max}(t)$ (dotted line) for (a) the undamped HONLS equation ($\epsilon = 0.05$) and (b) the linear damped HONLS equation ($\epsilon = 0.05$, $\Gamma = .005$, and $\beta = 0$) for initial condition (5.1.1) with $a = 0.5$, $\delta = 0.01$ and $L = 4\pi\sqrt{2}$. On this time frame the linear damped HONLS has two rogue waves while the undamped HONLS has only one. The damping alters the excitation time of the modes, allowing the modes to partially coalesce at $t \approx 30$ and produce the second rogue wave (Figure 5.5(b)). However, this is atypical

and with damping the average strength and lifetime of rogue events decreases, which we subsequently address more fully.

In the linear damped HONLS experiments, $0 < t < 100$, we use initial data (5.1.1) with $\delta = 0.1$, $L = 4\sqrt{2}\pi$, and where the amplitudes a_k vary in the three cases, $k = 1, 2, 3$ UMs regimes initially, i.e. we let $.25 \leq a_1 \leq .3, .45 \leq a_2 \leq .5$, and $.6 \leq a_3 \leq .65$. The perturbation parameters for the evolution equation are $\epsilon = 0.05, \beta = 0$, and $0 < \Gamma \leq 0.1$. For each value of $\Gamma = .002 * j, j = 0, ..., 50$, five numerical experiments were carried out by varying the amplitude a_k in the initial condition for each of the three cases. For each value of Γ the data for the strength and lifetime of the rogue waves was averaged over the five numerical experiments for each k. Figure 5.6(a) shows the maximum strength $S_{max}(\Gamma)$ attained for $0 < t < 100$. The maximum strengths decrease to the strength of the initial plane-wave as linear damping is increased. This indicates there exists a Γ^* such that for $\Gamma > \Gamma^*$ linear damping stabilizes the modulational instability on the time frame examined and prevents exponential growth. Figure 5.6(b) shows that the lifetime of rogue waves are generally decreasing in those experiments that have rogue waves in the undamped cases ($N \geq 2$ UMs initially). For Γ sufficiently large, rogue waves do not develop in the time series: this occurs at approximately $\Gamma = .01$ when averaged over the experiments initially in the two UMs regime and $\Gamma = .03$ when averaged over the experiments initially in the three UMs regime. Similarly, the number of rogue waves and the time of the last rogue are generally decreasing as linear damping is increased (not shown).

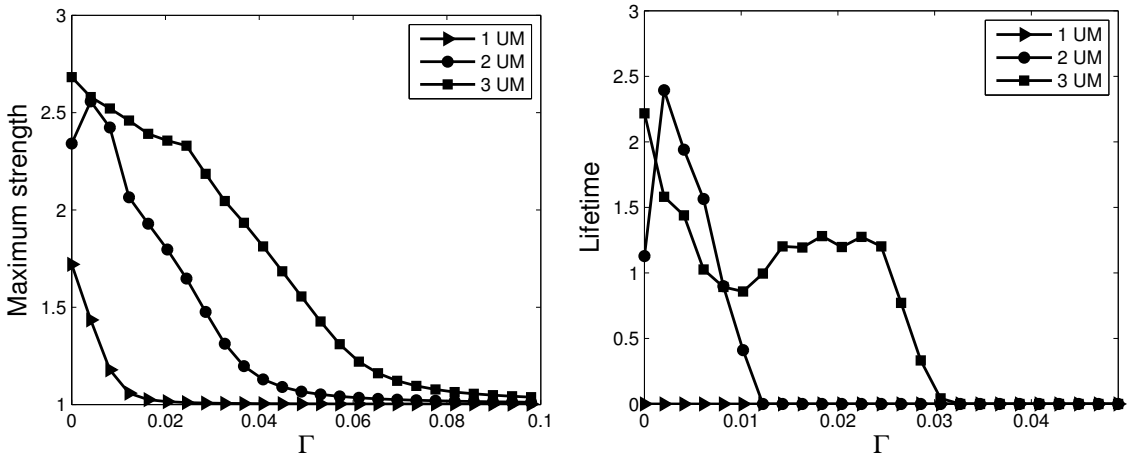

Figure 5.6: The (a) maximum strength, and the (b) lifetime of rogue waves as a function of Γ for the linear damped HONLS with $\epsilon = 0.05$, $\beta = 0$, and $0 < \Gamma < 0.1$ using the initial condition $u(x,0) = a_k(1 + 0.1\cos\mu x)$ and $0 < t < 100$.

5.4 Rogue waves and downshifting in nonlinear damped HONLS

Nonlinear damping has quite a different effect on the Fourier spectrum than linear damping. Instead of being uniformly damped, equation (4.2.6) shows when $\beta \neq 0$ and $\Gamma = 0$, the individual Fourier modes are damped at different rates causing k_{peak} to shift to a lower mode. To demonstrate the basic mechanism by which the nonlinear damping induces a permanent downshift in the spectrum, consider the solution of equation (4.1.1) with $\epsilon = 0.05$, $\beta = 0.6$ and $\Gamma = 0$, for initial data (5.1.1) with $a = 0.45$ and $\delta = 0.01$, $0 < t < 200$. The amplitude of the surface $|u(x,t)|$ and the strength $S(t)$ are shown in Figures 5.7(a-b). Only one rogue wave appears in the time series at $t \approx 25$. The onset of downshifting occurs when the first large wave (albeit not a rogue wave) appears at $t \approx 16$ which produces an abrupt decay

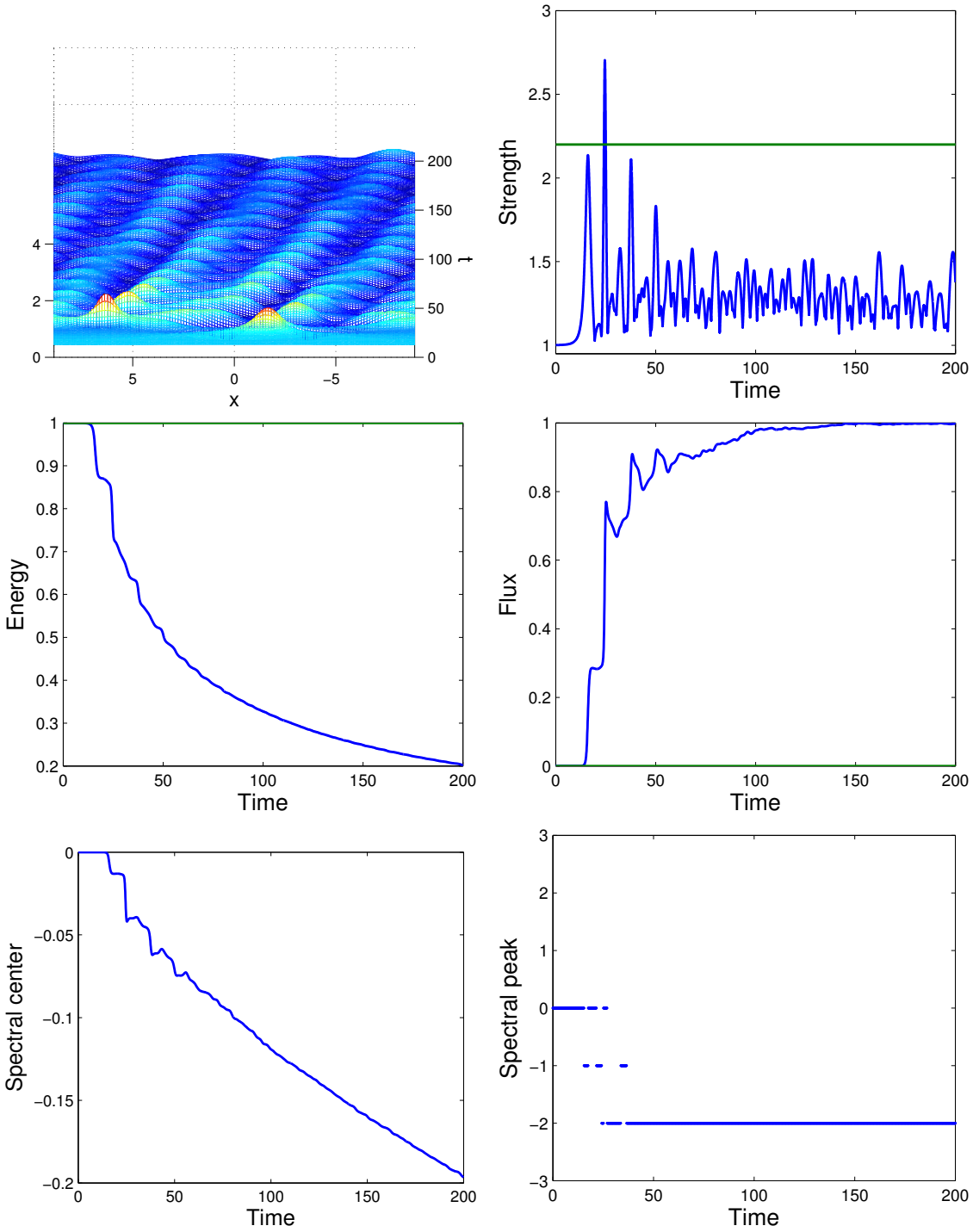

Figure 5.7: Nonlinear damped HONLS with $\beta = .6$, $\Gamma = 0$, $\epsilon = 0.05$, using initial condition (5.1.1) with $a = .45$, $\delta = 0.01$, $L = 4\sqrt{2}\pi$. The (a) amplitude of the surface, (b) maximum strength, (c) energy, (d) flux, (e) spectral center, and (f) spectral peak.

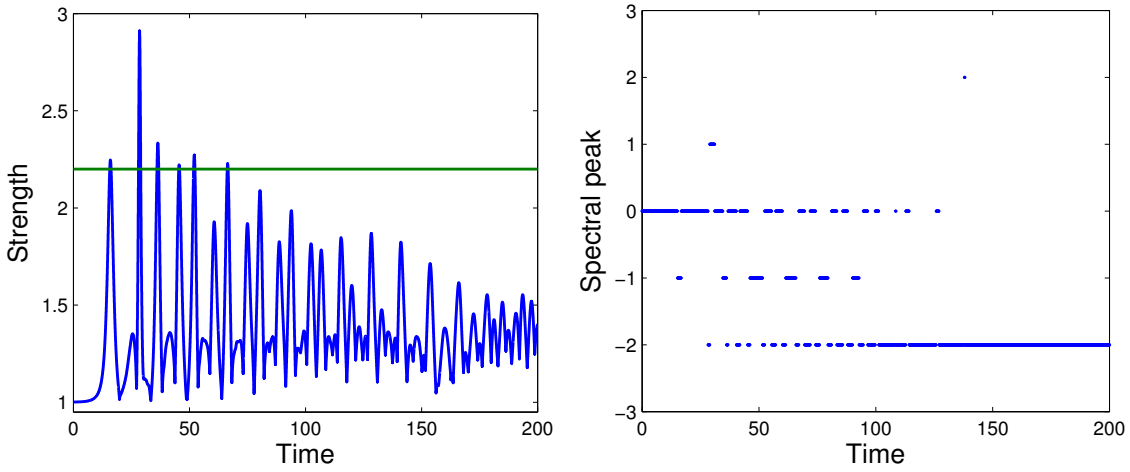

Figure 5.8: HONLS with nonlinear damping, $\epsilon = 0.05$, $\beta = 0.15$, $\Gamma = 0$. The (a) strength and (b) the spectral peak k_{peak} obtained using $u(x,0) = 0.45(1+0.01\cos\mu x)$, with $\mu = 2\pi/L$, $L = 4\sqrt{2}\pi$, for $0 < t < 200$.

in the energy seen in Figure 5.7(c) and growth in the flux as seen in Figure 5.7(d). This results in a rapid downward shift in the spectral center k_m and the spectral peak, k_{peak} at $t \approx 16$, Figures 5.7(e-f). The energy and flux vary only slightly until the rogue wave is excited at $t \approx 25$. This triggers a further rapid decay in the energy and growth in the flux. Figure 5.7(f) shows k_{peak} is active until the third large wave occurs at $t \approx 38$, at which time the spectrum permanently downshifts.

The time of permanent downshift, t_{PDS}, is determined using k_{peak}, i.e. t_{PDS} is the last time $k_{peak} = 0$. The subsequent numerical experiments are presented on the timeframe $0 < t < 200$; however each experiment was run for $0 < t < 250$ to ensure k_{peak} achieved its asymptotic state. The smaller the value of β, the slower the change in the energy and the flux, delaying a permanent downshift. As a case in point, Figure 5.8 shows the (a) strength

and (b) spectral peak of the solution of the nonlinear damped HONLS equation ($\epsilon = 0.05$, $\beta = 0.15$) for the same initial data as in Figure 5.7. For $\beta = 0.15$ the spectral peak, k_{peak}, permanently downshifts at $t \approx 127$, in contrast with the permanent downshift at $t \approx 27$ for $\beta = 0.6$. Further, for $\beta = 0.15$ the last rogue wave appears at $t \approx 67$, much later than for $\beta = 0.6$.

Downshifting does not occur for initial data which are perturbations of stable plane waves. To explore the dependence of downshifting and rogue waves on β we use initial data (5.1.1) with $\delta = 0.1$ in both the (a) one UM regime ($L = 2\sqrt{2}\pi$, $.5 \leq a_1 \leq .625$) and the (b) two UM regime ($L = 4\sqrt{2}\pi$, $.4 \leq a_2 \leq .48$). The parameters for the evolution equation are $\epsilon = 0.05$, $\Gamma = 0$, and $0 < \beta \leq 0.75$. For each of fourteen values of β, five experiments were conducted in each of the one and two UMs regimes by varying the amplitude a_k in the initial condition.

Figure 5.9 (a-b) provides the time of permanent downshift (x) and the time of the last rogue wave (square) averaged over the amplitudes in the a) one UM regime and b) two UMs regime. The plots for a single amplitude a are qualitatively the same. Significantly, in the set of experiments summarized in Figure 5.9 we find : 1) Permanent downshift is observed in all the experiments for all $\beta > 0$ and for all modulated unstable plane wave initial data ($N \geq 1$ UMs regimes). 2) The time of permanent downshift is a decreasing function of β, occurring rapidly for larger values of β. 3) A downshifted sea-state does not allow for any further rogue waves. Rogue waves typically do not develop after permanent downshifting occurs.

Several comments are in order. First, although rogue waves do not occur in the one UM regime, the data in Figure 5.9(a) shows that the wave strengths are sufficient to trigger a permanent downshift for all β. Second, in 94% of the experiments in the two UM regime the last rogue wave occurs before permanent downshifting (Figure 5.9(b)). Of the remaining 4 experiments (6%), the last rogue wave occurs either almost simultaneously with the time of permanent downshift or else the rogue waves is already forming. That is, given the time required for the instability to saturate or grow to its maximum amplitude, t_{SAT}, for these four experiments $t_{LRW} - t_{PDS} < t_{SAT}$. Finally, unlike the linear damped HONLS (as shown in Figure 5.6), it is not possible for nonlinear damping alone to cause the solution to settle into a nearly steady state. In Figure 5.10(b) we see that even for an extremely large nonlinear damping parameter ($\beta = 100$) the maximum strength is still approximately 1.1, indicating there is always initial growth in the timeseries. The same behavior can be seen for initial conditions with only one UM in Figure 5.10(c).

5.4.1 Characteristic features of the nonlinear damped evolution

Further features of the nonlinear damped evolution can be extracted from the previous set of experiments described in Figure 5.9. Figure 5.11(a) shows the effect of β on the terminal spectral center, i.e. $k_m(200)$, for different amplitudes in the one UM regime. In the plots the solid curve is the average over the amplitudes. For each amplitude, $k_m(200)$ is a decreasing function of β. Further, for fixed β as the amplitude of the initial condition increases the

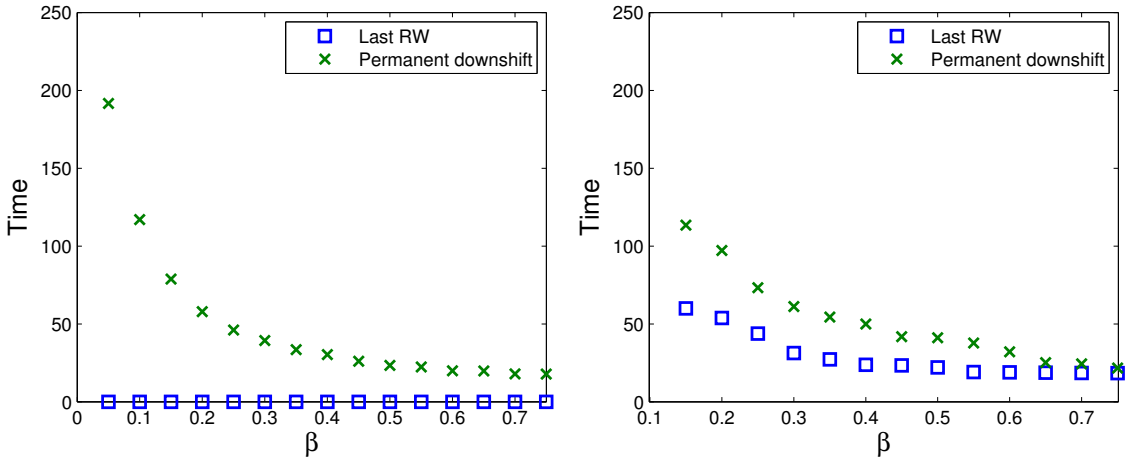

Figure 5.9: Time of permanent downshift (x) and time of last rogue wave (square) for one and two UM initial conditions in nonlinear damped HONLS with various β, and $\Gamma = 0$, using the initial condition $u(x,0) = a(1 + 0.1\cos\mu x)$ with $\mu = 2\pi/L$, $\epsilon = 0.05$ in Trulsen (4.1.1) for $0 < t < 250$, averaged over 5 amplitudes with initial conditions in the (a) one UM regime ($L = 2\sqrt{2}\pi$, $.5 \le a \le .625$ (b) two UM regime $L = 4\sqrt{2}\pi$, $.4 \le a \le .48$.

terminal spectral center k_m decreases. Figure 5.11(b) shows for each initial amplitude in the one UM regime the maximum strength $\max_{t\in[0,200]} S(t)$ is a strictly decreasing function of β. Similarly, for fixed β, the maximum strength is a strictly decreasing function of the amplitude. This is in contrast to the behavior observed for $N \ge 2$ UMs (see Fig 5.12(b)) where due to a chaotic sea state averaged quantities must be examined.

For initial amplitudes in the two UMs regime, $0.5 < a < 0.625$, Figure 5.12 shows the effects of β on: (a) the terminal spectral center k_m, (b) the maximum strength $\max_{t\in[0,200]} S(t)$, (c) the time of the last rogue wave and d) the lifetime of rogue waves for $0 < t < 200$. Figure 5.12(a) shows the terminal spectral center behaves similarly in the one and two UMs

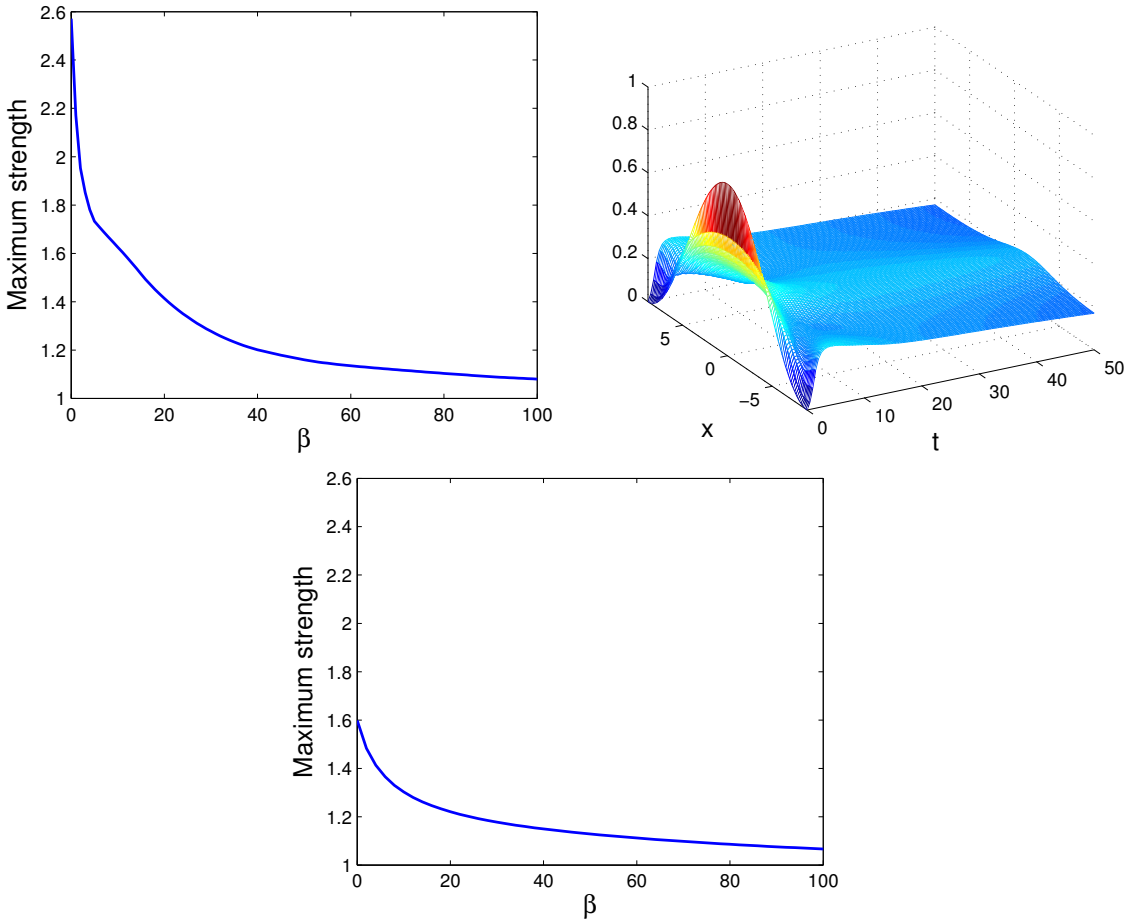

Figure 5.10: (a)The maximum strength of the two UMs initial condition $u(x,0) = .4(1 + 0.1\cos\mu x)$, $L = 4\sqrt{2}\pi$, evolved by nonlinear damped HONLS $\epsilon = 0.05$, $0 \leq \beta \leq 100$, $\Gamma = 0$, for $0 < t < 200$ as a function of β; (b) the surface amplitude for $\beta = 100$, $0 < t < 50$; and (c) the maximum strength of the one UM initial condition $u(x,0) = .25(1 + 0.1\cos\mu x)$ with the same parameter values as (a).

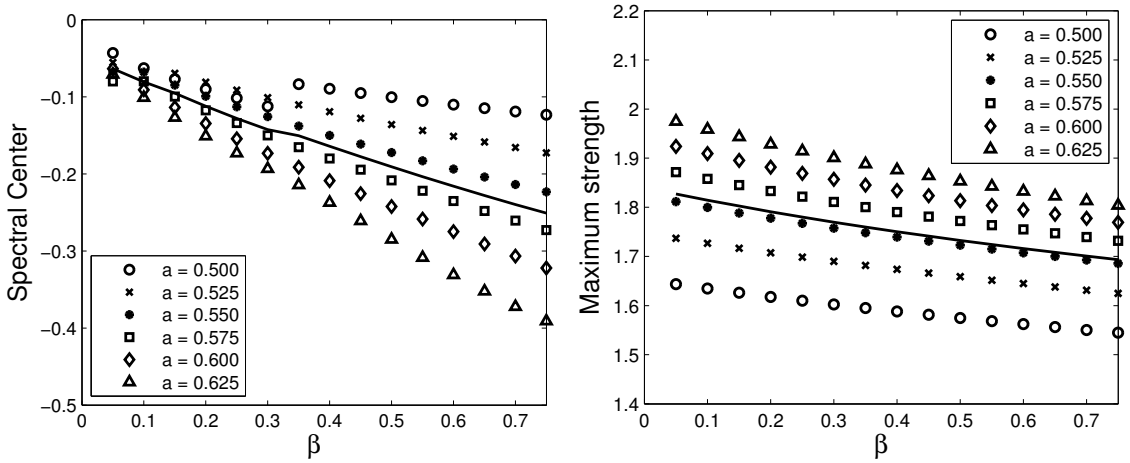

Figure 5.11: One UM initial condition in nonlinear damped HONLS, $\epsilon = 0.05$, $0 \leq \beta \leq .75$, $\Gamma = 0$, for $0 < t < 400$. The (a) terminal spectral center and the (b) maximum strength obtained using initial condition (5.1.1) with $L = 2\sqrt{2}\pi$, $\delta = 0.1$, and specified amplitudes in the one UM regime. The solid line is the average over the amplitudes.

regimes. Namely, for fixed amplitude, the $k_m(200)$ is a decreasing function of β while for fixed β, $k_m(200)$ is a decreasing function of the amplitude.

Figure 5.12(b) shows the smaller values of β can be thought of as providing a nonlinear "underdamping" of the waves since the maximum strength, as a function of β, has several critical points before it relaxes to its final state. Recall one may obtain larger waves when small damping is present due to changes in the focusing times and coalescence of the modes, as is illustrated in Figure 5.6. However, for a given amplitude a and for the average over the amplitudes, there exists a critical β^* for which the maximum strength decreases for $\beta > \beta^*$. In the earlier study of the effects of nonlinear damping on a carefully selected coalesced three mode rogue wave, significant damping of the maximum strength occurred since the largest rogue wave was typically not the first large wave excited [7]. For $N \leq 2$ UMs the maximum strength does not decrease as strikingly since the strength of the first large wave, which is needed to trigger the nonlinear damping, is typically the maximum strength in the time series. For all values of the initial amplitude, the first rogue wave is only slightly delayed ($t \approx 6$) for all β considered (not shown). Averaging the data over the amplitudes in the $N = 2$ UMs regime, Figures 5.12(c-d) show as β increases the time of the last rogue wave $\rightarrow 20$ and the average lifetime and number (not shown) of rogue waves decreases.

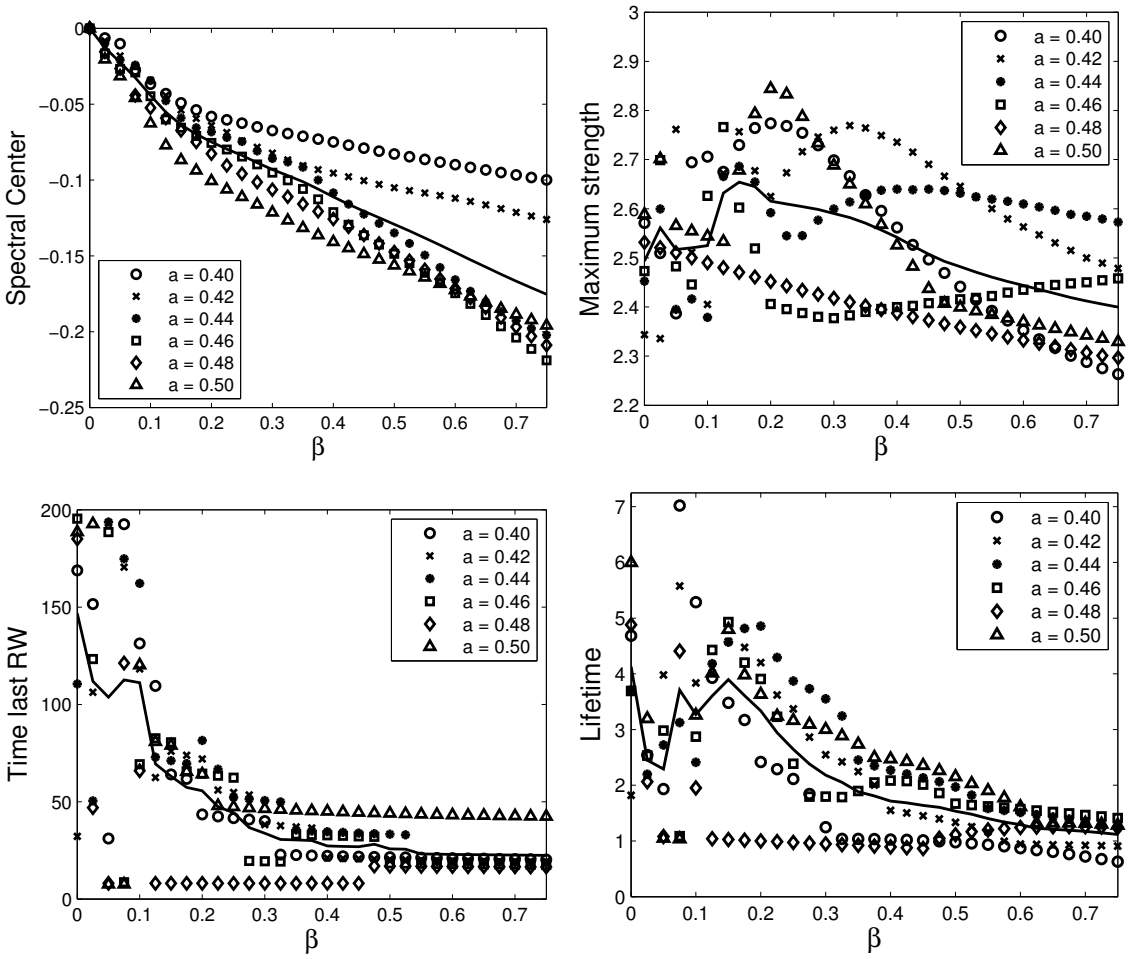

Figure 5.12: Two UMs initial condition in nonlinear damped HONLS, $\epsilon = 0.05$, $0 \leq \beta \leq .75$, $\Gamma = 0$, for $0 < t < 200$. The (a) terminal spectral center, (b) the maximum strength obtained, (c) the time of the last rogue wave on this time frame, (d) the lifetime of rogue events on this time frame, and (e) the number of rogue waves. using initial condition (5.1.1) with $L = 4\sqrt{2}\pi$, $\delta = 0.1$, and specified amplitudes in the two UMs regime. The solid line is the average over the amplitudes. [90 experiments]

5.4.2 The effect of proximity to instabilities on rogue waves

In this section we examine how altering the proximity of the initial data to the plane wave and its instabilities affects the characteristic features of the solution. Significantly, we show that as the initial data gets closer to the plane wave, the maximum strength of the waves as well as the number and lifetime of rogue waves increase on average while the time of permanent downshift decreases.

For the nonlinear damped HONLS equation with $\epsilon = 0.05$, $\beta = .15$, $\Gamma = 0$, Figure 5.13 shows the evolution of the (a) strength $S(t)$ and (b) spectral peak k_{peak} for initial condition $u(x,0) = .45(1 + \delta \cos \mu x)$ with $\delta = .0005$, $\mu = 2\pi/L$, $L = 4\sqrt{2}\pi$, $0 < t < 200$. Notice this experiment differs only in δ, the perturbation of the plane wave, from the experiment in Figure 5.8 where $\delta = 0.01$.

Although for $\delta = 0.0005$ spectral activity continues until $t \approx 110$, k_{peak} permanently downshifts from the zeroth mode at $t \approx 90.2$ and the last rogue wave occurs at $t = 88$. In contrast, for $\delta = 0.01$ k_{peak} permanently downshifts from the zeroth mode at $t = 127$ and the last rogue wave occurs at $t = 66$. These experiments illustrate the trend that decreasing the perturbation from the plane wave in the initial condition decreases the length of time it takes for the solution to permanently downshift. Restated, larger δ values in the initial condition take longer to downshift, and smaller δ values (which are closer to the plane wave) downshift sooner.

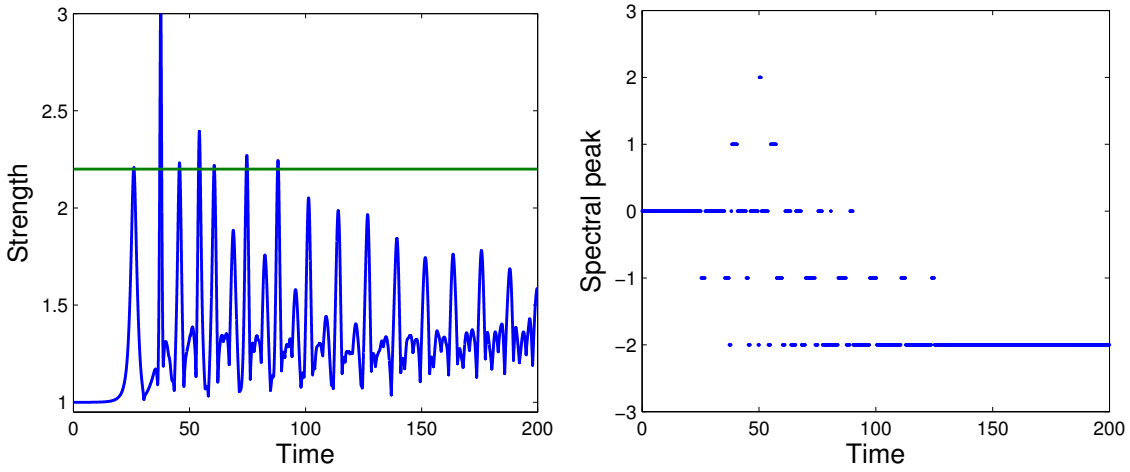

Figure 5.13: Nonlinear damped HONLS with $\epsilon = 0.05$, $\beta = .15$, $\Gamma = 0$. Evolution of the (a) strength $S(t)$ and (b) spectral peak k_{peak} for initial condition $u(x,0) = .45(1+\delta\cos\mu x)$ with $\delta = .0005$, $\mu = 2\pi/L$, $L = 4\sqrt{2}\pi$, $0 < t < 200$.

In Figure 5.14 we see how the proximity to the plane wave affects many of the features of the nonlinear damped HONLS solution ($\epsilon = 0.05$, $\beta = 0.1$, $\Gamma = 0$) discussed thus far in this paper. The initial data for the set of experiments in the two UMs regime is obtained by choosing for each of nine values of the amplitude in (5.1.1) , $0.4 \leq a \leq 0.48$, $L = 4\sqrt{2}\pi$ 15 values of the modulation parameter δ in the range $0.01 \leq \delta \leq 0.1$.

The result of a single experiment is displayed as a data point. The solid line represents the average of the (a) lifetime, (b) maximum strength, (c) number of rogue waves, and (d) terminal spectral center obtained over 15 uniform bins in the $a\delta$ range. We see that on average, as $a\delta$ increases, the lifetime, maximum strength and number of rogue waves decrease. Additionally, the time of the last rogue wave and the time of the maximum strength is slightly delayed (not shown).

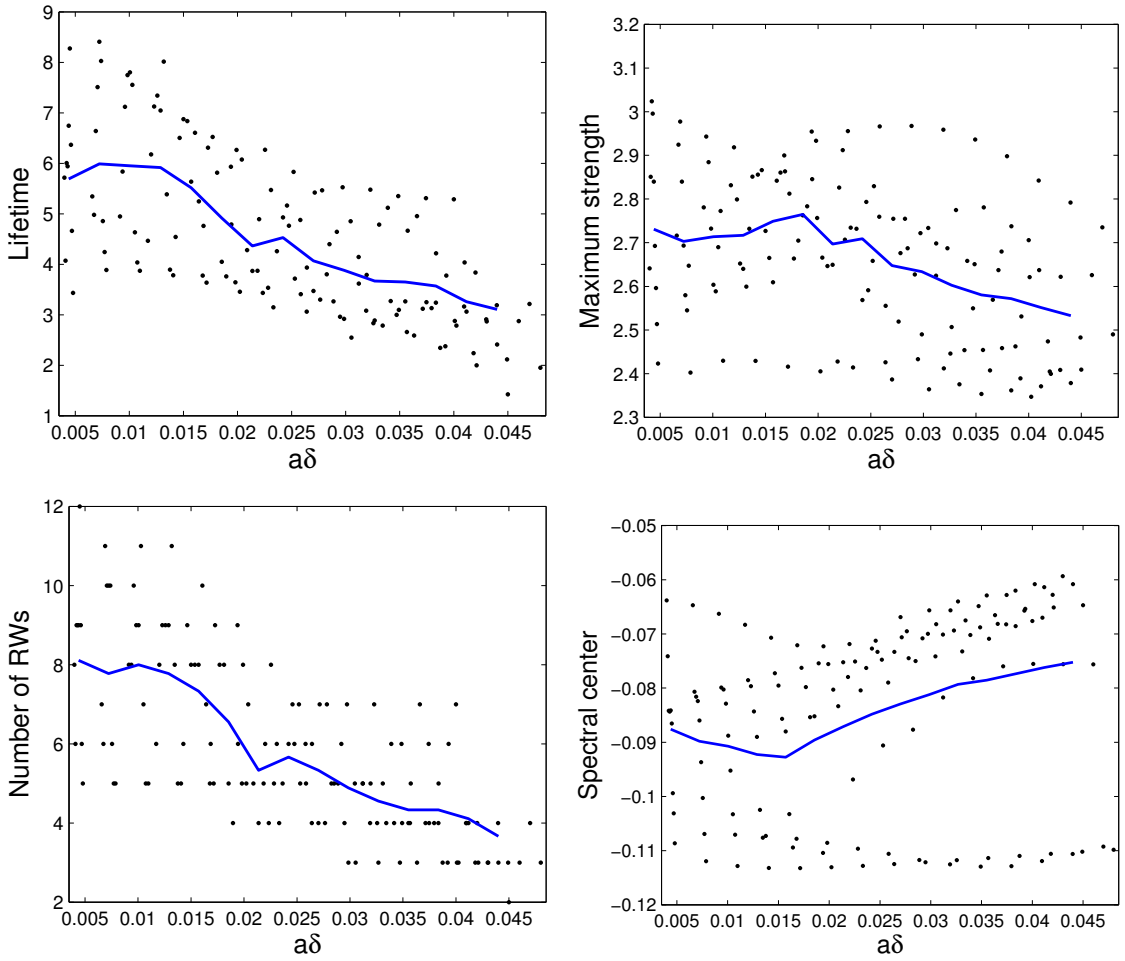

Figure 5.14: Nonlinear damped HONLS, $\epsilon = 0.05$, $\beta = .1$, and $\Gamma = 0$, for $0 < t < 600$ with fifteen δ values, $0.01 \leq \delta \leq 0.1$, and nine initial amplitudes, $0.4 \leq a \leq 0.48$ in (5.1.1). The amplitude and modulation parameter δ in initial condition are varied in the two UMs regime. The solid line represents the average of the (a) lifetime, (b) maximum strength, (c) number of rogue waves, and (d) terminal spectral center. [135 experiments]

5.4.3 The effect of wave strength on the time of permanent downshift

Alternatively one may ask how the time of permanent downshift is affected by rogue wave activity. Recall Figure 5.13 and Figure 5.7 provide an example of two experiments, differing only by their initial perturbation from the plane wave, which yielded different maximum strengths. Further the solution with the larger maximum strength downshifted more quickly. This raises the question of how the time of permanent downshift depends upon features of the waves such as their maximum strength or lifetime and number of rogue waves.

To address this question a set of experiments was carried out using the nonlinear damped HONLS equation, $\epsilon = 0.05$, $\Gamma = 0$ for $\beta = 0.1$, $\beta = 0.2$, and $\beta = 0.4$. Nine values of the amplitude in initial condition (5.1.1) are chosen in the two UMs regime, $0.4 \leq a \leq 0.48$, $L = 4\sqrt{2}\pi$, and for each amplitude nine values of the modulation parameter δ are chosen, $10^{-3} \leq \delta \leq 10^{-1}$. Similarly, nine values of the amplitude in initial condition (5.1.1) are chosen in the three UMs regime, $0.57 \leq a \leq 0.65$, $L = 4\sqrt{2}\pi$, and for each amplitude nine values of the modulation parameter δ are chosen, $10^{-3} \leq \delta \leq 10^{-1}$.

Figure 5.15 provides the time of permanent downshift for the nonlinear damped HONLS, $\epsilon = 0.05$, $\Gamma = 0$, and $\beta = .1$ (circle), $\beta = .2$ (square), or $\beta = .4$ (triangle), as a function of the average maximum strength (a) in the two UMs regime and (b) in the three UMs regime. The average is computed by binning the data over 10 uniform bins.

For the smaller value $\beta = 0.1$ the average time of permanent downshift, in general, decreases as the strength of the wave increases in both the two and three UMs regimes. As β

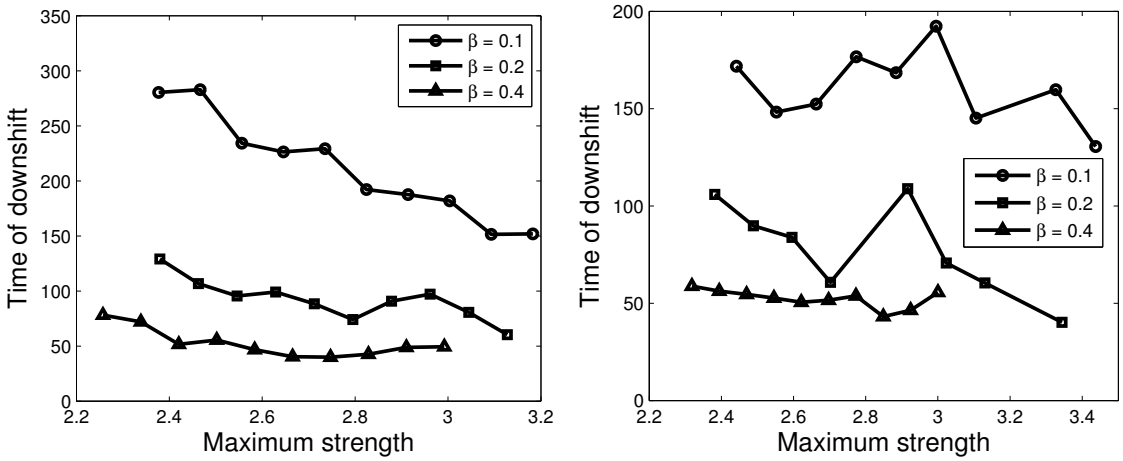

Figure 5.15: Two and three UMs initial condition (5.1.1) in nonlinear damped HONLS, $\epsilon = 0.05$, $\Gamma = 0$, and $\beta = .1$ (circle), $\beta = .2$ (square), or $\beta = .4$ (triangle) for $0 < t < 450$ with experiments required to downshift by $t = 400$. The time of permanent downshift as a function of the maximum strength in the (a) two UMs regime, $0.4 \leq a \leq 0.48$ and (b) three UMs regime, $0.57 \leq a \leq 0.65$. [81 experiments]

increases, the dependence of the time of permanent downshift on the strength is less striking in the two UMs regime. In the three UMs regime the time of permanent downshift is almost uniform as the strength increases.

5.5 Rogue waves and downshifting in the linear and nonlinear damped HONLS

In this section we explore the combined effects of wind and nonlinear damping on the HONLS evolution. Initial data (5.1.1) is used with $\delta = 0.1$ and an appropriate amplitude and period for each of the $N = 1, 2, 3$ UMs regimes. For each initial condition, seventy-five experiments were carried out by selecting five values of β, i.e. $\beta = 0.1, ..., 0.5$, where for each value of β fifteen values of Γ are considered where the linear term is active in the experiment for differing lengths of time (T_{wind}) as specified in the figure labels. The ranges in Γ, chosen to ensure stability of the forced experiments, depend on the number of nearby unstable modes. For each T_{wind}, the lines presented are the averages over the five β values considered.

Figure 5.16 provides the (a) terminal spectral center, $k_m(200)$, and the (b) maximum strength obtained for the HONLS equation with $\epsilon = 0.05$ and various (T_{wind}, Γ) pairs using initial data in the one UMs regime, $u(x, 0) = 0.3(1 + 0.1 \cos \mu x)$, $\mu = 2\pi/L$, $L = 4\sqrt{2}\pi$ for $0 < t < 200$. Figure 5.16(a) shows that for a given T_{wind} the terminal spectral center is an increasing function of Γ. We also see in the individual experiments for a given β, the frequency downshift (from zero) decreases as Γ increases (not shown). Moreover, as T_{wind}

increases, linear forcing causes the terminal spectral center to decrease more, and linear damping causes the terminal spectral to decrease less. Thus linear damping inhibits the downshifting effect of the nonlinear damping, while linear forcing enhances the downshifting effects of the nonlinear damping. Figure 5.16(b) shows the maximum strength is a decreasing, approximately linear, function of Γ for each T_{wind}. The same behavior is seen for individual β values (not shown). In the one UM regime there are no rogue waves in the HONLS evolution. Similarly, for the β, Γ, and T_{wind} values considered in the damped/forced HONLS evolution, there are also no rogue waves in the one UM regime.

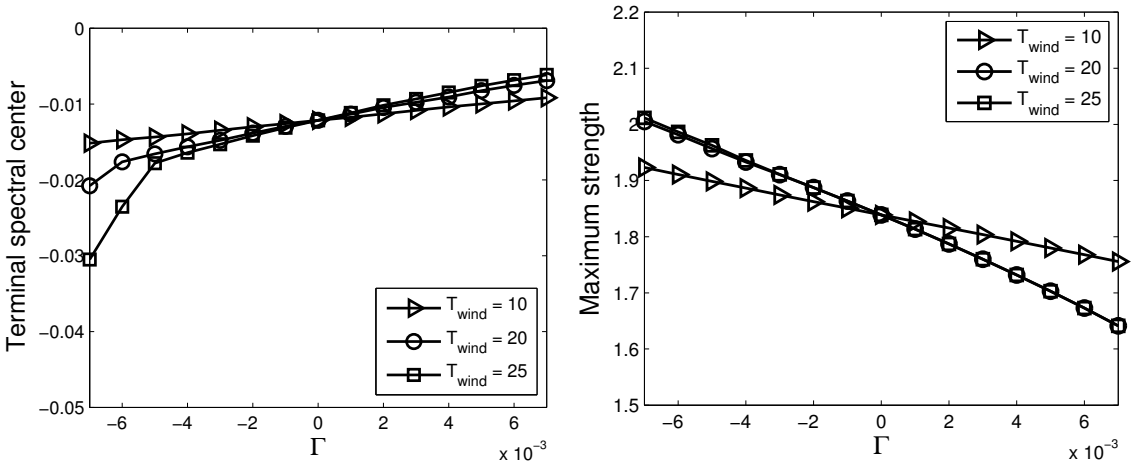

Figure 5.16: One UM initial condition (5.1.1) with $a = 0.3$, $\delta = 0.1$, and $L = 4\sqrt{2}\pi$ in the nonlinear damped HONLS ($\epsilon = 0.05$, $\beta = .1, .2, .3, .4, .5$, $-0.007 \leq \Gamma \leq 0.007$) for $0 < t < 200$ with linear forcing for $0 < t < T_{wind}$: (a) the terminal spectral center, and (b) the maximum strength obtained averaged over five β values.

When there are $N \geq 2$ unstable modes nearby, the inclusion of linear forcing results in a more striking enhancement of downshifting. Figure 5.17 shows the terminal spectral

center for the HONLS equation, with $\epsilon = 0.05$ and various β, Γ, and T_{wind}, for $0 < t < 200$, using initial conditions (a) $u(x,0) = 0.48(1 + 0.1\cos\mu x)$ with $\mu = 2\pi/L$, $L = 4\sqrt{2}\pi$ (two UMs regime), and (b) $u(x,0) = 0.67(1 + 0.1\cos\mu x)$ with $\mu = 2\pi/L$, $L = 4\sqrt{2}\pi$, (three UMs regime). The solid curve represents the averages over β for a given T_{wind}. In Figures 5.17(a) and 5.17(b), the behavior of each initial condition shows that linear forcing causes the spectral center to decrease further, whereas linear damping yields results that have decreased less than in the cases with no linear term. The experiments for a given T_{wind} also demonstrate that for each β the terminal spectral center is an increasing function of Γ (not shown). Clearly, as in the one UM regime, for a given β, the addition of linear forcing enhances the downshifting effect, whereas linear damping diminishes the downshifting effect of the nonlinear damping.

As discussed previously, when only nonlinear damping is present, one could expect that features of the rogue events such as strength, number of events, lifetime would increase with linear forcing and decrease with linear damping. However, for a given β, this is not always the case for the small variations in Γ examined. The additional damping changes the focusing time and coalescence of the modes. However, when averaged over β, the maximum strength of rogue events are generally decreasing across the Γ ranges examined in the two and three UMs regimes as seen in Figures 5.18(a-b). Figure 5.18(c-d) shows that the dynamics are more complicated when considering the lifetime of rogue events.

The number of rogue waves is a decreasing function of Γ for each β in the two UMs and three UMs cases (not shown). Linear damping causes fewer rogue waves in most cases shown, whereas linear forcing causes an increase in the number of rogue waves. This effect

is seen more starkly in the case of three UMs, but is also present in the two UMs case when comparing to the cases with no linear effects ($\Gamma = 0$).

The time of the last rogue wave is much later for the smaller β values when linear forcing is included (not shown). This indicates that rogue waves are continuing to occur when the experiment terminates. For the larger values of β however, increasing the amount of linear forcing in this range has little impact on the time of last rogue wave. For $\Gamma > 0$, rogue waves cease earlier than they do for $\Gamma = 0$ in nearly all of the experiments in both two UMs and three UMs regimes.

The behavior of the system is determined largely by whether the linear term is damping or enhancing the waveform. In general, we see that the forcing of two UMs allows for a larger number of rogue waves that occur later in the time series and are, on average, stronger (not shown). The maximum strength is also larger, in general, and the downshifting effects of the nonlinear damping term are enhanced by linear forcing. For longer lengths of T_{wind}, the maximum strength is larger when linear forcing is applied. Interestingly, this does not vary much for the larger lengths of T_{wind}. The lifetime of rogue events in the two UMs case is longer for $T_{wind} = 200$ when $\Gamma < 0$ and shorter when $\Gamma < 0$. Similarly, the smallest length of linear term, T_{wind} is shortest when $\Gamma < 0$ and largest when $\Gamma > 0$. This illustrates further that as T_{wind} increases, the change from the Γ term also increases.

Unlike the two UMs case in Figure 5.18(a-b), the three UMs case (seen in Figure 5.18(c-d)) shows comparatively little change as T_{wind} changes. For these experiments, the maximum strength occurs early in the timeseries. The large wave early in the exper-

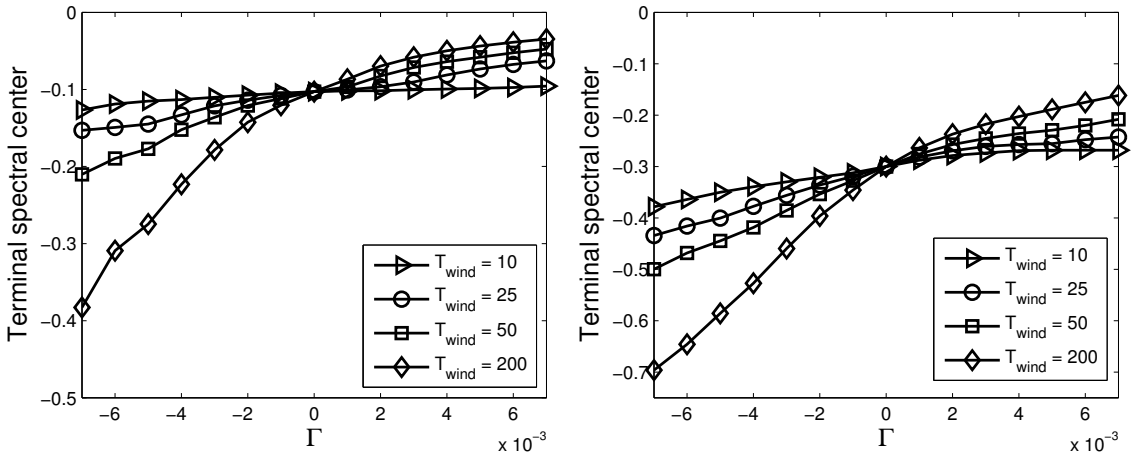

Figure 5.17: The terminal spectral center for the two and three UMs initial conditions in the damped HONLS, with $\epsilon = 0.05$ and various β and Γ, for $0 < t < 200$ with linear term applied until $0 < t < T_{wind}$, using initial condition (5.1.1) with $\delta = 0.1$, $L = 4\sqrt{2}\pi$: (a) $a = 0.48$, and (b) $a = 0.67$ averaged over the five β values for each T_{wind}.

iment causes the nonlinear term to act strongly to lessen the likelihood of further waves of the same strength. Consequently, the maximum strength changes proportional to the Γ term as long as it acts until the first large wave is formed. We still see that the inclusion of linear forcing causes the maximum strength to increase whereas linear damping causes the maximum strength to decrease. The lifetime for the three UMs cases behaves similarly. There is a slight increase, on average, as Γ is more largely negative, and a slight decrease in the lifetime as Γ increases in the positive direction.

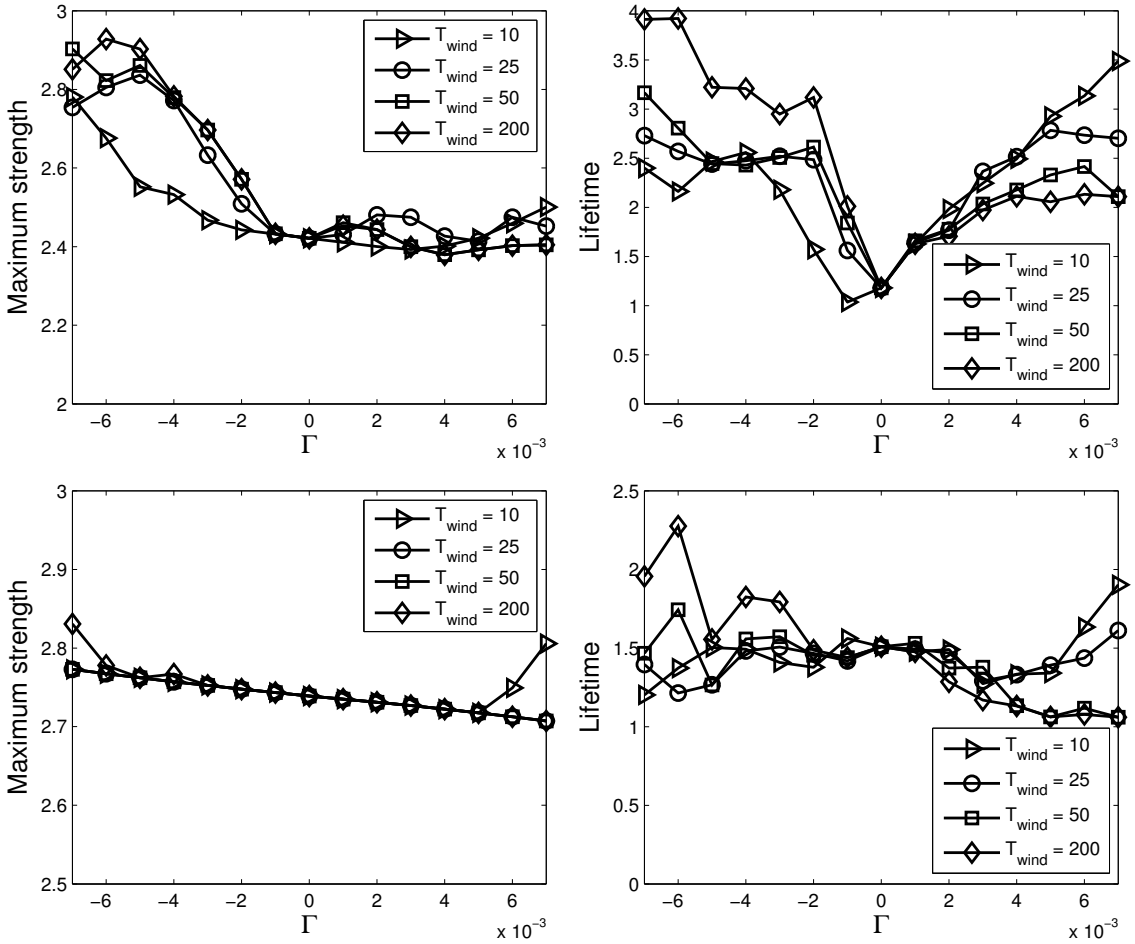

Figure 5.18: Nonlinear damped HONLS with various Γ applied for $0 < t < T_{wind}$ averaged over five β values using initial condition (5.1.1) with $\delta = 0.1$, $L = 4\sqrt{2}\pi$, $\epsilon = 0.05$ for $0 < t < 200$: (a) the maximum strength and (b) the lifetime of rogue events for two UMs ($a = .48$); (c) the maximum strength and (d) the lifetime of rogue events for three UMs ($a = .67$).

5.5.1 Time of permanent downshift and time of the last rogue wave

In section 5.4 it was shown permanent downshifting occurs $\forall \beta > 0$ when $\Gamma = 0$ (for $N \geq 1$ UMs) and that rogue waves do not occur after permanent downshifting in the two and three UMs regimes. Here we examine this issue when both nonlinear damping and linear damping/forcing are present. Figure 5.19 presents the time of permanent downshift (x) and the time of the last rogue wave (square) for fourteen values of β in the range of $0 < \beta \leq .75$, $\Gamma = \pm 0.005$, in (4.1.1) with initial condition (5.1.1) for 5 different initial amplitudes in the two UMs regime ($.4 \leq a \leq .48$) and 5 different initial amplitudes in the three UMs regime ($.57 \leq a \leq .65$). Figure 5.19 provides the times averaged over the relevant amplitudes. The plots for a single amplitude a are qualitatively the same.

When $\Gamma = .005$ for the two UMs initial conditions, 65 of the 65 experiments downshifted. Recall the nonlinear damping term is $\mathcal{O}(\epsilon\beta)$. As a result, linear damping interferes with the downshift mechanism for the smallest β considered, $\beta = 0.10$, so they are not considered. The last rogue wave occurs before the time of permanent downshifting in 62 of the 65 (95%) downshifted cases. In the two cases where the last rogue wave occurred after the last time the spectral peak returned to the zeroth mode, the last rogue wave occurred before the spectral peak ceased activity. Figure 5.19(a) shows these results averaged over the different initial amplitudes in the experiment set. As β increases, the time of permanent downshifting and the time of the last rogue wave move closer.

The behavior was similar in the three UMs experiments, with 61 of the 70 experiments experiencing permanent downshifting, 58 of those experiments doing so after the last rogue wave and one additional experiment having its last rogue wave just after the time of permanent downshifting (98%). In the three UMs experiments, there were experiments which had a rogue wave long after the time of permanent downshifting (21.5 and 28 time units later).

When the waves are forced, $\Gamma = -.005$, permanent downshifting occurred on the timeframe considered in 46 of the 65 numerical experiments, primarily for the larger values of β. Only one of the downshifted experiments did not have its last rogue wave before the time of permanent downshift, but the instability that caused the last rogue wave in that case had already begun growing at the time of permanent downshift. With the exception of this single experiment, the remainder of the experiments that experienced permanent downshifting the permanent downshifting occurred after the last rogue wave (98%).

For the three UMs initial conditions, 68 of the 70 experiments permanently downshifted on this timeframe, 59 of which had their last rogue wave before permanent downshifting and 7 further that had a rogue wave which formed before the time of permanent downshifting occur shortly after the time of permanent downshift (97%). From this set, two experiments had a rogue wave approximately 21 time units after the time of permanent downshifting.

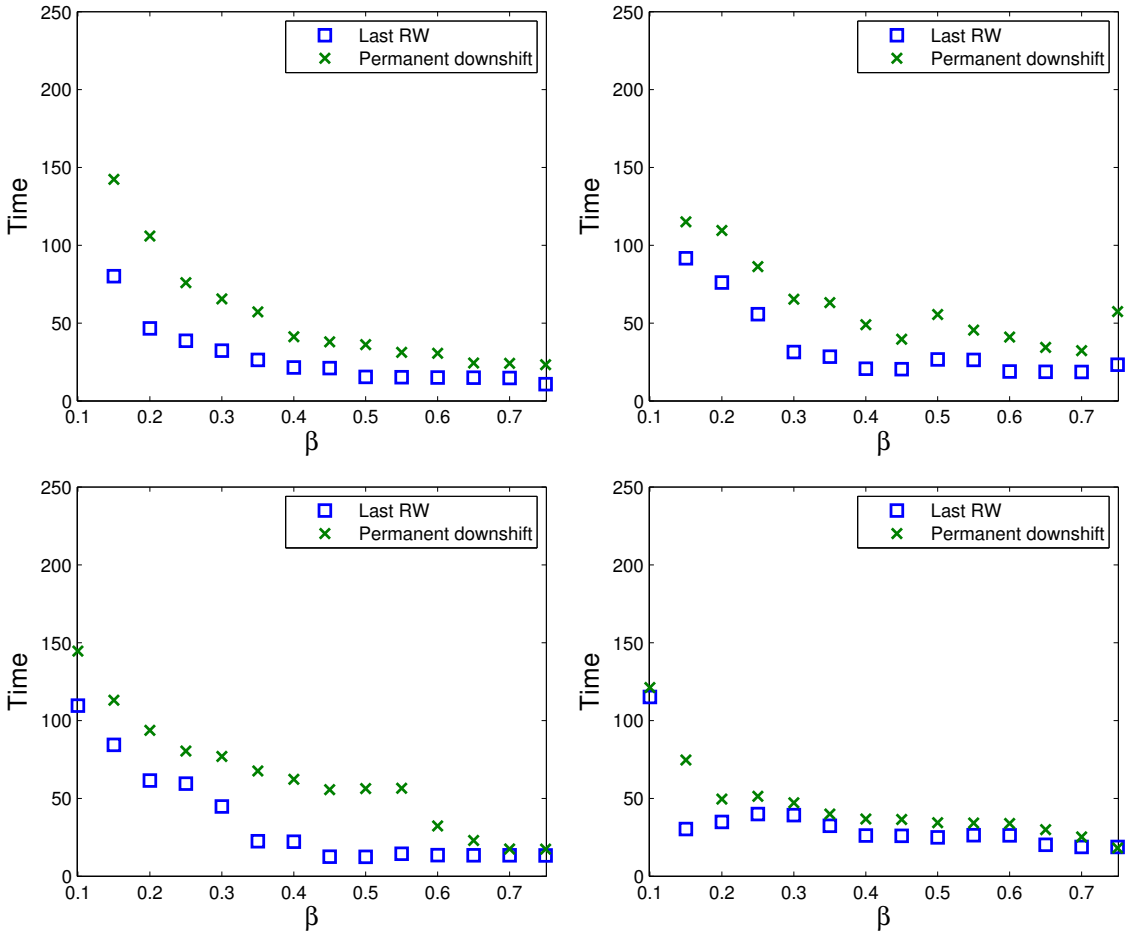

Figure 5.19: Time of downshifting (x) and time of last rogue wave (square) in the nonlinear damped and linear damped/forced HONLS with various β, and Γ, using initial condition (5.1.1) with $\delta = 0.1$, $L = 4\sqrt{2}\pi$, $\epsilon = 0.05$ for $0 < t < 200$ with the linear term active for $0 < t < 20$. The figures are (a) the downshifted cases for $\Gamma = 0.005$ and (b) the downshifted cases for $\Gamma = -0.005$ averaged over 6 amplitudes in the two UMs regime $.4 \leq a \leq .48$, and (c) the downshifted cases for $\Gamma = 0.005$ and (d) the downshifted cases for $\Gamma = -0.005$ averaged over 6 amplitudes in the three UMs regime $.57 \leq a \leq .65$.

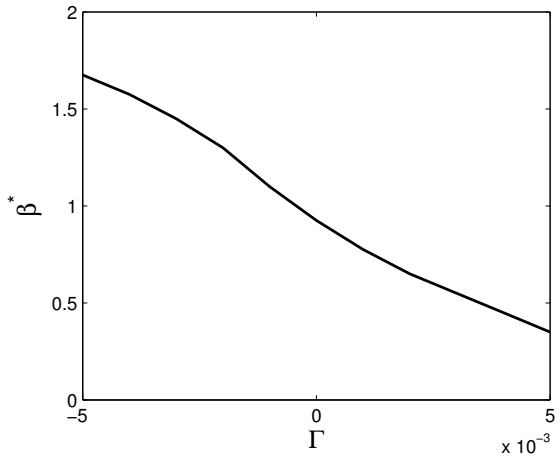

Figure 5.20: A sufficient amount of nonlinear damping to prevent the formation of any rogue waves on the timeframe for a given Γ in nonlinear damped HONLS ($\epsilon = 0.05$, $0 \leq \beta \leq 2$, $-.005 \leq \Gamma \leq .005$) with initial condition (5.1.1) , with $a = 0.4$, and $L = 4\sqrt{2}\pi$ for $0 < t < 200$.

5.5.2 Eliminating rogue waves

The initial condition (5.1.1) with $\delta = 0.1$ is a small perturbation of the plane wave. The initial condition has two UM for $a = 0.1$ with $L = 4\sqrt{2}\pi$. These instabilities quickly grow, which typically forms a rogue wave early in the timeseries. In figure 5.6 we showed that linear damping can cause the initial growth to not be a rogue wave, and furthermore that no rogue waves occur later. Figure 5.20 extends this idea to the cases including nonlinear damping and allowing for the cases with linear forcing. For each Γ in the range, β^* is the first β value that was able to prevent all rogue waves from forming. Because the experiment

set is run for β values in steps of .025, the β^* indicated is sufficient to prevent all rogue waves, but it may not be the minimal such β value.

APPENDIX

NUMERICAL INTEGRATOR

1 The exponential integrator

The governing equation (4.1.1) is solved numerically using a very accurate smoothing exponential integrator [27]. The integrator combines Fourier-mode decomposition in space with a fourth-order exponential Runge-Kutta method in time which uses Padé approximations of the matrix exponential terms.

Break down the equation into linear and nonlinear components:

$$u_t = (\mathcal{L} + \mathcal{N})u,$$

where

$$\begin{aligned}
\mathcal{L}u &= iu_{xx} + i\Gamma u - \frac{\epsilon}{2}u_{xxx} \\
\mathcal{N}u &= 2i|u|^2u + 8\epsilon|u|^2u_x + 2i\epsilon u(1+i\beta)\left[\mathcal{H}\left(|u|^2|\right)\right]_x .
\end{aligned}$$

Let $\mathcal{F}(u) = \hat{u}$ be the Fourier transform in space. Then,

$$\begin{aligned}
\hat{u}_t &= \mathcal{F}(\mathcal{L}u + \mathcal{N}u) \\
&= \left[i(ik)^2 + i\Gamma - \frac{\epsilon}{2}(ik)^3\right]\mathcal{F}(u) + \mathcal{F}\left(\mathcal{N}(u)\right) \\
&= \left(-ik^2 + i\Gamma + i\frac{\epsilon}{2}k^3\right)\hat{u} + \mathcal{F}\left(\mathcal{N}(u)\right) \\
&= -A\hat{u} + F(t),
\end{aligned}$$

where

$$A = ik^2 - i\Gamma - i\frac{\epsilon}{2}k^3 \qquad F(t) = \mathcal{F}\left(\mathcal{N}(u)\right).$$

Using an integrating factor we see that

$$\hat{u}_t + A\hat{u} = F(t)$$

$$e^{At}\hat{u}_t + Ae^{At}\hat{u} = e^{At}F(t)$$

$$\frac{\partial}{\partial t}\left[e^{At}\hat{u}\right] = e^{At}F(t)$$

$$\left[e^{At}\hat{u}\right]\Big|_{t_n}^{t_{n+1}} = \int_{t_n}^{t_{n+1}} e^{At}F(t)\,dt.$$

Evaluating the integral we have

$$e^{A(t_n+\Delta t)}\hat{u}(t_n+\Delta t) - e^{At_n}\hat{u}(t_n) = \int_0^{\Delta t} e^{A(t_n+\tau)}F(t_n+\tau)\,d\tau$$

$$e^{At_n}e^{A\Delta t}\hat{u}(t_n+\Delta t) - e^{At_n}\hat{u}(t_n) = e^{At_n}\int_0^{\Delta t} e^{A\tau}F(t_n+\tau)\,d\tau$$

$$\hat{u}(t_n+\Delta t) = e^{-A\Delta t}\hat{u}(t_n) + e^{-A\Delta t}\int_0^{\Delta t} e^{A\tau}F(t_n+\tau)\,d\tau.$$

But now we need to evaluate the resulting integral. Because the integral cannot typically be evaluated exactly, we approximate.

The simplest approximation is assuming F is piece-wise constant, i.e. assume $F(t) = F_n$ for $t_n \le t \le t_{n+1}$. Then,

$$\int_0^{\Delta t} e^{A\tau}F(t_n+\tau)\,d\tau \approx F_n\int_0^{\Delta t} e^{A\tau}\,d\tau = \frac{F_n}{A}\left[e^{A\Delta t} - 1\right].$$

Given $u_0 = u(x,0)$ we can now step forward in time.

$$\hat{u}(t_{n+1}) = e^{-A\Delta t}\hat{u}(t_n) + \frac{F_n}{A}\left[1 - e^{-A\Delta t}\right].$$

With this assumption, the error at each time step is $\mathcal{O}\left((\Delta t)^2\right)$.

In application, we can achieve much better accuracy. In this work we implement a fourth-order Runge-Kutta method. In general, if $y'(t) = g(y(t), t)$, then we can approximate the solution at the next time step, $t_{n+1} = t_n + \Delta t$ by

$$y(t_{n+1}) = y(t_n) + \frac{\Delta t}{6}\Big(k_1 + 2(k_2 + k_3) + k_4\Big),$$

where

$$\begin{aligned}
k_1 &= g(y(t_n), t_n), \\
k_2 &= g(a_n, t_n + \tfrac{\Delta t}{2}), & a_n &= y(t_n) + k_1\tfrac{\Delta t}{2}, \\
k_3 &= g(b_n, t_n + \tfrac{\Delta t}{2}), & b_n &= y(t_n) + k_2\tfrac{\Delta t}{2}, \\
k_4 &= g(c_n, t_n + \Delta t), & c_n &= y(t_n) + k_3\Delta t.
\end{aligned}$$

In our case, $y(t) = e^{At}\widehat{u}$, and $g(y(t), t) = e^{At}F(t)$. Approximating the matrix exponential introduces many problems. Following the work of [28], we use a Padé approximation to help minimize some of the issues. In general, a Padé approximation, $R_{m,n}(z)$ to a function $h(z)$ is a rational function of polynomials whose numerator degree is $m \geq 0$ and denominator degree is $n \geq 1$ with the requirement that $h^{(k)}(z_0) = R^{(k)}_{m,n}(z_0)$. In this case, we need to expand e^z around $z = 0$, and we find

$$\begin{aligned}
e^{-z} &\approx R_{2,2}(z) \equiv \frac{1 + \frac{1}{2}(-z) + \frac{1}{12}(-z)^2}{1 - \frac{1}{2}(-z) + \frac{1}{12}(-z)^2} = \frac{12 - 6z + z^2}{12 + 6z + z^2}, \\
e^{-z/2} &\approx \widetilde{R}_{2,2}(z) \equiv \frac{1 + \frac{1}{2}(-\frac{z}{2}) + \frac{1}{12}(-\frac{z}{2})^2}{1 - \frac{1}{2}(-\frac{z}{2}) + \frac{1}{12}(-\frac{z}{2})^2} = \frac{48 - 12z + z^2}{48 + 12z + z^2}.
\end{aligned}$$

In our case, we are interested in finding $\widehat{u}_{n+t}$, not simply $y(t_{n+1})$, so the coefficients on $\widehat{u}_{n+t}$ must be moved to the other side after approximating. We end up at the system

$$\widehat{u}_{n+1} = R_{2,2}(A\Delta t)\widehat{u}_n + P_1(A\Delta t)F(\widehat{u}_n, t_n) + P_2(A\Delta t)\left[F(\widehat{a}_n, t_n + \tfrac{\Delta t}{2}) + F(\widehat{b}_n, t_n + \tfrac{\Delta t}{2})\right]$$

$$+ P_3(A\Delta t)F(\widehat{c}_n, t_n + \Delta t).$$

where,

$$\widehat{a_n} = \widetilde{R}_{2,2}(A\Delta t)\widehat{u}_n + \widetilde{P}(A\Delta t)F(u_n, t_n),$$

$$\widehat{b_n} = \widetilde{R}_{2,2}(A\Delta t)\widehat{u}_n + \widetilde{P}(A\Delta t)F(u_n, t_n + \tfrac{\Delta t}{2}),$$

$$\widehat{c_n} = \widetilde{R}_{2,2}(A\Delta t)\widehat{u}_n + \widetilde{P}(A\Delta t)\big[F(b_n, t_n + \tfrac{\Delta t}{2}) - F(u_n, t_n)\big],$$

$$P_1(M) = \Delta t \left(\frac{2I - M}{12I + 6M + M^2}\right),$$

$$P_2(M) = \Delta t \left(\frac{4}{12 + 6M + M^2}\right),$$

$$P_3(M) = \Delta t \left(\frac{2I + M}{12 + 6M + M^2}\right).$$

The final step is to invert the Fourier transform using the Fast Fourier Transform (FFT).

The accuracy of the integrator for the HONLS used in this document was compared to another state of the art methods in [29]. Specifically, they compared the accuracy and the computational efficiency of this method to the split-step method and found the exponential time differencing method to be more computationally efficient than the split-step method when trying to obtain a specific accuracy by comparing to exact solutions.

2 Accuracy

The initial data used in the numerical experiments are small perturbations of the unstable plane wave, i.e.

$$u(x,0) = a\left(1 + \delta\cos 2\pi x/L\right),$$

where $\delta << 1$ and the amplitude a and period L are chosen so that $\lfloor aL/\pi \rfloor = N = 1, \ldots, 3$. Initial data (5.1.1) is referred to as the N unstable mode (UM) "regime" as the background plane wave has N unstable modes *initially*. It is also close to initial data for the N-mode SPB solutions of the NLS equation.

The number of Fourier modes and the time step used in the experiments depends on the complexity of the solution. For example, for initial data in the two UMs regime, typically $L = 4\sqrt{2}\pi$ and $N = 256$ Fourier modes are used with time step $\Delta t = 10^{-3}$. This space - time resolution allows for the three global invariants of the conservative HONLS equation, the energy E, momentum P, and Hamiltonian $\mathcal{H}$, to be conserved with an accuracy of $\mathcal{O}(10^{-12})$, $\mathcal{O}(10^{-11})$, $\mathcal{O}(10^{-11})$, respectively for $0 < t < 200$. For the linear perturbed HONLS, $k_m = \frac{-P}{2E}$ is invariant and, in the case of linear damping, is conserved with an accuracy of at least $\mathcal{O}(10^{-11})$ for experiments in the $N = 1, 2, 3$ UMs regimes for $0 < t < 200$.

The spectral center, E, P, and $\mathcal{H}$ are not invariant for the HONLS equation with nonlinear damping and linear forcing. As a result, we appeal to error results for the linear forced HONLS equation to provide an upper bound on the error in the numerical experiments which also include nonlinear damping. That is, when both nonlinear damping and linear

forcing are present we use the space-time mesh and parameter range in Γ that allows for an acceptable conservation in the spectral center for the linear forced HONLS equation.

To determine the accuracy in the linear forced HONLS experiments for $0 < t < 200$ with wind acting until $T_{wind} = 25$, for each of nine values of Γ, $-0.007 \leq \Gamma \leq 0.001$, five experiments using different amplitudes in the initial data were carried out in each of the $N = 1, 2, 3$ UMs regimes, (a) $.25 \leq a \leq .33$, (b) $.4 \leq a \leq .48$, (c) $.57 \leq a \leq .65$, respectively. For each value of Γ the terminal spectral center $k_m(200)$ is averaged over the five experiments in each of the regimes. Figure A.21 shows that for $T_{wind} = 25$, the maximum error in the spectral center at $T = 200$ is $\mathcal{O}(10^{-12})$, $\mathcal{O}(10^{-10})$, and $\mathcal{O}(10^{-4})$ for initial data in the N = 1,2,3 UMs regimes, respectively. The error in the spectral center decreases as T_{wind} decreases (not shown).

We have decided based on previous short-time forcing experiments to consider $-.007 \leq \Gamma$ for forcing times of $T_{FORCED} = 10, 20, 25$. Figure A.21 displays that for this range, when run to $T_{MAX} = 200$ as we do in the experiments.

Most of the experiments are over the timeframe $0 < t < 200$. Key experiments, e.g. those relating the time of permanent downshift and the time of the last rogue wave, are run longer than presented, to ensure the validity of the results. To avoid aliasing we eliminate the high frequency modes at every time step, e.g. when $N = 256$ Fourier modes are used we let $\hat{u}_k = 0$ for $|k| > 120$. This does not have a significant effect on the exchange of energy between the dominant low wave number modes and thus does not change our results related to frequency downshifting and rogue waves (it was also verified that varying the number of

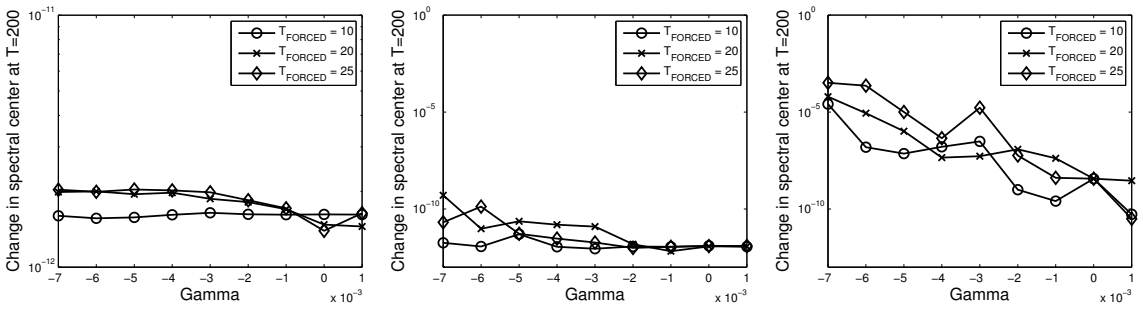

Figure A.21: Nonlinearly damped HONLS, $\epsilon = 0.05$, $\beta = 0$, $-0.007 \leq \Gamma \leq 0.001$, $T_{max} = 200$ with linear forcing until $T_{forced} = 10, 20, 25$, as specified in the labels. The terminal spectral center averaged over (a) 5 initial amplitudes $.25 \leq a \leq .33$, (b) 9 initial amplitudes $.4 \leq a \leq .48$, (c) 5 initial amplitudes $.57 \leq a \leq .65$ using initial condition $u(x, 0) = a(1 + 0.1 \cos \mu x)$ with $L = 4\sqrt{2}\pi$. [45,81,45 experiments per forcing time]

frequencies being eliminated does not change the behavior). Additionally, the behavior of the solution and of the dominant modes does not change when the mesh is refined.

LIST OF REFERENCES

[1] K. Trulsen and K. B. Dysthe, "Frequency downshift in three-dimensional wave trains in a deep basin," *Journal of Fluid Mechanics*, vol. 352, pp. 359–373, 1997.

[2] W. Rosenthal and S. Lehner, "Rogue waves: Results of the MaxWave project," *Journal of Offshore Mechanics and Arctic Engineering*, vol. 130, no. 2, p. 021006, 2008.

[3] B. M. Lake, H. C. Yuen, H. Rungaldier, and W. E. Ferguson, "Nonlinear deep-water waves: theory and experiment. part 2. evolution of a continuous wave train," *Journal of Fluid Mechanics*, vol. 83, no. 01, pp. 49–74, 1977.

[4] M. Tulin, Y. Yao, and P. Wang, "The simulation of the deformation and breaking of ocean waves in wave groups," 1994.

[5] T. B. Benjamin and J. Feir, "The disintegration of wave trains on deep water part 1. theory," *Journal of Fluid Mechanics*, vol. 27, no. 03, pp. 417–430, 1967.

[6] A. Calini and C. Schober, "Observable and reproducible rogue waves," *Journal of Optics*, vol. 15, no. 10, pp. 105–201, 2013.

[7] A. Islas and C. Schober, "Rogue waves, dissipation, and downshifting," *Physica D: Nonlinear Phenomena*, vol. 240, no. 12, pp. 1041–1054, 2011.

[8] C. Kharif, E. Pelinovsky, and A. Slunyaev, "Deterministic and statistical approaches for studying rogue waves," in *Rogue Waves in the Ocean*, pp. 33–61, Springer, 2009.

[9] H. Segur, D. Henderson, J. Carter, J. Hammack, C. Li, D. Pheiff, and K. Socha, "Stabilizing the Benjamin–Feir instability," *Journal of Fluid Mechanics*, vol. 539, pp. 229–271, 2005.

[10] M. Ablowitz and H. Segur, *Solitons and the inverse scattering transform*, vol. 4. SIAM, 1981.

[11] A. Shabat and V. Zakharov, "Exact theory of two-dimensional self-focusing and one-dimensional self-modulation of waves in nonlinear media," *Soviet Physics JETP*, vol. 34, no. 1, p. 62, 1972.

[12] G. Biondini and E. Fagerstrom, "The integrable nature of modulational instability," *SIAM Journal on Applied Mathematics*, vol. 75, no. 1, pp. 136–163, 2015.

[13] E. R. Tracy and H. H. Chen, "Nonlinear self-modulation: An exactly solvable model," *Physical Review A*, vol. 37, no. 3, p. 815, 1988.

[14] R. Grimshaw, *Nonlinear ordinary differential equations*. CRC Press, 1991.

[15] K. B. Dysthe and K. Trulsen, "Note on breather type solutions of the NLS as models for freak-waves," *Physica Scripta*, vol. 1999, no. T82, p. 48, 1999.

[16] A. R. Osborne, M. Onorato, and M. Serio, "The nonlinear dynamics of rogue waves and holes in deep-water gravity wave trains," *Physics Letters A*, vol. 275, no. 5, pp. 386–393, 2000.

[17] A. Calini and C. Schober, "Homoclinic chaos increases the likelihood of rogue wave formation," *Physics Letters A*, vol. 298, no. 5, pp. 335–349, 2002.

[18] N. Akhmediev, A. Ankiewicz, and J. Soto-Crespo, "Rogue waves and rational solutions of the nonlinear Schrödinger equation," *Phys. Rev. E*, vol. 80, p. 026601, Aug 2009.

[19] D. Peregrine, "Water waves, nonlinear Schrödinger equations and their solutions," *The Journal of the Australian Mathematical Society. Series B. Applied Mathematics*, vol. 25, no. 01, pp. 16–43, 1983.

[20] A. R. Osborne, "Classification of homoclinic rogue wave solutions of the nonlinear Schrödinger equation," *Natural Hazards and Earth System Sciences Discussions*, vol. 2, no. 1, pp. 897–933, 2014.

[21] K. Konno and M. Wadati, "Simple derivation of Bäcklund transformation from Riccati form of inverse method," *Progress of Theoretical Physics*, vol. 53, no. 6, pp. 1652–1656, 1975.

[22] A. Calini and C. M. Schober, "Dynamical criteria for rogue waves in nonlinear Schrödinger models," *Nonlinearity*, vol. 25, no. 12, p. R99, 2012.

[23] M. J. Ablowitz, D. J. Kaup, A. C. Newell, and H. Segur, "The inverse scattering transform-Fourier analysis for nonlinear problems," *Studies in Applied Mathematics*, vol. 53, pp. 249–315, 1974.

[24] M. G. Forest and J.-E. Lee, "Geometry and modulation theory for the periodic nonlinear schrodinger equation," in *Oscillation Theory, Computation, and Methods of Compensated Compactness*, pp. 35–69, Springer, 1986.

[25] O. Gramstad and K. Trulsen, "Hamiltonian form of the modified nonlinear Schrödinger equation for gravity waves on arbitrary depth," *Journal of Fluid Mechanics*, vol. 670, pp. 404–426, 2011.

[26] Y. Uchiyama and T. Kawahara, "A possible mechanism for frequency down-shift in nonlinear wave modulation," *Wave Motion*, vol. 20, no. 2, pp. 99–110, 1994.

[27] S. Cox and P. Matthews, "Exponential time differencing for stiff systems," *Journal of Computational Physics*, vol. 176, no. 2, pp. 430–455, 2002.

[28] A. Khaliq, J. Martin-Vaquero, B. Wade, and M. Yousuf, "Smoothing schemes for reaction-diffusion systems with nonsmooth data," *Journal of Computational and Applied Mathematics*, vol. 223, no. 1, pp. 374–386, 2009.

[29] M. Hederi, A. Islas, K. Reger, and C. Schober, "Efficiency of exponential time differencing schemes for nonlinear Schrödinger equations," *Mathematics and Computers in Simulation*, 2013.